

Michigan International Copper Analogue (MICA) project – Phase I

Ismo Aaltonen, Theodore J. Bornhorst, Xuan Liu, Heini Reijonen and Timo Ruskeeniemi

GTK Open File Research Report 22/2023



GEOLOGICAL SURVEY OF FINLAND

Open File Research Report 22/2023

Ismo Aaltonen, Theodore J. Bornhorst, Xuan Liu, Heini Reijonen and Timo Ruskeeniemi

Michigan International Copper Analogue (MICA) project – Phase I

Unless otherwise indicated, the figures have been prepared by the authors of the report.

Front cover: Historic Number 2 shaft-rock house of the Quincy Mine, Keweenaw Peninsula native copper district, Michigan USA which is a Heritage Site of the Keweenaw National Historic Park.

The mine has been dormant for over 75 years but limited underground mine workings are accessible for sampling of in-situ native copper for Phase II. Photo: Theodore J. Bornhorst, Michigan Technological University.

Layout: Elvi Turtiainen Oy

Espoo 2023

Aaltonen, I., Bornhorst, T. J., Liu, X., Reijonen, H. & Ruskeeniemi, T. 2023. Michigan International Copper Analogue (MICA) project – Phase I. *Geological Survey of Finland, Open File Research Report 22/2023*, 42 pages, 6 figures, 7 tables and 3 appendices.

The long-term prediction of engineered barrier system materials is generally supported by: demonstrating a mechanistic understanding of the degradation processes, conducting large-scale in situ tests, and developing computer models. The study of analogues can be used to support long-term predictions relevant for copper as part of waste canisters. Copper is an important part of many disposal concepts, e.g., KBS-3 developed in Sweden and Finland and Mark II developed in Canada.

The Michigan International Copper Analogue (MICA) Project focuses on the general stability of native copper in the world's largest native copper dominated deposits of the Keweenaw Peninsula native copper district in Michigan, U.S.A. One of the key requirements for the deep geological disposal of high-level nuclear waste is the assessment of its long-term performance and safety for upwards of one million years. Observations made from the geological systems, i.e., natural analogues, can be utilized in the safety case and can provide information far beyond one million years. Both natural and archaeological analogue studies are reported in the literature, but only a few studies have focussed on the stability of native copper within its natural setting. The goal of the MICA Project is to provide a unique data source to describe natural analogue processes governing long-term corrosion behaviour of the pure copper used in waste canisters. This information will support disposal safety cases as well as stakeholder communications.

The Keweenaw Peninsula native copper district occurs within the ca. 1.1 billion years old North American Midcontinent Rift system (MCR). Metamorphogenic ore-forming hydrothermal fluids precipitated native copper and associated minerals in primary and secondary open spaces of the host rocks at depth about 1.04 to 1.07 billion years ago. Subsequent erosion resulted in exposure of the native copper deposits at the surface. The Keweenaw deposits were commercially mined from 1845 to 1968.

Keweenaw Peninsula native copper occurrences have been mentioned as a qualitative source of information to support the use of copper as part of nuclear waste canisters. However, data on natural corrosion of native copper for geological disposal process-based safety assessments is lacking. In Phase I of the MICA Project, the combination of geologic setting and geologic and environment history was used to group natural native copper occurrences into several different potential analogues. For each potential analogue, the geologic history, environmental condition, length of exposure, and uncertainties and assumptions are presented based on existing data. The feasibility of obtaining sufficient representative or new samples with a reasonably high potential for being exposed to water have been assessed for each analogue. Water is an essential component to initiate corrosion of native copper as illustrated by native copper inclusions encased in calcite and other minerals which do not show visible corrosion. Availability of supportive information such as estimates of water composition is also evaluated. All these data have been reviewed against disposal concepts and degradation processes. While all the analogues have the potential to provide insight into corrosion of copper, some of the analogues are ranked to have higher potential than others. Native copper encased in bedrock or minerals with limited to no exposure to waters provides a baseline analogue or background level of corrosion. A few of the corrosion analogues identified as the most promising and relevant are:

1. Bedrock native copper with long and varied history – Cumulative corrosion under different probable conditions over time frames of up to 100s of millions of years and more and at depths up to 2 km.
2. Cumulative corrosion observed in subaqueous Lake Superior native copper gravel and in native copper in glacial deposited sediments.
3. Copper in clay – Bedrock native copper formed in situ in hydrothermal fracture-filling clay.
4. Copper exposed to copper sulfides – bedrock native copper effected by sulfur-bearing waters and native copper in contact with sulfide minerals.

The results from Phase I of the MICA Project provide a context and a starting point to further investigate the corrosion of native copper samples during Phase II.

Keywords: radioactive waste, nuclear waste, final deposition, copper, natural analogs, Keweenaw Peninsula, Michigan, USA

Ismo Aaltonen, Xuan Liu, Heini Reijonen and Timo Ruskeeniemi
Geological Survey of Finland
P.O. Box 96
FI-02151 Espoo, Finland

E-mail: ismo.aaltonen@gtk.fi, xuan.liu@gtk.fi, heini.reijonen@gtk.fi, timo.ruskeeniemi@gtk.fi

Theodore J. Bornhorst
Department of Geological and Mining Engineering and Sciences
Michigan Technological University
Houghton
Michigan, USA

Aaltonen, I., Bornhorst, T. J., Liu, X., Reijonen, H. & Ruskeeniemi, T. 2023. Michigan International Copper Analogue (MICA) project – Phase I. *Geologian tutkimuskeskus, Tutkimustyöraportti 22/2023*, 42 sivua, 6 kuvaa, 7 taulukkoa ja 3 liitettä.

Pitkän aikavälin ennusteet teknisten vapautumisesteiden materiaaleista perustuvat yleensä mekanistiseen tietoon niihin vaikuttavista rappeutumisprosesseista sekä in situ -koejärjestelyihin ja mallinnukseen. Kuparikapselin kannalta oleellisten kehityskulkujen ymmärtämiseksi voidaan käyttää lisäksi analogiatutkimuksia. Kupari on tärkeä komponentti useissa loppusijoituskonsepteissa, kuten Ruotsissa ja Suomessa kehitetyssä KBS-3:ssa ja Kanadassa kehitetyssä Mark II:ssa.

MICA-projektissa keskitytään kuparin yleisen stabiiliuden tutkimukseen Keweenawin niemimaalla Yhdysvaltojen Michiganissa sijaitsevien maailman suurimpien natiivikupari-esiintymien avulla. Korkea-aktiivisen ydinjätteen syvän geologisen loppusijoituksen tärkeimpiä edellytyksiä on arvioida sen pitkäaikainen toimintakyky ja osoittaa turvallisuus miljoonaksi vuodeksi. Geologisista ympäristöistä saatuja tietoja (luonnonanalogioita) voidaan hyödyntää turvallisuusperustelussa, ja joissain tapauksissa ne tarjoavat tietoa paljon pidemmältäkin ajanjaksoilta kuin miljoona vuotta. Sekä luonnollisia että arkeologisia analogiatutkimuksia on esitetty kirjallisuudessa, mutta vain harvoissa tutkimuksissa on keskitytty kuparin stabiiliuteen sen luonnollisessa ympäristössä. MICA-projektin tavoitteena on tarjota ainutlaatuista täydentävää tietoa kuvaamaan pitkäaikaisen korroosion prosesseja puhtaasta kuparista tehdyissä loppusijoituskapseleissa ja siten tukea loppusijoituksen turvallisuutta sekä keskustelua sidosryhmien kanssa.

Keweenawin niemimaan kuparialue sijaitsee noin 1,1 miljardin vuoden ikäisen Pohjois-Amerikan hautavajoaman (Midcontinent Rift, MCR) alueella. Esiintymät muodostuivat metamorfogeenisten hydrotermisten fluidien mineralisoidessa metallista kuparia isäntäkiven huokostilavuuksiin 1,04–1,07 miljardia vuotta sitten. Myöhemmät erosionaaliset vaiheet ovat tuoneet kupariesiintymät maanpinnalle. Keweenawin esiintymiä louhittiin kaupallisesti vuosina 1845–1968.

Keweenawin natiivikupariesiintymät on mainittu kvalitatiivisena tietolähteenä liittyen kuparin käyttöön osana loppusijoituskapselia. Geologisen loppusijoituksen turvallisuusarvioinnissa tarvittavaa tietoa natiivikuparin luonnollisesta korroosiosta ei kuitenkaan ole saatavilla. Alueen geologisen historian ja ympäristön tuntemusta käytettiin MICA-projektin ensimmäisessä vaiheessa natiivikupariesiintymien ryhmittelyyn useisiin potentiaalsiin luonnonanalogiatyyppeihin. Jokaisesta mahdollisesta analogiasta esitetään geologinen historia, ympäristöolosuhteet, altistumisen kesto, epävarmuudet ja oletukset olemassa olevan tiedon perusteella. Jokaisesta analogiasta on arvioitu riittävän edustavien tai uusien näytteiden saatavuus korroosioaltistumisen varmistamiseksi. Vesi on tärkeä tekijä natiivikuparin korroosion käynnistymisessä, kuten havaitaan kalsiitin ja muiden mineraalien ympäröimissä natiivikupari-inkluusioissa, joissa ei havaita näkyvää korroosiota. Tukevien tietojen saatavuutta esimerkiksi veden koostumuksessa on myös arvioitu. Kaikkia näitä tietoja on tarkasteltu loppusijoituskonseptien ja rappeutumisprosessien kannalta. Vaikka kaikilla analogioilla on potentiaalia tarjota tietoa kuparin korroosiosta, jotkin niistä ovat muita lupaavampia. Muiden kivilajien tai mineraalien sisällä sulkeumana oleva natiivikupari, joka ei ole ollut kosketuksissa veden kanssa, voi tarjota tietoa kuparin lähtötilanteesta ja toimia korroosioprosessien vertailukohtana. Muutamia olennaisimmista korroosioanalogoista ovat seuraavat:

1. Kallioperän kupari, jolla on pitkä ja monivaiheinen historia – kumulatiivista korroosiota monissa erilaisissa olosuhteissa satojen miljoonien vuosien aikana ja jopa 2 km:n syvyydelle asti.
2. Yläjärven subakvaattisessa natiivikuparisorassa ja glasiaalisedimenteissä havaittavan natiivikuparin kumulatiivinen korroosio.
3. Saven ympäröimä kupari – kallioperän kupari, jota tavataan hydrotermisten savien yhteydessä siirrostäyhteissä.
4. Kupari- ja kuparisulfidisysteemit – kallioperän kupari, johon ovat vaikuttaneet rikki-pitoiset vedet, sekä sulfidimineraalien kanssa kosketuksissa oleva kupari.

MICA-projektin ensimmäinen vaihe tarjoaa taustan ja lähtökohdan kallioperän natiivikuparin korroosiotutkimukselle projektin toisessa vaiheessa.

Asiasanat: radioaktiiviset jätteet, ydinjätteet, loppusijoitus, kupari, luonnonanalogiat, Keweenawin niemimaa, Michigan, USA

Ismo Aaltonen, Xuan Liu, Heini Reijonen ja Timo Ruskeeniemi
Geologian tutkimuskeskus
PL 96
02151 Espoo

Sähköposti: ismo.aaltonen@gtk.fi, xuan.liu@gtk.fi, heini.reijonen@gtk.fi, timo.ruskeeniemi@gtk.fi

Theodore J. Bornhorst
Department of Geological and Mining Engineering and Sciences
Michigan Technological University
Houghton
Michigan, USA

CONTENTS

GLOSSARY	8
1 INTRODUCTION	9
2 SAFETY CASE FRAMEWORK	10
2.1 Disposal concepts	10
2.1.1 Radioactive waste disposal options in general	10
2.1.2 Concepts with copper as part of the engineered barrier system	11
2.1.3 Copper composition in repository designs	13
2.2 Important aspects regarding copper stability considerations in safety cases	13
2.3 Nuclear Energy Agency (NEA) Features, Events and Processes (FEP) database	14
3 BACKGROUND	15
3.1 Geologic setting of native copper	15
3.1.1 Primary (magmatic) native copper	16
3.1.2 Primary (hydrothermal) native copper	16
3.1.3 Secondary native copper	17
3.1.4 Secondary supergene native copper	17
3.2 Natural analogue studies on copper	17
3.2.1 Hyrkkölä – native copper in fractured crystalline rock (Finland)	17
3.2.2 Littleham Cove – native copper in Permian mudstone formation (UK)	18
3.2.3 NWMO copper analogue review	18
4 KEWEENAW GEOLOGY	19
4.1 The Midcontinent Rift	19
4.2 Geological setting of the Keweenaw native copper mining district	20
4.3 Younger geological evolution	21
4.4 Composition of native copper	21
5 THE GEOLOGIC CONTEXT AND SEQUENCE OF EVENTS	22
5.1 Keweenaw Peninsula bedrock native copper	22
5.1.1 Generation of Main-Stage Hydrothermal Fluids	22
5.1.2 Conditions of Hydrothermal Precipitation of Native Copper	22
5.1.3 Spatial Setting of Keweenaw Peninsula bedrock native copper	23
5.2 Native Copper at the White Pine Mine	23
5.2.1 Spatial Setting	23
5.3 Float copper masses	23
5.3.1 Spatial Setting	24
5.3.2 Glacial Event Uncertainty	24
5.4 Lake copper	24
5.4.1 Lake copper formations	24
5.4.2 Spatial Setting	25

5.5	Chisel chips of native copper	25
5.5.1	Spatial Setting	26
5.6	Mining and post-mining processes	26
5.7	Generalized sequence of events.....	26
6	POTENTIAL NATURAL ANALOGUES AND AVAILABILITY OF RESEARCH MATERIALS.....	31
6.1	Analogue Type A. Long and Varied History of Keweenaw Peninsula Bedrock Native Copper in the Subsurface.....	31
6.2	Analogue Type B. Keweenaw Peninsula Deep Bedrock Native Copper – Long and Varied Native Copper History, likely less exposed to oxic conditions	32
6.3	Analogue Type C. White Pine Mine Bedrock Native Copper – Long and Varied Native Copper History, likely less exposed to oxic conditions.....	32
6.4	Analogue Type D. Keweenaw Peninsula Shallow Bedrock Native Copper – Long and Varied Native Copper History, likely more exposed to oxic conditions	32
6.5	Analogue Type E. Lake Superior Shallow Bedrock Native Copper.....	33
6.6	Analogue Type F. Keweenaw Peninsula Bedrock Native Copper Exposed to Supergene Weathering	33
6.7	Analogue Type G. Keweenaw Peninsula Bedrock Native Copper Exposed to Hydrothermal Sulfur.....	34
6.8	Analogue Type H. White Pine Mine – Bedrock Native Copper in contact with sulfide minerals	34
6.9	Analogue Type I. Lake Superior Shallow Native Copper with Glaciated Surface (Great Sand Bay lake copper)	34
6.10	Analogue Type J. Lake Superior Native Copper Gravel (Great Sand Bay lake copper nuggets)	34
6.11	Analogue Type K. Glacial Native Copper (“Float Copper”)	35
6.12	Analogue Type L. Native Copper Chisel Chips.....	35
6.13	Native copper in clay (Type M)	35
6.14	Other Analogues related to human activity	35
7	ANALYTICAL METHODS UNDER CONSIDERATION FOR PHASE II	36
7.1	Metallurgical properties	36
7.2	Supporting geological investigations related to copper samples.....	36
8	DISCUSSION AND RECOMMENDATIONS	37
9	CONCLUSIONS	38
	REFERENCES	39
	APPENDICES.....	43

GLOSSARY

AAS	Atomic Absorption Spectroscopy
APT	Atom Probe Tomography
BC	Before Christ
BGE	Federal Company for Radioactive Waste Disposal (WMO in Germany)
B.P.	Before Present
CANDU	Canada Deuterium Uranium (Canadian pressurized heavy-water reactor design)
DSDP	Deep Sea Drilling Project
EBS	Engineered Barrier System
EPMA	Electron Probe MicroAnalysis
FEP	Features, Events, Processes
FI	Fluid Inclusion
GTK	Geological survey of Finland
HLW	High Level Waste
IAEA	International Atomic Energy Agency
ICP-OES	Inductively-Coupled Plasma Optical Emission Spectroscopy
INAA	Instrumental Neutron Activation Analysis
KBS-3	Swedish repository concept developed to dispose spent nuclear fuel
KBS-3V	Variant of KBS-3 where vertical disposal holes are used to dispose waste packages
LA-ICP-MS	Laser Ablation Inductively Coupled Plasma Mass Spectrometry
LIP	Large Igneous Province
Mark II	NWMO repository concept
MCR	(North American) MidContinent Rift
Micro-XCT	Micro X-ray Computed Tomography
Micro-XRF	Micro X-Ray Fluorescence
NAGRA	National Cooperative for the Disposal of Radioactive Waste (WMO in Switzerland)
NEA	Nuclear Energy Agency
NWMO	Nuclear Waste Management Organization (WMO in Canada)
NWS	Nuclear Waste Services (WMO in UK, see also RWM)
ODP	Ocean Drilling Program
PLV	Portage Lake Volcanics
RWM	Radioactive Waste Management (see also NWS)
SEM-EDS	Scanning Electron Microscopy analysis - Energy Dispersive Spectroscopy
SKB	Swedish Nuclear Fuel and Waste Management Co. (WMO in Sweden)
SRB	Sulfate Reducing Bacteria
TDS	Total Dissolved Solids
UFC	Used Fuel Container
VSHE	Volts vs. Standard Hydrogen Electrode
WMO	Waste Management Organization
XRD	X-Ray Diffraction
XRF	X-Ray Fluorescence

1 INTRODUCTION

Long-term metallic copper stability is of interest in assessing long-term performance of high-level radioactive waste repositories (e.g., Hall et al. 2021). Metallic copper is an important part of many disposal concepts, e.g., KBS-3 used in Sweden and Finland (SKB 2010a) and Mark II used in Canada (Boyle & Meguid 2015). One of the key parts for the high-level nuclear waste (HLW) disposal is the assessment of long-term performance of the engineered canister encasing the waste. Assessment of performance of the copper waste packages has been mainly conducted with extrapolation of short-term investigation data, and via mass balance and mass transport calculations.

Studying natural analogues over geological time scales can be an important way of obtaining a better understanding of long-term safety (e.g., IAEA 1989, Miller et al. 2000). In this report, natural metallic copper deposits are referred to as ‘native’. Natural analogues for native copper have been extensively used in safety cases, but mainly at a qualitative level (Alexander et al. 2015, Reijonen et al. 2015). A generally accepted definition for natural analogues comes from Côme and Chapman (1987): “... an occurrence of materials or processes which resemble those expected in a proposed geological waste repository”. This has been further defined by IAEA (1999): “Natural analogues can include both natural and human-made materials provided the processes that affect them are natural. Thus, studies of archaeological and historical artefacts, ancient buildings, anthropogenic sources of radionuclides such as nuclear weapons fallout, and examples of pathways in plants and animals can be regarded as natural analogue studies.”

The Keweenaw Peninsula in Michigan provides a wealth of occurrences of natural native copper subjected to several different environmental histories (see Fig. 1). Geological samples have been studied for decades (mainly regarding ore formation and local/regional geology). The use of copper in the area dates back thousands of years in the cultures of indigenous peoples. In addition to geological and archaeological samples, historical artefacts of native copper from the area are available for study. Of the sample types mentioned above, archaeological samples are not the scope of project Phase I work.

The potential corrosion of metallic copper in the underground repositories is primarily driven by the composition of water in contact with the copper canisters used to contain the nuclear waste and to a lesser degree by contact with air prior to saturation with water. The natural metallic copper of the Keweenaw Peninsula site has been exposed to a variety of compositions of water over short to long periods of time applicable to disposal relevant time scales (from 100s to millions of years).

The objective of MICA Project Phase I is to systematically collect and review the existing literature and data on the environmental setting of metallic copper occurrences of Keweenaw Peninsula and availability of samples for study in collaboration with local experts. In addition, Phase I, includes testing analytical methods to study metallic copper samples and develop methodologies to describe the properties of unaltered samples as well as the corrosion and/or alteration phenomena.

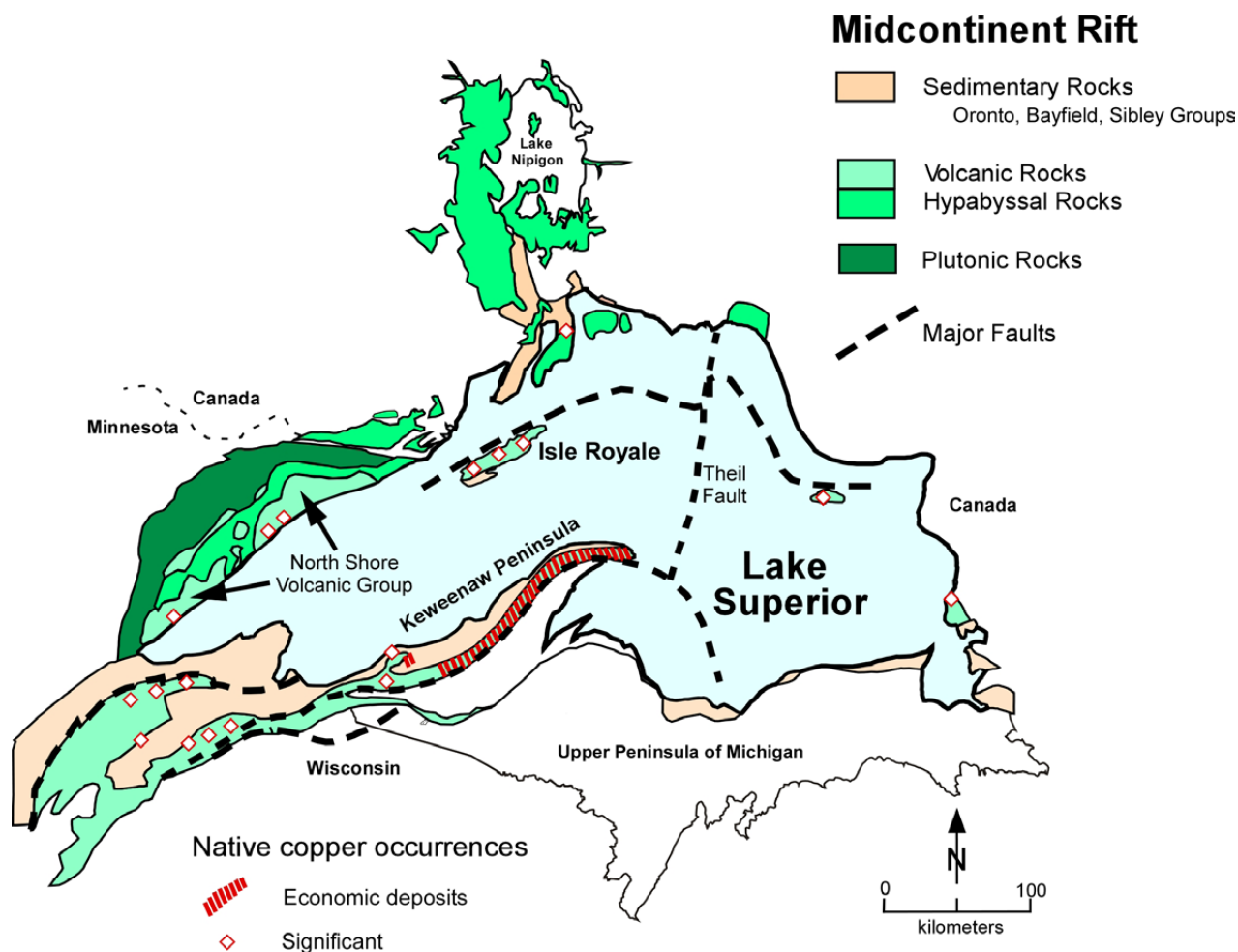


Fig. 1 Geologic setting of the Mesoproterozoic Midcontinent Rift showing area of economic native copper deposits in the Keweenaw Peninsula and occurrences of native copper in exposed rocks of the Midcontinent Rift. Figure modified from Bodden et al. (2022).

2 SAFETY CASE FRAMEWORK

2.1 Disposal concepts

2.1.1 Radioactive waste disposal options in general

Commonly accepted disposal options are based on either near-surface or deep geological concepts. Near-surface options are implemented with or without an engineered barrier system with disposal at ground level and/or underground several tens of meters below ground level. These shallow disposal facilities are strongly affected by long-term changes in the surface environment and are therefore, typically used only for low-level radioactive waste disposal consisting of short-lived radioactive isotopes (e.g., World Nuclear Association 2020).

Deep geological concepts, needed for high level waste (HLW) disposal, are based on isolation pro-

vided by a combination of natural and engineered barriers (multi-barrier concept), and typically planned to be passive, i.e., without need to maintain the facility after the closure. These concepts can be divided into deep boreholes and mined repositories. Deep borehole disposal has been considered as an option for geological isolation but has been abandoned in many countries due to economic considerations and insufficient knowledge and technology. The most commonly planned deep geological disposal concept is for a mined repository comprising tunnels into which packaged waste would be placed (e.g., World Nuclear Association 2020).

All mined repository concepts selected or under development for deep geological disposal of HLW

are based on a series of engineered barriers combined with the natural barrier of the host rock for the repository (e.g., NEA 2000). The engineered barrier system (EBS) can include, for instance, spent nuclear fuel packed into a metal container surrounded by compacted bentonite. The EBS is designed to contain the radionuclides, retain them, and retard their dispersion into the environment. The natural barrier provides a favorable and stable environment for the EBS and isolates the repository from the surface environment (e.g., Boyle & Meguid 2015, Posiva SKB 2017).

2.1.2 Concepts with copper as part of the engineered barrier system

The Swedish Nuclear Fuel and Waste Management Co. (SKB) is planning to construct a repository for spent nuclear fuel at the Forsmark site in Östhammar Municipality, Sweden. In their KBS-3

concept, spent fuel is placed in corrosion-resistant copper canisters with a cast iron insert providing mechanical strength. The sealed copper canisters will be placed in tunnels approximately 500 meters deep in the bedrock and embedded in bentonite. The bentonite protects the canisters from minor rock movements and limits the inflow of the groundwater. The host rock provides a stable environment for the canisters and the bentonite (Fig. 2; SKB 2010a, 2011). The primary option for implementing the KBS-3 concept is use of vertical placement of the canisters (KBS-3V, Fig. 2). Also, Posiva in Finland has selected the KBS-3 method for final disposal. Posiva and SKB have been jointly formulating the long-term safety principles guiding the design and production of a KBS-3 repository (Posiva SKB 2017). Posiva has already submitted the application for the operating license based on this concept to the Finnish authorities on December 2021.

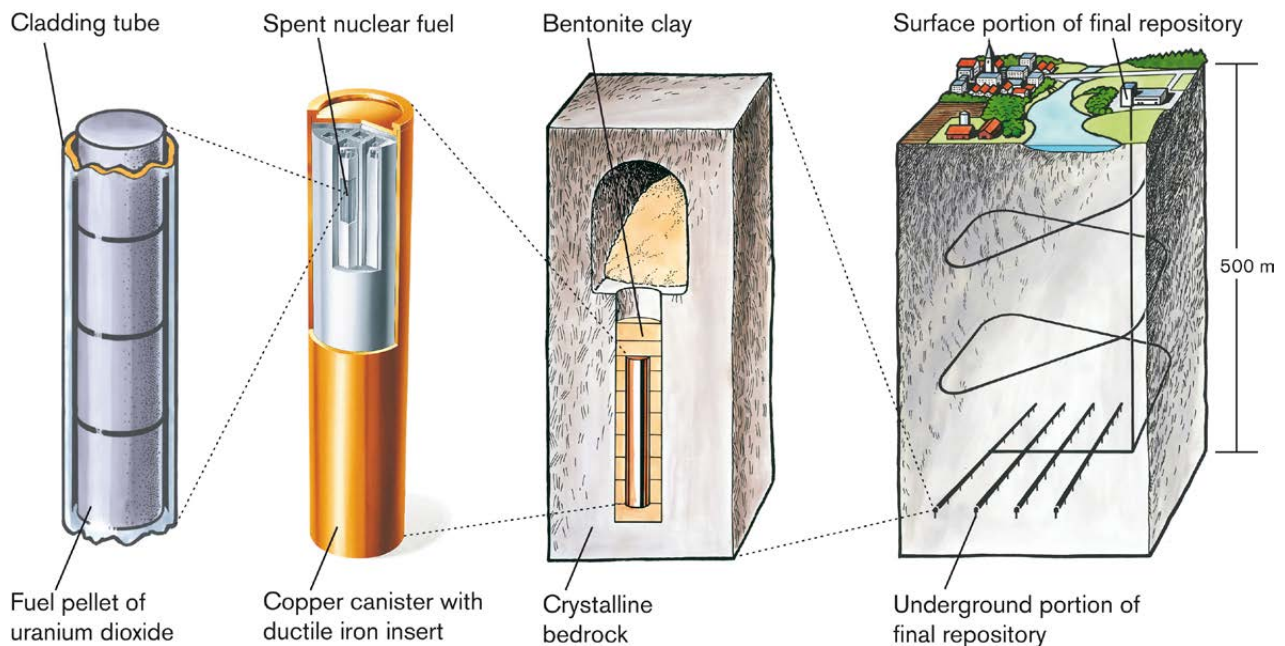


Fig. 2. SKB's KBS-3 concept (SKB 2010a).

Based on Nuclear Waste Services (NWS; former Radioactive Waste Management Ltd.) the requirements for geological disposal consist of isolation and containment of the high-level radioactive waste; confidence in long-term safety; and low probability of future generations unintentionally intruding into the disposal facility. The Engineered Barrier System (EBS) needs to be physically and chemically compatible with the geological envi-

ronment. RWM (2016) is considering three different host rock types: higher strength rock, lower strength sedimentary rock, and evaporite rock. In case of higher strength rock (igneous or metamorphic), NWS considers using a sealed canister fabricated from copper, with a cast iron insert (Fig. 3; RWM 2016).

In Canada, due to specific reactor technology (CANDU), the fuel bundles and therefore spent

nuclear fuel containers (UFC) are smaller than, for example, in the KBS-3 concept. However, the Canadian disposal concept relies more on the EBS system than the KBS-3 concept. The Nuclear Waste Management Organization (NWMO), Canada, has designed a method based on a smaller sized can-

ister consisting of standard pressure vessel grade steel for structural containment and a copper coating applied to its surface for corrosion protection termed the Mark II concept (Fig. 4; Boyle & Meguid 2015).

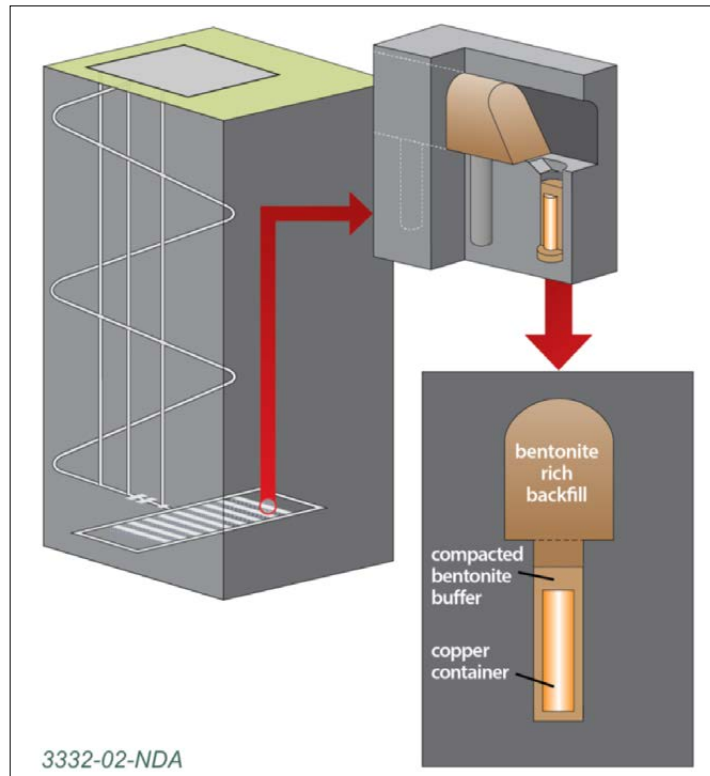


Fig. 3. Schematic of illustrative disposal concept for high heat generating waste. Disposal in higher strength rock. (RWM 2016).

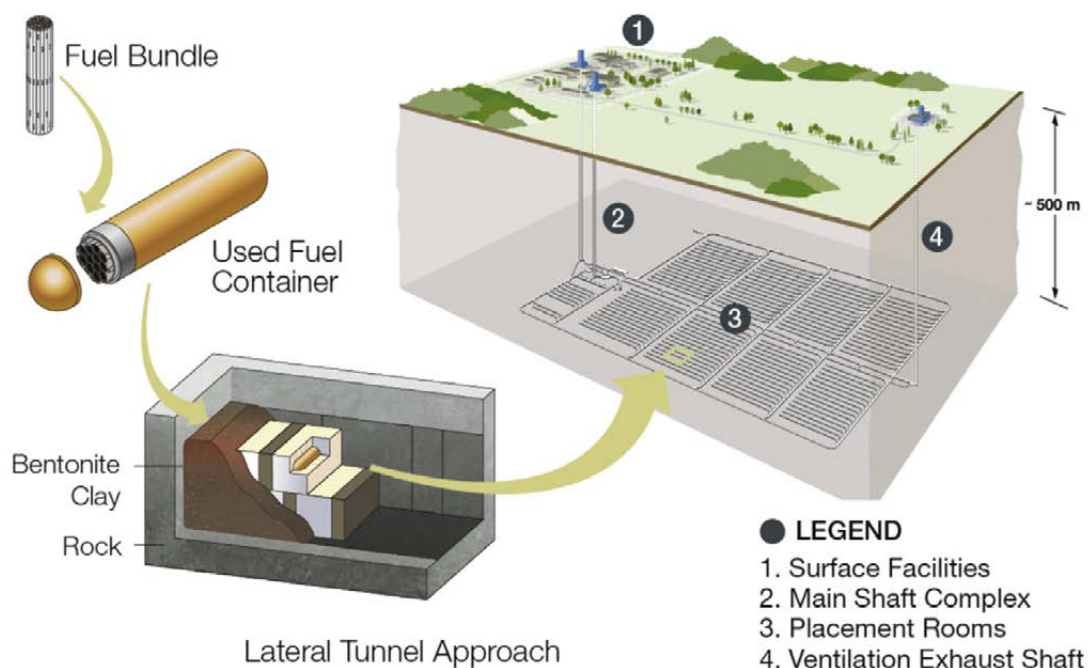


Fig. 4. NWMO's Mark II concept (Boyle & Meguid 2015).

National Cooperative for the Disposal of Radioactive Waste (NAGRA), Switzerland, is developing design concepts of canisters for the deep geological disposal of HLW. The high-level waste canister is an integral part of the multi-barrier system. A wide range of designs and materials has been considered for the canister, including a steel canister or canister with corrosion resistant coating. Feasibility of candidate canister designs have been recently assessed by Diomidis et al. (2017) by considering e.g., mechanical integrity, environmental damage, and potential impact on the geological barrier. A canister concept based of a thick-walled forged carbon steel substrate coated with copper, was favorably assessed.

In addition to canister material, copper is considered as a potential material to be used in some of the borehole sealing concepts as well (e.g., Jackson et al. 2014), where the disposal is closer to the land surface and therefore likely subjected to a wider range of hydrogeochemical conditions than those expected for deeper disposal.

2.1.3 Copper composition in repository designs

The copper used in canister designs is carefully tested to fulfil the design specifications. As examples, SKB's specification for the copper composition and preliminary specification for NWMO's copper coating are presented in Table 1 and Table 2 below.

Table 1. Material specifications for copper canisters (SKB 2010b). All elements specified in wt-ppm except copper content in wt.%.

Cu %	P	O	S	H	Ag	As	Bi	Cd	Fe	Mn	Ni	Pb	Sb	Se	Sn	Te	Zn
≥99.99	30–100	<5	<8	<0.6	<25	<5	<1	<1	<10	<0.5	<10	<5	<4	<3	<2	<2	<1

Table 2. Preliminary material specifications for copper coating (Mehran Behazin, NWMO, personal communication, February 28th, 2023). All elements specified in wt.ppm except copper content in wt.%.

Cu %	P	O	S	H	C
>99.9	<100	<400	<100	<10	<50

2.2 Important aspects regarding copper stability considerations in safety cases

Copper integrity described in long-term safety assessments by SKB, Posiva and NWMO are relevant to the MICA project goals. The state-of-the-art for safety cases has been presented in dedicated reports of the WMOs (e.g., Posiva 2021a,b). The WMOs' work over decades has identified possible substances with potential to cause copper corrosion in the repository at some stage of the future evolution (assessment time frame is 1 Ma) of the system (e.g., King et al. 2001, 2012), which have been considered in requirements set for repository designs (e.g., POSIVA SKB 2017). Below, the most important findings on corrosion substances relevant to MICA are briefly listed:

1. Sulfide is the most important cause of corrosion of copper canisters in the repository.
 - a. Sulfide (HS⁻) can be present in the groundwater, but its concentration is highly site specific. Expected (and observed by groundwater sampling) sulfide concentrations in the Swedish and Finnish repository sites

at Forsmark and Olkiluoto are quite low, at Forsmark mostly < 0.4 mg/L (Tullborg et al. 2010) and in Olkiluoto 0–3.0 mg/L (Posiva 2021c). However, it is known that during the transient conditions in the groundwater system, i.e., during operation of an underground repository, the sulfide levels may locally be higher due to microbial sulfate reduction (SRB) processes. Sulfide can also be locally produced from sulfate (SO₄) by microbial activity, in the buffer and backfill, but the activity is suppressed in compacted bentonite.

- b. For MICA, the aim is to seek, whether we could find evidence of copper stability in environments where dissolved sulfide has existed in connection with native copper. The presence of sulfur-bearing minerals or hydrothermal fluids in contact with native copper could provide new insight for safety case assumptions. Potentially, also samples

where copper has been subjected to alternating conditions (regarding presence of sulfide and oxygen, see below) would be of interest.

2. Oxygen is another corrodent to copper, but its availability is limited in the SKB and Posiva repository systems to early phases after closing the underground openings (Posiva SKB 2017).
 - a. Additional oxygen could be introduced into the disposal unit by the unlikely case of infiltration of oxygen rich groundwaters, e.g., in connection with melting of future glaciers.
 - b. For MICA, exposure to oxygen needs to be considered in selecting the samples for studies since some of the samples may represent very extreme cases for corrosion from the safety case point of view, and thus their relevance as analogues may be of little value.
3. Salinity as such is not considered an issue for copper performance, as in general Cl⁻ inhibits passivation and localized corrosion of the copper (e.g., King et al. 2012). This is beneficial from the safety case point of view as uniform corrosion of copper can be tolerated in the system, while pitting corrosion causes more significant impact to integrity of the copper canisters.
 - a. Both SKB and Posiva have evaluated higher salinities than currently observed at the repository sites when assessing the copper stability in the long-term. For Olkiluoto up to 5 mol/kg have been considered in the

modeling (4 times higher than the Olkiluoto bounding brine composition). This high salinity does not affect copper stability (King et al. 2021), even though some uncertainties in the modeling results are reported, involving the higher salinities.

- b. At Olkiluoto salinity is rarely higher than 100 g/L (TDS) (Posiva 2021c). At Forsmark salinity is even lower (SKB 2008). However, at Bruce site in Canada (NWMO 2011), TDS can be above 300 g/L. Thus, for NWMO and NWS (who have not selected the site yet) higher salinities in the host rocks could be of higher significance than for SKB/Posiva, depending on the site selected. Salinity is considered as potential issue for copper corrosion in conditions where the main corroding agents oxygen and sulfur are absent. Cl affects the copper equilibrium in the system and hence can facilitate corrosion. See Lilja et al. (2020) for a thorough discussion.
- c. Overall, for MICA, a large salinity range is relevant to repository concepts considered here and should be assessed for its effect on copper stability.

While the above (points 1–3) considers conditions identified in safety cases most affecting corrosion of the copper canisters, also other aspects can be of relevance to the safety case. These are discussed in terms of process understanding and they are further elaborated in the section below.

2.3 Nuclear Energy Agency (NEA) Features, Events and Processes (FEP) database

An overview on the processes relevant to copper stability in international geological disposal concepts can be found for example by looking at Nuclear Energy Agency (NEA) Features, Events and Processes (FEP) database 3.0 (NEA 2019). In this report, a short overview is provided in Table 3 on the FEPs of potential significance in the MICA

project. The objective of listing these FEPs here is because the focus of Phase II will be set on safety case relevant processes. NEA FEP database provides a high-level starting point for processes of interest and more specific processes may need to be accounted for in future phases of MICA.

Table 3. NEA FEPs relevant to copper waste packages and the potential significance for MICA project objectives.

FEPs (NEA 2019)	Context	Processes of relevance to MICA	MICA input for process understanding
2.3.3	Mechanical processes [waste package]	Deformation Material volume changes Stress corrosion cracking Mechanical processes may operate over time periods that are very short compared to the assessment period (e.g., loading caused by seismic shearing) or over time periods that are very long compared with the assessment period (e.g., loading by creep of the surrounding geosphere)	MICA project can potentially provide some textural information (e.g. evidence of shearing, grain size) on the massive native copper that can be of use for comparing mechanical properties of the native copper in comparison to copper in the waste packages. Stress corrosion cracking is related to geochemical conditions (availability of nitrite, ammonium and acetate). Less likely to find relevant sites within MICA.
2.3.4	Chemical processes [waste package]	Evolution of pH conditions Evolution of redox conditions Corrosion Alteration Precipitation Complexation Colloid formation Chemical processes acting within and/or upon a waste package may alter the chemical and/or physical forms of the waste package components.	In MICA project scope, most of the mentioned processes are of relevance when investigating natural occurrences of native copper and compilation of understanding of the past and current conditions that affect the copper stability.
2.3.5	Biological processes [waste package]	Microbial growth and decline Microbially/biologically mediated processes Biological/biochemical processes may affect the characteristics of engineered components, and potentially their performance. For example, microbes may influence corrosion of metals ('microbially-influenced corrosion')	In MICA project, the potential influence of microbial processes needs to be considered when assessing potential sources of corroding agents.

3 BACKGROUND

3.1 Geologic setting of native copper

Gold, silver, and meteoric iron were probably the first metals to be worked into tools and other artefacts, but native copper was the first to be used in significant ways (e.g., Murr 2015, Mindat.org 2021). Native copper was first used approximately 10000 years ago by Neolithic humans at least in the Middle East and North America (Martin 1993, Murr 2015, Britannica 2020, Pompeani et al. 2021, Bebbler & Key 2022). Smelting of native copper from the ore and casting in molds was the beginning of the metallurgy in Mesopotamia c. 6000 years B.P. (Murr 2015, Britannica 2020). Approximately 5500 years ago, metallic copper was first produced from other than native copper ores. Copper was alloyed with tin to make bronze (Murr 2015). Availability, quality,

and price of copper have been important issues for people for a long time (e.g., Nanni 1750 BC).

Native copper occurs in a wide variety of geological environments (Cornwall 1956, Marcos 1989, Ikehata et al. 2016) that include basaltic lavas and interbedded sedimentary rocks; intrusive rocks, typically mafic and ultramafic; clastic sediments; oxidized copper ores, and modern swamps and lakes.

Deposits dominated by native copper are rare because reduced sulfur-poor hydrothermal systems are uncommon (Wang et al. 2006). Based on several studies, for example Ikehata et al. (2016) and Marcos (1989), the origin of native copper can be divided into four generalized types:

1. primary (magmatic) native copper crystallizing contemporaneously with silicate minerals from:
 - a. mafic magma (e.g., Ikehata et al. 2016, Hofmeister & Rossman 1985, Zhang et al. 2006, Ikehata & Hirata 2012);
 - b. pegmatite (e.g., Räisänen 1986, Marcos 1989, Marcos & Ahonen 1999);
2. primary (hydrothermal) native copper precipitated from hydrothermal fluids hosted by:
 - a. ancient oceanic pillow basalt (spilite) (e.g., Nagle et al. 1973);
 - b. continental flood basalt (e.g., Stoiber & Davidson 1959, Bornhorst et al. 1988, Białowolska et al. 2002, Emetz et al. 2005, Zhu et al. 2007, Pinto et al. 2010, Zhang et al. 2013), and
 - c. ocean island alkali basalt (Ikehata et al. 2016).
3. secondary native copper from serpentinization of copper sulfide minerals in mafic or ultramafic rocks (e.g., Ikehata et al. 2016, Lorand 1987) resulting in native copper, copper sulfide minerals, and/or awaruite (alloy of nickel and iron);
4. secondary supergene native copper resulting from galvanic reactions of pre-existing metallic sulfides and metals in a media of percolating groundwater, such as in the Malankhand porphyry deposit (e.g., Ikehata et al. 2016, Sikka et al. 1991);

In addition, native copper, of unknown origin, has been observed and documented by the Deep Sea Drilling Project (DSDP) and Ocean Drilling Program (ODP) in oceanic sediments covering the igneous basement, and in the basement rocks themselves (e.g., Hekinian 1974, LeHuray 1989).

Selected examples of native copper occurrences are presented in the sections below.

3.1.1 Primary (magmatic) native copper

Copper-rich sulfide minerals and native copper in plagioclase lherzolite, spinel lherzolite, and harzburgite are reported in the Horoman peridotite complex, Hokkaido, Japan. It is suggested that copper and the copper sulfides are primary, and not related to low-temperature processes such as serpentinization (e.g., Kitakaze 1998, Ikehata & Hirata 2012, Kitakaze et al. 2011).

Native copper grains are observed from a picrite lava of the Emeishan Large Igneous Province in

the Lijiang area, SW China (Zhang et al. 2006). The native copper fits into the mineral paragenetic sequence which suggests that the primary magmas were S-unsaturated. Native gold and native copper grains are xenocrysts from the mantle, transported to shallow depths, and captured by the picritic melts (Zhang et al. 2006).

Native copper is hosted in granite pegmatite at Hyrkkölä, Finland. This native copper is connected to the late stages of the Svecokarelian orogenic events approximately 1.8–1.7 Ga ago (Räisänen 1986, Marcos 1989, Marcos & Ahonen 1999, Räisänen 1989). The pegmatites are 0.05–0.5 m thick foliation-parallel veins hosted in amphibolite and quartz-feldspar gneisses. Native copper occurs as thin flakes in and between feldspar grains and around tourmaline grains (Marcos & Ahonen 1999).

Other primary occurrences include a Miocene basaltic lava flow in Lake County, Oregon, U.S. (Hofmeister & Rossman 1985) and Lesnaya Varaka ultramafic alkaline complex in the Kola Peninsula, NW Russia (Barkov et al. 1998).

3.1.2 Primary (hydrothermal) native copper

The volcanic rocks that fill the Midcontinent rift system host widespread and locally abundant native copper in the Keweenaw Peninsula native copper district, Michigan, U.S. (Bornhorst & Lankton 2009). Native copper is mainly hosted by the Portage Lake Volcanics (PLV) and occurs in brecciated and amygdaloidal flow tops, interflow conglomerate beds, and cross cutting vein systems (e.g., Houghton 1841, Lane 1911, Butler & Burbank 1929, White 1968, Bornhorst et al. 1988, Mauk et al. 1992, Bornhorst & Lankton 2009). In addition to PLV, the rift-filling sedimentary units host native copper especially in the far western Upper Peninsula southwest of the main native copper district (White 1968, Mauk et al. 1992, Bornhorst & Lankton 2009). Please also refer to Section 4.2 for more details.

Bell et al. (2020) defined the Kiffaannngissuseq metallogenic province in NE Greenland and described a basalt-hosted native copper formation related to a 1250 Ma orogenic event. A significant amount of native copper occurs in aphyric basalts of the Zig-Zag Formation as part of a mineral assemblage of prehnite, quartz, and calcite (Bevins et al. 1991). Bell et al. (2020) reported many similarities between Zig-Zag Formation of Kiffaannngissuseq and PLV of Keweenaw Peninsula. Both are associated with low-grade metamorphic minerals and

host native copper in void spaces within basalt lava flows.

Other hydrothermal native copper occurrences include Vista Alegre district in Paraná basaltic province, southern Brazil (Pinto et al. 2011); Mineoka belt of Boso Peninsula, central Japan (Ikehata et al. 2016); some of the Chilean manto-type deposits (Muñoz 1975, Kojima et al. 2009); Darhand and Mejdard deposits in the Orumieh–Dokhtar magmatic belt in Iran (Nezafati et al. 2005, Akbarpour et al. 2012, Alireza et al. 2019).

3.1.3 Secondary native copper

The layered Muskox Intrusion in Nunavut, Canada is reported to contain native copper mineralization as well as awaruite, wairauite, and native iron (Chamberlain et al. 1965). Mineral distributions and textures indicate that the native metals formed in situ during the serpentinization of the host dunites and related rocks. Conditions during the alteration are interpreted to be more reducing in the central and lower parts of the layered series because the native metals are abundant in the central regions and are lacking in other parts. This suggests that reducing conditions were generated internally and

possibly because of serpentinization (Chamberlain et al. 1965).

Other secondary native copper occurrences include Table Mountain and Blow-Me-Down Mountain ophiolite massifs, Bay of Islands area, Newfoundland, Canada (Lorand 1987); The Acoje massif, Zambales ophiolite complex, Philippines (Abrajano & Pasteris 1989).

3.1.4 Secondary supergene native copper

Supergene native copper can form in many systems, such as in porphyry copper ores, where redox weathering of copper sulfide minerals is taking place and preexisting copper sulfides are breaking down by downward percolating groundwater and subsequently reprecipitated as native copper. (e.g., Ikehata et al. 2016).

For example, Cook (1988) described six copper-bearing supergene mineral assemblages at the Lakeshore Mine, Pinal County, Arizona, U.S. The deposit is hosted by a granodiorite stock which is cut by a normal fault, the Lakeshore fault. Supergene sulfides are overlain by native copper, sulfates, silicates, and cupric oxides.

3.2 Natural analogue studies on copper

Native copper analogue studies (both geological and archaeological) have been reported in the literature and have been extensively reviewed by various authors for their applicability to nuclear waste disposal (e.g., Miller et al. 2000, Alexander et al. 2015, Reijonen et al. 2015, King 2021). WMOs have used natural analogues for safety analysis (e.g., Posiva 2012), but only few studies have focused on the general stability of native copper hosted by natural media (e.g., Milodowski et al. 2000, Marcos 2002).

Keweenaw Peninsula native copper occurrences have been mentioned as a qualitative source of information in relation to the safety assessments of geological repositories (e.g., in Miller et al. 2000), however, the data available to be used in safety assessments for geological disposal is very limited, especially regarding corrosion processes. Based on the reviews made by e.g., Posiva (2012), the two best studied natural native copper analogues are Hyrkkölä (Finland) and Littleham Cove (UK). These are briefly presented below.

3.2.1 Hyrkkölä – native copper in fractured crystalline rock (Finland)

Native copper occurs in small quantities in fractures of crystalline rocks at the Hyrkkölä and Askola sites, Finland. The age of the U–Cu mineralisation is about 1 700 Ma (see Section 2.1.1 for overview on magmatic copper deposits).

Post-emplacement corrosion under both oxidizing and reducing conditions has been reported (Marcos & Ahonen 1999) and the native copper has been subjected to sulfur-bearing fluids. Despite contact with sulfur-bearing fluids the native copper has survived, and only thin films of sulfide minerals are observed e.g., non-stoichiometric cuprous sulfide phases (djurleite ($\text{Cu}_{1.934}\text{S}$)). Oxygen-bearing groundwater (O concentration 0.5 to 4 mg/L) is present at the site today and likely from 10 000 to 100 000 years ago (Marcos & Ahonen 1999). Oxidation of the native copper is ongoing, albeit very slow (Marcos & Ahonen 1999), possibly due to hindering mechanism, such as smectite surrounding the native copper.

3.2.2 Littleham Cove – native copper in Permian mudstone formation (UK)

The Permian mudstone formation at Littleham Cove has been studied as a natural native copper analogue where the host material is clay (Milodowski et al. 2002). Native copper occurs here as cylindrical plates (up to 160 mm in diameter and 4 mm thick). Copper is closely associated with uraniferous–vanadiferous concretions and reduction spots within the red mudstone and is interpreted to be formed before the maximum compaction of the local strata. After initial diagenetic reactions, the native copper occurrences have been considered to be preserved by the clay matrix without further alteration over 170 million years, before being exposed by the uplift and erosion. Some very late–stage alterations of native copper have been observed in the samples e.g., copper oxyhydroxides, copper carbonate and copper sulfate minerals. Alexander et al. (2015) note that some uncertainties remain, including:

- The permeability of the mudstone host rocks has not been examined but the permeability is likely to be greater than would be the case for an engineered bentonite buffer in a repository (i.e., more corrosion would be expected at Littleham Cove).
- Similarly, the porewaters today and for the past 170 million years in the Littleham Mudstone Formation may have been significantly different than those anticipated in a radioactive waste repository.

3.2.3 NWMO copper analogue review

King (2021) has recently reviewed the copper natural analogues for their use in supporting the prediction of the long-term corrosion of the NWMO's copper-coated UFC. In this review, the relevance of natural analogues has been estimated from the point of view of long-term safety assessment methodology (and its data needs) utilized in the NWMO's safety case. King (2021) has also listed potential future studies of interest to NWMO. King identified potential natural analogue studies include some that could be part of Phase II of the MICA project. These studies are (based on Table 2 in King 2021):

- The detailed properties of Cu₂S films on native copper
 - Evidence to support position that Cu₂S films formed under repository conditions are porous, rather than being passive and susceptible to localized film breakdown.
- Localized corrosion under anaerobic conditions
 - Evidence for pitting
- Effect of impurity levels on copper corrosion
 - Cold spray copper has relatively high O content, electrodeposited copper can contain amounts of P, S, and/or H depending upon the process
- Localized corrosion under aerobic conditions
 - Evidence for surface roughening versus pitting, under both saturated and unsaturated conditions is needed
- Mechanism of suppression of microbial activity by bentonite (note: this would require samples from clay pockets)
- Mechanical performance (NB: not identified a site yet)
 - Maximum external load considered by NWMO is 45 MPa
- Fate of initially trapped O₂
 - Determines duration of oxic phase, as well as extent of general and localized corrosion. Current uncertainty regarding processes responsible for O₂ consumption under deep geological repository conditions
- Conversion of Cu₂O to Cu₂S

In MICA, the scope is broader than what is presented in the above list, due to the needs of different WMOs with differing boundary conditions. The list above is therefore useful to potentially define topics of future activities of MICA Phase II, but it should be not taken as an exhaustive list. King (2021) points out that the safety assessment models for copper corrosion are based on mass transport calculations, and not corrosion rate estimates. However, this is not seen as a reason to not to seek better corrosion rate estimates for the copper (King 2021, considered corrosion rate of copper via natural analogue as less-worthwhile analogue to be studied). As discussed in Section 3.2 so far, the corrosion rate data from natural analogues are very limited.

4 KEWEENAW GEOLOGY

The Keweenaw Peninsula native copper district (Fig. 5) occurs within the ca. 1.1 Ga old North American Midcontinent Rift system (MCR). The rift was filled with thick succession of about 25 km of dominantly subaerial basaltic lava flows with minor interbedded clastic sedimentary rocks overlain by about 8 km of clastic sedimentary rocks. Ore-forming hydrothermal fluids were generated by burial metamorphism of the rift-filling mafic volcanic rocks about 15 to 30 Ma after the end of significant magmatism during regional compression. These fluids moved upward from the source zone into the zone of precipitation where native copper and associated minerals were precipitated in primary and secondary open spaces. Subsequent

erosion during the Precambrian likely exposed the deposits at the land surface. A Paleozoic sea covered the area and resulted in deposition of sedimentary rocks on the Precambrian erosional surface and saline ocean waters penetrating downward. Quaternary glaciations stripped away most of the Paleozoic rocks and once again exposed the native copper deposits at the surface. Some basic description of the geology of the Keweenaw Peninsula geology are provided below. For detailed discussions, reader is referred to the following papers and references therein: Butler & Burbank 1929, White 1968, Bornhorst 1997, Bornhorst & Lankton 2009, Bornhorst & Barron 2011, Bornhorst & Mathur 2017, Bodden et al. 2022.

4.1 The Midcontinent Rift

The bedrock of the Keweenaw Peninsula is almost entirely composed of rift-related rocks (Bornhorst & Lankton 2009). The MCR is a major tectonic feature in the Precambrian crust of Northern America. Heaman et al. (2007) dated the onset of the Midcontinent rift to be approximately 1.15 Ga and Hodgin et al. (2022) dated the outcrops of the rift-flanking Jacobsville Sandstone to be approximately 950 Ma or the end of rift-related bedrock strata. Volcanic materials began filling the rift about 1.15 Ga because of a rising and laterally-spreading mantle plume that extended the over-riding lithosphere (Bornhorst & Lankton 2009). The continental crust had a long and complex history but was a rigid crustal block for hundreds of millions of years prior to rifting (Klasner et al. 1982).

The PLV is a geologic formation that includes rift-filling subaerial basaltic lava flows and interbedded clastic sedimentary rocks. The exposed thickness of the PLV is about 5 km. Subaerial lava flows of the PLV are typically about 10–20 m thick and consist of a massive interior, capped by a vesicular and/or brecciated flow top (Bornhorst & Lankton 2009).

Between periods of active volcanism, gravels and sand with lesser silt and mud were transported from the edges of the rift and deposited on top of the relatively flat-lying lava flows. Upon burial, these sediments lithified into conglomerates, sandstones, siltstones, and shales. Individual layers of these sediments have thicknesses from a few cm up to tens of meters. When volcanism resumed these

clastic sediments were buried by new lava flows. The process repeated several times and resulted in the volcanic-dominated PLV with minor (<5%) interbedded clastic sediments (Bornhorst & Lankton 2009).

Volcanism waned and then ended but the rift continued to sag. This basin was filled with a significant thickness of clastic sediments (Bornhorst & Lankton 2009).

The PLV are overlain by rift-filling sedimentary rocks consisting of red-brown conglomerates and sandstones of the Copper Harbor Formation deposited in alluvial fans. Subaerial lava flows, informally termed the Lake Shore Traps, are interbedded in this rift-filling unit and represent some of the last significant volcanism of the rift system. The Copper Harbor Conglomerate is overlain by rocks of the Nonesuch Formation, which is composed mainly of gray to black siltstones and shales. The last rift-filling sediments were sands, silts, and muds of the Freda Sandstone, which were deposited by shallow rivers (Bornhorst & Lankton 2009). The last phase of the MCR was characterized by compression, probably caused by continental collision along the Grenville front about 1.07 Ga to 950 Ma (Bornhorst & Lankton 2009).

The MCR is both a rift system and a large igneous province (LIP) (Bornhorst 1997, Bornhorst & Barron 2011, Stein et al. 2015). There was a major compressional event late in the history of the MCR and distinguishes it from other LIPs in the world. The MCR is notable because of its abundant native copper

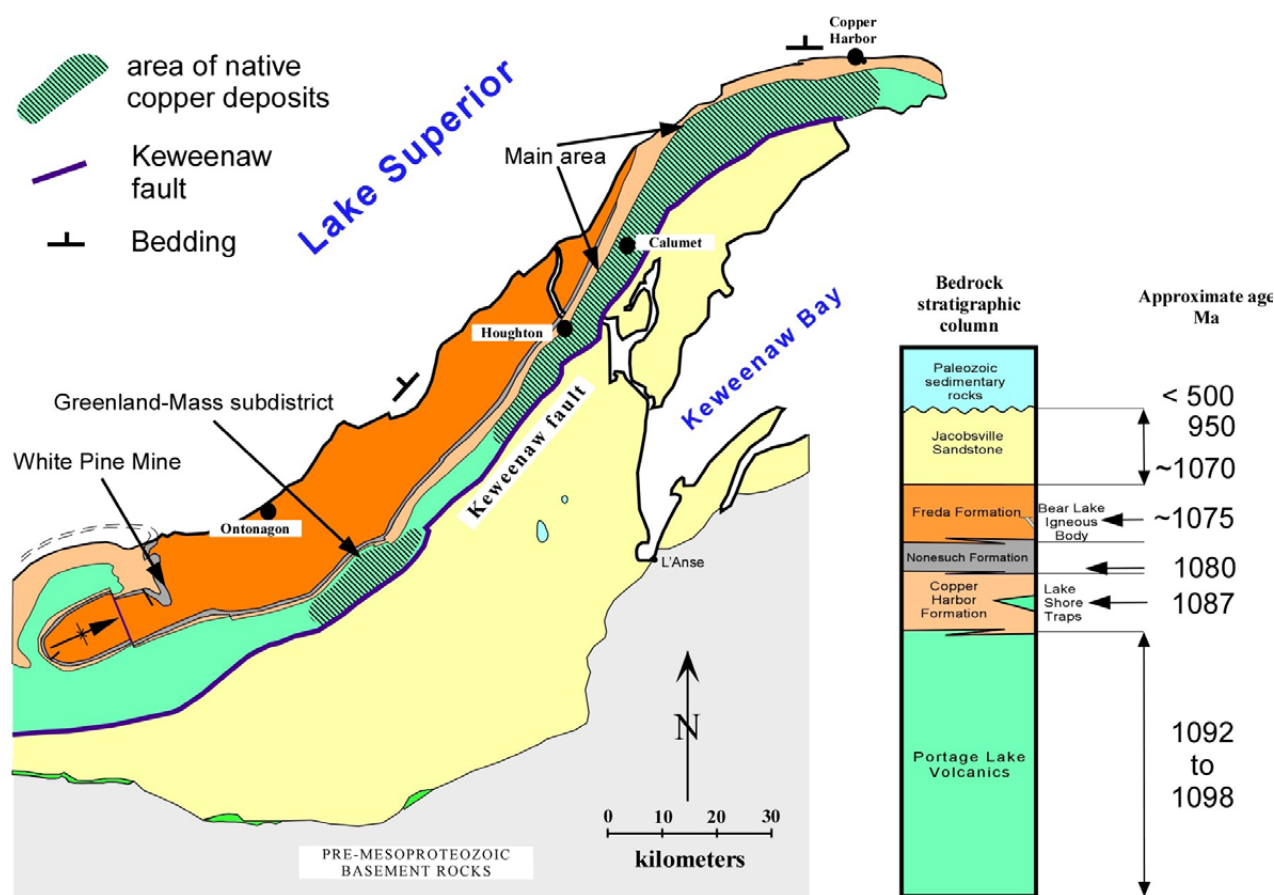


Fig. 5 Geologic map of Keweenaw Peninsula Native Copper District. Figure modified from Bodden et al. 2022.

deposits that are not associated with other rifts or LIPs. The late compressional event is hypothesized to have been critical to the generation of native copper deposits, as it likely provided a fracture network that integrated the plumbing system and

allowed for upward movement of the ore-forming fluids generated by burial metamorphic processes at depth below the native copper deposits (Bornhorst 1997, Bornhorst & Lankton 2009, Bornhorst & Mathur 2017, Bodden et al. 2022).

4.2 Geological setting of the Keweenaw native copper mining district

The native copper deposits of the Keweenaw Peninsula are hosted in the tops of subaerial basaltic lava flow, in interflow red-colored clastic sedimentary horizons, and in veins (White 1968, Bornhorst & Lankton 2009). Precipitation of native copper is accompanied by an assemblage of low-grade alteration minerals. Native copper and associated minerals were deposited as part of a regional hydrothermal event from about 1.07 to 1.04 Ga coincident with regional compression (Bornhorst & Mathur 2017, Bodden et al. 2022).

The copper-bearing fluids were generated by burial metamorphism of the rift-filling basalts

at temperatures of about 300–500°C (Bornhorst & Mathur 2017, Bodden et al. 2022). About 10 km thickness of basalt beneath the present ore horizons is suggested to be a sufficient source for the copper seen in the deposits (Bornhorst 1997). Degassing of sulfur from low-sulfur subaerial lava flows likely resulted in very low sulfur contents in the hydrothermal ore fluids generated by burial metamorphism of these rocks (Bornhorst & Mathur 2017, Bodden et al. 2022). The pathways of very low sulfur hydrothermal ore fluids through the very low sulfur basalts resulted in precipitation of native copper instead of copper sulfides.

4.3 Younger geological evolution

From ca. 950 Ma to 500 Ma, the Keweenaw Peninsula was subjected to erosion, long after formation of the native copper deposits with an age from 1.04 to 1.07 Ga. Many kilometers of rock were eroded which likely exposed the native copper deposits to the surface. Groundwater likely interacted with the native copper ores at shallow levels as the result of erosion and could have caused supergene alteration (Bornhorst & Robinson 2004). The expected supergene minerals would have been cuprite (Cu_2O), tenorite (CuO), malachite ($\text{Cu}_2\text{CO}_3(\text{OH})_2$), and chrysocolla ($((\text{Cu},\text{Al})_2\text{H}_2\text{Si}_2\text{O}_5(\text{OH})_4 \cdot n\text{H}_2\text{O})$). Today, these minerals are found near the surface but well below the water table (<300 m) in several deposits. They may be near the same position beneath the surface as they were 500 million years ago (Bornhorst & Lankton 2009).

Phanerozoic sediments associated with marine deposition in the Michigan basin buried the copper ores and their host rocks beginning ~500 Ma. This sedimentation took place from ca. 500 to 175 Ma (Catacosinos et al. 2001). Observations of isolated outliers of Ordovician limestone, e.g., Limestone Mountain and Sherman Hill, ca. 35 km south of Houghton, are evidence of the presence of these overlying rocks. The Phanerozoic geologic processes were nontectonic and without major faulting. This long period of marine conditions overlying the rocks

of the rift and the native copper deposits likely resulted in deep penetration of saline brines into the bedrock (Bodden 2022). Saline brines encountered during mining of the native copper deposits are likely of Phanerozoic origin (Kelly et al. 1986). Another period of long-term erosion followed, from the middle Jurassic to the Pleistocene glacial period (Bornhorst & Lankton 2009). The extent of erosion during this time is unknown but it seems likely that Paleozoic rocks remained at the bedrock surface over the entire Keweenaw Peninsula until after Pleistocene glaciation.

Pleistocene glaciers effectively eroded the Phanerozoic rocks of the western Upper Peninsula. The amount of erosion of underlying rift-related rocks is uncertain although it seems likely that there was limited glacial erosion of the more competent rocks such as the PLV. The weaker sandstones, siltstones, and shales were eroded into lowlands. The current bedrock topography is a result of the cumulative effect of a series of glacial episodes. The elevated ridge making up the Keweenaw Peninsula consists of competent rocks of the PLV and adjacent Lake Superior consists of less competent rift-filling sandstones, siltstones, and shales. By the end of the most recent glacial retreat, native copper ores were once again exposed at the surface (Bornhorst & Lankton 2009).

4.4 Composition of native copper

The native copper of the Keweenaw Peninsula typically consists of >99% copper (often >99.9% copper), but it does contain trace elements, which are likely not separate phases. Native copper does contain fluid inclusions that could be the source of low amounts of trace elements but it is more likely that trace elements substitute into the crystalline structure of native copper. The variation in the composition of natural native copper may be of interest from a corrosion point of view.

Silver is a well-known element associated with Keweenaw Peninsula native copper and the term “lake copper” was used to indicate that smelted (not electrolytically refined) copper from the Keweenaw Peninsula contained silver. Native silver occurs as a separate visible phase in some samples of native copper and likely also occurs as a separate phase only visible under high magnification using a SEM. The amount of silver that substitutes

into the crystalline structure of native copper is unknown. Carefully separated native copper analyzed by INAA contains about 300 wt.ppm Ag with maximum of about 2000 ppm (Rapp et al. 2000; sheet copper [sheet copper formed along thrust faults are likely time equivalent to native copper from the Keweenaw Peninsula] from Mauk and Hancock 1998). A reasonable assumption is that 300 ppm Ag substitutes into native copper and the maximum level is a result of a separate native silver mineral phase.

Native copper is also well-known to have higher amounts of arsenic which causes a different color of acid cleaned native copper. Rapp et al. (2000) reports a median of 54 ppm As whereas Mauk and Hancock (1998) report about 100 to 200 ppm As for sheet copper. Both report a large range with As of up to a few 1000s of ppm.

Aside from Ag and As, other trace elements typically do not exceed 10s of ppm. Rapp et al. (2000) reported low levels of Fe in native copper of about 250 ppm, but this was not confirmed by Mauk and Hancock (1998) who did not detect Fe.

Rapp et al. (2000) report Hg at levels up to 120 ppm as compared to Mauk and Hancock (1998) who report typically 2 to 10 ppm. The absolute abundance of 120 ppm Hg reported by Rapp et al. (2000) is not consistent with unpublished data of Bornhorst (pers. comm.) whose data is more con-

sistent with the level of Hg reported by Mauk and Hancock (1998). Bornhorst's data indicates a very strong correlation between the abundance of Ag and Hg.

Other reported elements in native copper based on a combination of Rapp et al. (2000) and sheet copper from Mauk and Hancock (1998) include Co of about 2 ppm and Sb of about 2 ppm (not detectable in Rapp et al. 2000). Typically, Sc, Cr, Sb, Zn, Co, Ni, Se, Br, Sm, Sn, Ti, Mn, La, and V are not detected in Keweenaw Peninsula native copper.

5 THE GEOLOGIC CONTEXT AND SEQUENCE OF EVENTS

This chapter contains descriptions of the geologic contexts and sequence of events related to native

copper and includes relevant uncertainty comments and questions.

5.1 Keweenaw Peninsula bedrock native copper

5.1.1 Generation of Main-Stage Hydrothermal Fluids

The hydrothermal system of the Keweenaw Peninsula native copper district consists of a main-stage event (1040 to 1070 Ma) during which native copper and associated minerals were precipitated followed by a late-stage event during which copper sulfide-bearing minerals were precipitated. The main-stage hydrothermal fluids are interpreted as being hybrid ore-forming fluids derived by mixing of burial metamorphic derived fluids and sulfur-depleted seawater (Bodden et al. 2022). This hybridization of fluids resulted in an ore-forming Ca-rich saline brine (Kelly et al. 2022, Kelly 2020) which contained copper in the 100s of ppm to perhaps as high as 1000s of ppm (Livnat 1983, Jolly 1974).

5.1.2 Conditions of Hydrothermal Precipitation of Native Copper

Oxygen and carbon isotopic data on main-stage hydrothermal calcite suggest that the hybrid ore-forming fluids were mixed with sulfur- and copper-depleted reducing meteoric water in the zone of precipitation (Bornhorst & Woodruff 1997, Bodden et al. 2022). Mixing of ore-forming fluids and dilute meteoric water along with metamorphic mineral reactions (Jolly 1974) facilitated precipitation of native copper. The temperatures of precipitation of native copper were spatially zoned varying from 150 to 300 °C (Bodden et al. 2022). Table 4 shows a compilation of the hydrothermal precipitation conditions.

Table 4. Composition of main-stage hydrothermal fluids. Information is mainly based on Jolly (1974), Livnat (1983), Kelly (2020), Bodden et al. (2022) and Kelly et al. (2022).

Temperature	150 to 300°C
Salinity	Ca-rich brine with 10 to 30 wt.% salinity (Kelly 2020, Kelly et al. 2022). Zone of precipitation: hybrid (metamorphic-seawater) ore-forming fluids mixed with meteoric water
Very low CO ₂	XCO ₂ < 0.01
Very low S	< 1 ppm ?
Cu	100s to 1000s ppm
pH	6 to 8
Pressure	likely 0.75 to 1.5 kbar at top of PLV with fluid pressure close to lithostatic

5.1.3 Spatial Setting of Keweenaw Peninsula bedrock native copper

Most native copper of the Keweenaw Peninsula fills open spaces within the tabular dipping tops of subaerial lava flows and clastic sedimentary layers. A small volume of native copper occurs in veins. Typical, masses of native copper range in size from mm disseminations to masses up to 25 kg. In general, the masses are larger in veins than in the lava flow tops and interbedded clastic sedimentary rocks. Masses of native copper in veins can be up to 10s of tons. Native copper is associated with a suite of hydrothermal minerals. Native copper occurs as inclusions in the associated hydrothermal minerals and itself contains inclusions of associated hydrothermal minerals (Bodden et al. 2022, Bornhorst & Lankton 2009). For the generalized sequence of events, see Table 5.

Native copper occurrences include following settings (not listed in order of importance):

- Amygdule fillings in top of subaerial basalt lava flows.
- Void space fillings in top of subaerial basalt lava flow with brecciated flow top.
- Fracture and vein fillings in the top of subaerial basalt lava flow which extend upward and downward into massive flow interior.
- Pore space fillings in clastic sedimentary rocks especially conglomerate and sandstone.
- Veinlet to veins filling open fractures (no stratigraphic offset) and faults that crosscut tabular stratigraphic units.
- Particle size μm to several meters; hard to predict spatial distribution due to “nugget effect”.
- Native copper as inclusions in associated minerals.
- Associated minerals found as inclusions in masses of native copper.
- Preservation of native copper in calcite in contact with fluid inclusions – not “dry” preservation.

5.2 Native Copper at the White Pine Mine

The White Pine Mine is a sediment-hosted stratiform copper deposit hosted by the rift-filling Nonesuch Formation deposited about 1.08 Ga (Bornhorst & Williams 2013). During diagenesis low-temperature, copper-bearing hydrothermal fluids were released by the compaction of pyrite- and organic-bearing muds and flowing upwards. The pyrite (FeS_2) was replaced by chalcocite (Cu_2S), the principal ore mineral at the White Pine Mine. Pyrite-poor oxidized sandstones at the top of the Copper Harbor Formation hosts diagenetic native copper disseminated in the pore spaces.

5.2.1 Spatial Setting

In the southwest part of the White Pine Mine native copper occurs in crosscutting veins filling thrust faults interpreted as associated with late-rift regional compression (Mauk et al. 1992). These native copper bearing thrust faults crosscut the stratiform diagenetic chalcocite ore. This fault/vein hosted native copper often occurs as sheets of copper mm square and mm thick up to 2 by 2 m square and 1 cm thick. The sheets of native copper are interpreted to be deposited by the same hydrothermal event (1070 to 1040 Ma) that precipitated native copper in the Keweenaw Peninsula proper. The generalized sequence of events is presented in Table 5.

5.3 Float copper masses

Float copper is an informal term used for masses of native copper that were carried in (“floated”) and transported by glacial ice. Float copper masses result from bedrock native copper that becomes entrained in glacial ice. The native copper masses were plucked from the bedrock by glacial ice or resulted from native copper already freed from the bedrock by erosional processes and lying on the

surface or being part of unconsolidated sediments that subsequently became entrained in the glacial ice. Float copper masses were deposited from melting of glacial ice and from glaciofluvial processes (Bornhorst & Lankton 2009) and are part of the current unconsolidated sediment cover on the bedrock.

5.3.1 Spatial Setting

The float copper masses vary in size just as in the bedrock native copper deposits. The size of masses may seem biased towards the larger masses, but no one has systematically looked for sand size or finer float copper masses. The float copper masses are found directly on the surface or covered by up to a few meters of unconsolidated sediments. Indigenous peoples and European explorers and settlers likely discovered most of those exposed to the surface. Excavations in unconsolidated glacial gravel deposits have yielded discovery of float copper masses. In modern times, metal detectors facilitate the discovery of float copper masses thinly covered by unconsolidated sediments and soil (Bornhorst & Lankton 2009).

Most float copper masses were deposited about 10 ka upon retreat of continental glaciers from the Lake Superior region. It is uncommon to find unconsolidated glacial deposits older than the most recent episode of glaciation in the Keweenaw Peninsula. Thus, it seems likely that the latest glacial episode incorporated pre-existing unconsolidated glacial sediments also containing float copper masses into the glacial ice. If the Paleozoic bedrock on top of the Precambrian of the Keweenaw Peninsula were removed before the latest glacial advance, the float copper masses could have been subjected to more than one glacial event.

The float copper masses occur along with rock of various sizes. These rocks round each other as

well as the float copper masses during glacial and glaciofluvial transport. The abrasion during glacial transport would result in exposed surfaces of the float coppers both lacking in alteration and associated secondary minerals. When the float copper masses are covered with hydrothermal minerals, such as cuprite and tenorite, these minerals may have protected the surface from alteration. Indentations or fractures within the float native copper masses could have copper alteration products far older than smooth rounded surfaces. Thus, establishing the context of the copper alteration products is critical for accurate interpretation.

5.3.2 Glacial Event Uncertainty

As noted above, only the last period of glaciation is well represented in the glacial formations of the Keweenaw Peninsula. The last glacial episode would have eroded previous unconsolidated deposits glacial episodes so float copper masses could have been through more than one glacial event (Bornhorst & Lankton 2009). In addition, the masses of native copper could have been separated from bedrock during Precambrian weathering and strewn about on the Precambrian weathering surface on which the Paleozoic was deposited. Upon removal of the Paleozoic rocks during glaciation these masses could have been incorporated into Pleistocene glacial ice. General level description of events is compiled in Table 5.

5.4 Lake copper

Lake copper is an informal term used by Bornhorst and Barron (2017) and the A. E. Seaman Mineral Museum of Michigan Tech to refer to native copper masses found on the bottomlands of Lake Superior nearby the Keweenaw Peninsula, especially Great Sand Bay. The lake copper was formed by the same hydrothermal ore-forming fluids and processes as the PLV bedrock native copper but at slightly lower temperatures (Bodden 2019, Bodden et al. 2022). Lake copper masses are subdivided by specific locality and by process of formation (see the following sections).

5.4.1 Lake copper formations

Great Sand Bay lake copper masses are massive tabular native copper deposits in subvertical veins that

crosscut bedrock. They are either connected to bedrock native copper veins or their context indicates they were not significantly moved. The large 19-ton block of lake copper on exhibit at the A. E. Seaman Mineral Museum belongs to this type as it was connected to the bedrock prior to removal (Bornhorst & Barron 2017). The smoothing and glacial grooving of the top surface by glacial ice resulted in exposed smoothed surfaces of lake copper to be pure copper and lacking alteration products prior to retreat of the glacier.

Great Sand Bay lake copper nuggets are included in the term lake copper as used by Bornhorst and Barron (2017) although their origin differs from the Great Sand Bay lake copper. The native copper nuggets range up to large boulder-sized masses (up to about 50 kg) not connected to veins in the

bedrock. Native copper nuggets often have smooth abraded and sculpted surfaces on all sides that are consistent with abrasion by water. Smaller masses from tens of g to 500 g are often found in crevasses within the bedrock. The high density of native copper results in its concentration in cracks and crevasses by water sorting. Since Great Sand Bay has been underwater below the wave base since glacial retreat about 10 ka ago, it is likely that the water abrasion and deposition occurred by subglacial streams. Their connection to the Great Sand Bay bedrock veins is not proven but it is likely that they are derived by this nearby deposit. The smoothing and rounding during transport resulted in exposed surfaces of float copper to be pure copper and lacking alteration products when the glaciers retreated about 10 ka ago. Surface alteration products were formed subsequently.

Great Sand Bay laker pocket is an in-place bedrock vein of crystalline native copper exposed on the bottomlands of Lake Superior in Great Sand Bay. The tabular Laker pocket vein is about 1 m thick and cross cuts the host rocks. It consists of finely crystallized native copper forming a very porous mass of interconnected crystals along with low temperature alteration minerals. Today, crystals of native copper are not encased in hydrothermal minerals but are surrounded by Lake Superior waters. No surface abrasion is seen on the small native copper crystals but the surfaces could have been surrounded by hydrothermal alteration products to a variable extent that were softened by soaking with water and removed by moving water. The copper alteration products on the crystal surfaces are the result of the cumulative exposure to corrosion events since formation in the Precambrian with the latest being submerged under glacial to modern Lake Superior waters. The laker pocket is described by Rosemeyer (2009).

Gull Rock native copper is an in-situ bedrock vein of entirely crystallized masses of native cop-

per encased in hydrothermal calcite at Grand Marais, Eagle Harbor area, Keweenaw County. The encasement of this native copper limits exposure to past corrosion events since formation in the Precambrian.

5.4.2 Spatial Setting

Great Sand Bay laker copper masses are connected or nearly connected to subvertical veins. They have been subjected to glacial abrasion, which stripped away copper alteration products from their surfaces prior to the latest glacial retreat. They are exposed on the bottomlands of Lake Superior and submerged under Lake Superior waters.

Granule- to boulder-sized Great Sand Bay laker copper nuggets are found on the bottomlands of Lake Superior in cracks and crevasses and scattered on the surface. The smoothed surfaces of the nuggets would have been stripped of copper alteration products prior to the latest glacial retreat.

Great Sand Bay laker pocket, a tabular vein of continuous interwoven network of small native copper crystals is exposed on the bottomlands of Lake Superior and submerged under Lake Superior waters. Typical size of copper crystals is about 5 mm across. These crystals have not been exposed to abrasion by glacial or glaciofluvial processes. Their copper alteration products represent the cumulative effect of exposure since the Precambrian which was likely uninhibited since the Precambrian.

Gull Rock native copper tabular vein of continuous interwoven network of native herringbone copper crystals encased in hydrothermal calcite is exposed on the bottomlands of Lake Superior and submerged under Lake Superior waters. These crystals have not been exposed to or abraded by glacial or glaciofluvial processes and their copper alteration products but since they are encased in hydrothermal calcite and thus, the exposure to past copper corrosion events is limited.

5.5 Chisel chips of native copper

Long dormant historic mines, especially those more than 125 years old (Cliff and Central mines), are known for having produced chisel chips. Since native copper is malleable, very large underground masses of native copper in these old mines were divided into smaller masses by chisels as powder explosives do not work on ductile materials as native copper. This resulted in chips of native

copper typically with length of <30 cm and width of about 2.5 cm with a chisel rippled surface. Some of these chisel chips were discarded as waste and thus, are found today in the poor rock piles. The surface of the chisel chips, immediately after they were formed, were highly likely to have been unaltered native copper except when other hydrothermal minerals are present. Any copper alteration

products present today are a result of downward percolating precipitation waters in the rock pile.

5.5.1 Spatial Setting

Chisel chips are found within poor rock piles typically coated with fine-grained mining muck. The

mining muck consists of fine sand to clay sized particles and the coating is usually much less than 5 mm thick. The muck is readily washed off with tap water and a soft brush. Chisel chips are more common in older mines that were focused on veins in which the native copper more often occurred as larger masses, readily up to tons.

5.6 Mining and post-mining processes

The mining and post-mining sample processing could have a dramatic effect on the observable corrosion of native copper and formation of alteration products. The explosive chemicals and by-products that contact surfaces of masses of native copper can result in chemical reactions leading to copper alteration products. Mining introduces oxygen into

the mine openings, which interacts with resident waters and the surfaces of minerals. Mine openings result in seepage of water into the mine. This water interacts with minerals in combination with oxygen and can result in copper alteration products. These are just some examples of mining and post-mining processes.

5.7 Generalized sequence of events

Native copper deposits formed at 5 to 10 km below the surface between 1.07 and 1.04 Ga accompanied and followed by compressional uplift that ended ~950 Ma. From ca. 950 Ma to 540 Ma the Keweenaw Peninsula underwent erosion. The vertical extent of erosion is unknown.

There were probably four or five global ice ages between ca. 751 to 550 Ma that could have affected erosion of the bedrock of the Keweenaw Peninsula (e.g., Hoffman et al. 1998, Pu et al. 2016, MacLennan et al. 2020). Neoproterozoic Cryogenian (720–635 Ma) and the Gaskiers glaciations (579 Ma) (e.g., Hoffman et al. 1998, Pu et al. 2016) may have resulted in glacial erosion. However, during these global ice ages, Laurentia was located near an equatorial position (Swanson–Hysell 2021). It is uncertain if there were significant ice sheets over the Keweenaw Peninsula and thus, large amounts of oxic glacial meltwater. The thickness of ice in the tropical regions was probably only tens of meters during a completely ice-covered “Snowball–Earth” (e.g., McKay 2000).

Regardless of the glacial impact on erosion rates, it seems likely that 5 to 10 km of bedrock could have been eroded in the Phanerozoic eon (541 Ma to present day) and the native copper deposits were exposed at the surface (Bornhorst & Robinson 2004; Table 5).

There was likely infiltration of fresh water below the surface from soon after the native copper deposits were formed at 1.07–1.04 Ga to ca. 540 Ma. Given the position of Laurentia during this

time interval, environmental conditions could have been arid with the water table being considerably below the surface. In this case, the infiltration of water in the zone of aeration could have resulted in supergene alteration of the native copper deposits in affected depths and with favorable paleohydrologic conditions. Deep supergene copper oxidation products are found in at least two mines at Keweenaw Peninsula (Bornhorst & Robinson 2004). Oxic conditions could have existed at the surface of the shallow parts of native copper deposits for a long period of time during the Neoproterozoic. However, the shallow parts of deposits would also be more likely to have been eroded away.

The region was submerged under marine conditions from ca. 540 Ma to 299 Ma. Sedimentation during this time interval began with Cambrian sandstone followed by Paleozoic limestone, dolomite, and shale. This long period of submersion beneath seawater could have readily resulted in penetration of these seawater brines deep into the bedrock replacing pre-existing waters. The brines found in the mines have a Phanerozoic stable isotope signature (Kelly et al. 1986).

The rock record from the end of the Pennsylvanian to the Pliocene (right before the beginning of Pleistocene glaciations) is lacking in Michigan. This time interval is called the “Lost Interval” (Velbel 2009). There is evidence that hundreds of meters of sedimentary rocks were deposited in the Lower Peninsula of Michigan during this time interval but by the middle Jurassic these same sedimen-

tary rocks were eroded away. During the middle Jurassic ca. 170 Ma continental redbed sands, muds, limestone and evaporites were deposited in erosion valleys on top of Pennsylvanian sedimentary rocks (Velbel 2009). The Upper Peninsula of Michigan was likely under continental conditions. The geologic evidence is lacking to propose erosion or deposition of sedimentary rocks during the time interval of 300 Ma to 2.5 Ma.

The Keweenaw Peninsula was impacted by all the episodes of Quaternary continental glaciation. The continental glaciers eroded away the Paleozoic and perhaps Mesozoic sedimentary rocks that covered the Mesoproterozoic to Neoproterozoic bedrock. The native copper deposits were uncovered and exposed at the surface by Quaternary glacial erosion. If the hypothesis by Bornhorst and Robinson (2004) of Neoproterozoic supergene alteration is correct, then the Quaternary continental glaciers did not erode much of the PLV, or else evidence of supergene alteration would have been eroded away. During the Quaternary, there is the possibility of infiltration of oxic glacial melt water into the bedrock. However, this infiltration must not have

been deep, otherwise brines found in the mines would have been displaced by glacial and freshwater infiltration.

Bedrock native copper would have been exposed to waters associated with all the events described above depending on the degree of encasement in associated hydrothermal minerals, the paleohydrologic accessibility of waters to the surfaces of native copper, and the degree to which waters penetrated the subsurface. Bedrock native copper corrosion is the cumulative result of these alteration processes over about a billion years. Native copper abraded by Quaternary glacial and/or glaciofluvial processes, or by Neoproterozoic erosion. These natural processes remove previous alteration products and thereby reset copper corrosion to zero and restart the corrosion “clock.” Human activities can also reset the copper corrosion “clock” as in the case of chisel chips.

The consolidated sequence of events for all the analogues are presented in Table 5. The stratigraphic context of the Keweenaw Peninsula is presented in Figure 6.

Table 5. Sequence of events for all analogues. The geological timeline is based on the International Chronostratigraphical Chart (Cohen et al. 2020).

Ma	EON	ERA	PERIOD	EPOCH	EVENTS
0	Phanerozoic	Cenozoic	Quaternary	Holocene	18. Minewaters, especially at depth, were often brines and likely related to deep penetration of seawater during deposition of Paleozoic Michigan basin sediments (see 10., this table). The brines are also present in unconsolidated glacial sediments today and seep to the surface in springs. These brines can be extremely saline. 17. Currently accessible mines above the water table offer possibility to study in situ native copper currently located in the zone of aeration. Shallow mine openings located in topographically higher areas may have been above of the water table prior to mining. 16. Profitable modern native copper mining begun in 1845 at the Cliff mine. Early techniques used chiseling to cut large amounts of native copper from veins. Native copper in poor rock pile started weathering. The degree of weathering is dependent on starting time on pile and the surrounding pulverized mine rock. 15. Native peoples collected float copper from the surface and mined native copper from shallow surface pits beginning about 7000 years ago. The items they made from native copper were widely traded throughout what is today the eastern US.
0,0117				Pleistocene	14. Glaciers exposed native copper in the bedrock on the bottomlands of Lake Superior and predecessor glacial lakes and glacially abraded surfaces started weathering. This "lake copper" is submerged today in Lake Superior water. 13. Native copper was transported during the last glacial episode and deposited upon glacial retreat ca. 10 ka ago. Glacial and glaciofluvial processes smoothed masses of copper and stripped away pre-existing copper alteration products from the surfaces. The native copper masses deposited with unconsolidated glacial sediments began weathering in the surface environment. These masses are informally termed "float copper." 12. Pleistocene glaciation took place from about 2.5 Ma to 10 ka. Glacial erosion stripped away most of the Michigan Basin strata but did not remove a significant amount of Precambrian bedrock. At 10 ka, the Precambrian bedrock and parts of the native copper deposits were exposed at or very near to the surface, There was selective replacement of brines near the bedrock surface with fresh water.
2,58		Neogene	Pliocene	Pliocene	11. There is a Mesozoic to Cenozoic gap from about 170 Ma to 2.5 Ma. Partial erosion of the Michigan basin strata is possible. (Likely scenario: Paleozoic remains on the top shield Precambrian bedrock from downward percolating groundwater).
5,333				Miocene	
23,03			Paleogene	Oligocene	
33,9				Eocene	
56				Paleocene	
66		Mesozoic	Cretaceous		10. Deposition from about 500 Ma to 170 Ma of marine sedimentary rocks of the Michigan Basin buried the Precambrian bedrock under multiple kms of strata. There was a deep penetration of seawater into the bedrock including all native copper occurrences of the Keweenaw Peninsula and the chalcocite and native copper at the White Pine mine.
145			Jurassic		
201,3			Triassic		
251,902		Paleozoic	Permian		
298,9			Carboniferous		
358,9			Devonian		
419,2			Silurian		
443,8			Ordovician		
485,4			Cambrian		

Table 5. Cont.

Ma	EON	ERA	PERIOD	EPOCH	EVENTS
541	Precambrian	Neo-proterozoic			9. Precambrian gap from 950 Ma to 540 Ma likely resulted in erosion to approximately the current bedrock surface and exposure of the native copper deposits at the surface. There has been possible impact of global periods of glaciation (Cryogenian 720–635 Ma, Gaskiers 579 Ma) on rate of erosion and infiltration of water. Hypothesized supergene alteration of native copper by downward percolating groundwater is recognized/preserved only in Algoma and Allouez mines.
1000		Meso-proterozoic			8. Late-stage district wide hydrothermal event was resulting in superposition of late-stage copper sulfides that crosscut Keweenaw Peninsula native copper but age is uncertain. The late-stage event could be as young as 950 Ma. 7. Regional compression and synchronous main-stage regional hydrothermal event at ~1.06 Ga related to the Grenville continental collision which took place some 400 km east of the Keweenaw Peninsula. Hydrothermal and compressional event resulted in precipitation of native copper multiple kms below the surface in the Keweenaw Peninsula and scattered throughout Mid-continent rift rocks of the Lake Superior region. Native copper precipitated in cross cutting thrust faults at the White Pine mine. 6. Continued deposition of rift-filling clastic sedimentary rock of the Freda Formation until about 1.06 Ga 5. Lithification of the Nonesuch Formation. 4. Upward moving ore-forming diagenetic fluids resulted in sedimentary rock-hosted stratiform copper deposits at the White Pine mine and Copperwood in the Nonesuch Formation (predominantly chalcocite with less native copper). 3. Deposition of the Nonesuch Formation interfingering with top of the Copper Harbor Formation (switch from oxidizing depositional environment of underlying Copper Harbor to reducing environment of Nonesuch). 2. Deposition of the Copper Harbor Formation with abundant sandstone close to top until ~1.08 Ma. 1. Deposition of Keweenaw PLV (native copper host rock formation) until ~1.092 Ga.
1600		Paleo-proterozoic			Basement bedrock in the Upper Peninsula of Michigan consists of metamorphosed igneous and sedimentary rocks.
2500		Neoproterozoic			
2800		Mesoproterozoic			
3200		Paleoproterozoic			
3600		Eoproterozoic			
4000		Hadean			

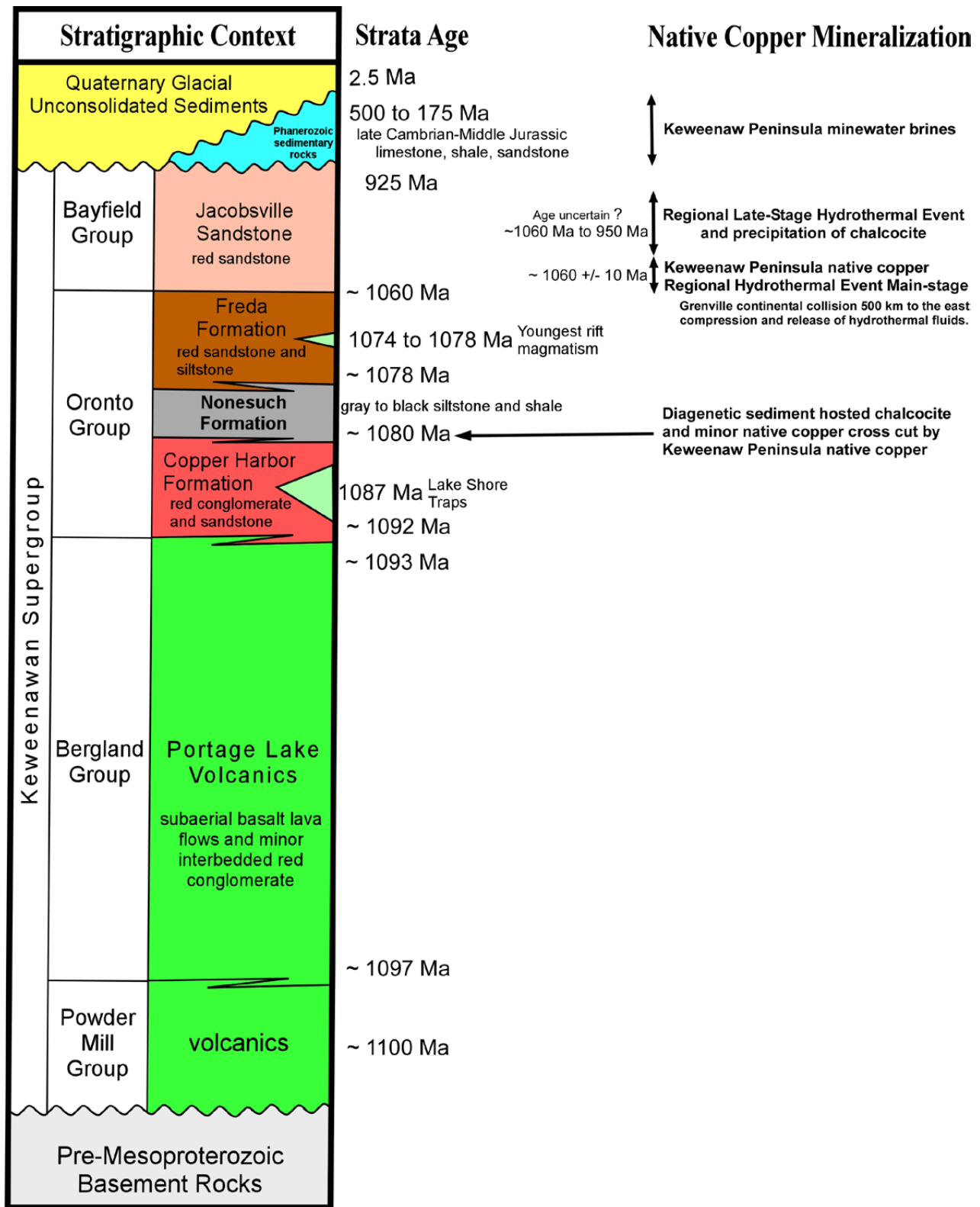


Fig. 6. Stratigraphic context of the Keweenaw peninsula.

6 POTENTIAL NATURAL ANALOGUES AND AVAILABILITY OF RESEARCH MATERIALS

This chapter presents the 13 types of native copper occurrences potentially suitable for natural analogue studies. They are distinguished from one another by their geologic history and their environ-

ments regarding the exposure to water (see Table 6 and Appendix 1). Description of the available samples and references are given in Appendix 1 for all analogue types except Type M.

Table 6. Potential occurrence types for analogue studies.

A	Long and Varied History of Keweenaw Peninsula Bedrock Native Copper in the Subsurface.
B	Keweenaw Peninsula Deep Bedrock Native Copper – Long and Varied Native Copper History, Likely Less Exposed to Oxidic Conditions.
C	White Pine Mine Bedrock Native Copper – Long and Varied Native Copper History, Likely Less Exposed to Oxidic Conditions.
D	Keweenaw Peninsula Shallow Bedrock Native Copper - Long and Varied Native Copper History, Likely More Exposed to Oxidic Conditions.
E	Lake Superior Shallow Bedrock Native Copper
F	Keweenaw Peninsula Bedrock Native Copper Exposed to Supergene Weathering
G	Keweenaw Peninsula Bedrock Native Copper Exposed to Hydrothermal Sulfur
H	White Pine Mine – Bedrock Native Copper in Contact with Sulfide Minerals
I	Lake Superior Shallow Native Copper with Glaciated Surface (Great Sand Bay Lake Copper)
J	Lake Superior Native Copper Gravel (Great Sand Bay Lake Copper Nuggets)
K	Glacial Native Copper (“Float Copper”)
L	Native Copper Chisel Chips
M	Native Copper in Clay

Analogue Type A encompasses all bedrock native copper in the subsurface of the Keweenaw Peninsula in which the cumulative environment of native copper corrosion over the past 1 billion years is generally known except the depth of extraction of the particular specimen of bedrock native copper. Analogue Type B and Type C are in essence subtypes of Type A in which the depth of extraction of the bedrock native copper is known to be deep and Type

D and E are known to be shallow. Analogue Types F, G, H, and I are special environmental considerations of bedrock native copper. These “subtypes” are distinguished to make assumptions on corrosion history simpler. Cumulative corrosion can be compared to native copper completely encased in other minerals. See Appendix 1 for sample availability and references.

6.1 Analogue Type A. Long and Varied History of Keweenaw Peninsula Bedrock Native Copper in the Subsurface

Analogue Type A represents cumulative corrosion of surface exposed native copper over about one billion years in the subsurface regardless of depth of extraction of the native copper from the bedrock or special environmental considerations excluding mining related or exposure to modern surficial conditions. The degree to which the surface of masses of bedrock native copper are exposed to water and/or air may be difficult to determine. Euhedral native copper crystals occurring within or protruding into

open cavities are examples where the surface of the native copper crystals could have been exposed to waters since ~1 Ga. It is reasonable that the cavities had open fracture interconnections with other cavities. We assume that corrosion of bedrock native copper completely encased in a mineral other than native copper is limited to negligible. Copper completely encased in another mineral, such as native copper inclusions in transparent calcite from the Quincy Mine, indicate little to no corrosion over the

past ~1 Ga as their surfaces are visually shiny native copper lacking typical surficial copper alteration minerals.

Since precipitation of Analogue Type A native copper, the surfaces of bedrock native copper not completely encased in another mineral have been exposed to potential corrosion events. In general,

the longest exposure has been to anoxic brines. Exposure to oxic low salinity meteoric water likely occurred in shallow settings. The general study of natural corrosion native copper will contribute to our understanding of native copper corrosion over long geologic time regardless of the details of corrosion history.

6.2 Analogue Type B. Keweenaw Peninsula Deep Bedrock Native Copper – Long and Varied Native Copper History, likely less exposed to oxic conditions

Analogue Type B is the same as Type A but with a known extraction depth. Analogue Type B encompasses all bedrock native copper in the subsurface of the Keweenaw Peninsula in which the cumulative environment of native copper corrosion over the past ~1 Ga is generally known and the deeper depth of extraction makes long-term oxic conditions unlikely. At great depths groundwater is generally reducing rather than oxic. For some native copper extraction localities, there is abundant evidence of that the bedrock is saturated with anoxic

brines. The presence of anoxic brines strongly supports limited exposure of the native copper to oxic conditions. See Table 2 in Appendix 1 for sample availability and references.

Since precipitation of Analogue Type B bedrock native copper, the surfaces of masses of deep bedrock native copper not completely encased in another mineral have been exposed to dominantly anoxic corrosion. Exposure time of the deep bedrock native copper to oxic conditions since formation is significantly less than Analogue Types D and E.

6.3 Analogue Type C. White Pine Mine Bedrock Native Copper – Long and Varied Native Copper History, likely less exposed to oxic conditions

Analogue Type C is similar to Type B in that the depth of extraction of the particular specimen is known to be relatively deep and the bedrock native copper was surrounded by anoxic brines. Analogue Type C encompasses only bedrock native copper in the subsurface of the White Pine Mine in which bedrock native copper veins (sheets) occur along thrust faults and related structures. The evolution affecting this native copper corrosion over the past ~1 Ga is generally known and the depth of extraction makes extended exposure to oxic conditions less likely. The presence of anoxic brines strongly supports limited exposure of the native copper to

oxic conditions. See Table 3 in Appendix 1 for sample availability and references.

Since precipitation of Analogue Type C native copper, the non-encased native copper surfaces have been exposed to anoxic brines. Anoxic brines seeped from fractures adjacent to native copper veins during mining. The bedrock native copper veins crosscut disseminated chalcocite mineralization. The chalcocite has been exposed to limited oxidation since formation about ~1 Ga ago (Bornhorst, personal communication), hence this type of bedrock native copper was also only exposed to little or no oxic conditions.

6.4 Analogue Type D. Keweenaw Peninsula Shallow Bedrock Native Copper – Long and Varied Native Copper History, likely more exposed to oxic conditions

Analogue Type D is the same as Type A and B except the extraction of the particular specimen is shallow. Analogue Type D encompasses all bedrock native copper in the subsurface of the Keweenaw Peninsula in which the cumulative environment of native copper corrosion over the past ~1 Ga is generally known and the shallowness of extraction makes an extended exposure of the native copper to oxic conditions more likely. In all mines, there

is documented evidence of oxic water at shallow depths of native copper extraction, which is consistent with current shallow depth of the bedrock native copper. Meteoric water infiltrates into mine openings along fractures/faults and interconnected pore space ultimately contributing to flooding of the mines. Mine sites allow careful description of the surrounding structural geology (potential groundwater flow paths). These shallow depths

of bedrock native copper may have first occurred between ~1 Ga–500 Ma ago caused by Precambrian erosion. Hence, those masses of bedrock native copper extracted from shallow depths may have been exposed to oxic waters over a significant amount of time prior to present exposure since removal of bedrock by erosion during Pleistocene glaciation. Type D has very likely been significantly more exposed to oxic waters than Types B and C. See Table 4 in Appendix 1 for sample availability and references.

6.5 Analogue Type E. Lake Superior Shallow Bedrock Native Copper

Analogue Type E is a subtype of Type D in which bedrock native copper is at the surface of the bottomlands of Lake Superior. Analogue Type E is otherwise the same as Analogue Type D shallow bedrock native copper except that the native copper has been submerged under fresh lake water since about 10 ka. Type E native copper has been exposed to the surface by the most recent glacial erosion, which ended about 10 ka ago and then subsequently

Since precipitation of Analogue Type D bedrock native copper, the surfaces of shallow bedrock native copper not completely encased in another mineral have been exposed to anoxic brines followed by oxic waters. Exposure time of the shallow bedrock native copper to oxic conditions since formation is significantly longer than Analogue Type B or C.

submerged under Lake Superior. Type E consists of *Great Sand Bay laker pocket* and *Gull Rock native copper* (see Section 5.4). Analogue Type E bedrock native copper is subject to potential corrosion as described above. *Great Sand Bay laker pocket* consists of cavity filling native copper crystals and represents an ideal target for the study of cumulative copper corrosion. See Table 5 in Appendix 1 for sample availability and references.

6.6 Analogue Type F. Keweenaw Peninsula Bedrock Native Copper Exposed to Supergene Weathering

Analogue Type F is proposed to be extreme oxic alteration of bedrock native copper by downward percolating oxic waters in the zone of aeration during the Precambrian. After precipitation of native copper at depth within the bedrock from main-stage hydrothermal fluids about 1.05 Ga ago, the region was exposed to a very long period of erosion from ~1.05 Ga to 500 Ma ago. This period of erosion is proposed to have resulted in the bedrock native copper, which formed at depth to end up near the Earth's surface. During this time interval, downward percolating oxic (meteoric) water within the zone of aeration would have led to supergene weathering of the native copper. The percolating water may have been slightly acidic. This oxic supergene weathering resulted in partial to near complete dissolution of native copper and precipitation of copper oxides, carbonates, and silicates. Only a few of the native copper deposits of the Keweenaw Peninsula clearly show supergene-style weathering. After the supergene weathering the rocks were submerged in anoxic brine for 100s

of million years followed by a variable interval of exposure to oxic–anoxic meteoric groundwater. See Table 6 in Appendix 1 for sample availability and references.

Since supergene weathering is restricted to few locations, it is possible that hydrologic conditions did not favor supergene weathering elsewhere. Alternatively, supergene weathering could have occurred at many deposits but subsequently eroded by the extended late Precambrian erosion episode prior to deposition of Paleozoic rocks. Paleozoic rocks covering the Keweenaw Peninsula made supergene weathering unlikely until all of the Paleozoic rocks were eroded, likely by Pleistocene glaciation. The water table after glacial retreat was near the surface making supergene alteration during the Pleistocene unlikely. It is possible that some of the Paleozoic rocks were removed during the Mesozoic to Cenozoic although there is no evidence to support this hypothesis. Removal during the Mesozoic to Cenozoic could have facilitated a second interval of supergene weathering.

6.7 Analogue Type G. Keweenaw Peninsula Bedrock Native Copper Exposed to Hydrothermal Sulfur

Analogue Type G can encompass all Keweenaw Peninsula bedrock native copper, where native copper mineralization is crosscut by late-stage hydrothermal veins and veinlets containing copper sulfide minerals. The contact between bedrock native copper and these late-stage veins or veins with demonstrated connection to late-stage hydrothermal fluids provides an opportunity for hydrothermal sulfur-related native copper corrosion. The late-stage hydrothermal fluids occurred throughout the district and thus, it is possible that

all native copper analogues of Types A, B, D, and E have been exposed to sulfur-bearing low temperature late-stage hydrothermal fluids. This late-stage hydrothermal event may have resulted in secondary hydrothermal fluid inclusions. After the late-stage hydrothermal event, the environment history follows the description of Types A, B, D, and E with significant exposure to anoxic brines for at least 100s of millions of years. See Table 7 in Appendix 1 for sample availability and references.

6.8 Analogue Type H. White Pine Mine – Bedrock Native Copper in contact with sulfide minerals

Analogue Type H represents bedrock native copper at the White Pine Mine that occurs along thrust-related faults and fractures (sheets) and is in physical contact with chalcocite (copper sulfide mineral) for ~1 Ga. Type H is a special subset of Analogue Type C in which the native copper is in physical contact with earlier precipitated disseminated, diagenetic chalcocite. This analogue only occurs at the

White Pine Mine in the southwest part of the mine. The physical contact between bedrock native copper and chalcocite would be a place for the native copper to undergo sulfur-bearing chemical reactions. The environmental history of Type H is otherwise identical to Type C. See Table 8 in Appendix 1 for sample availability and references.

6.9 Analogue Type I. Lake Superior Shallow Native Copper with Glaciated Surface (Great Sand Bay lake copper)

Analogue Type I is shallow bedrock native copper (Type D) on the bottomlands of Lake Superior, which has been glaciated during the last advance of continental glaciers about 10 ka ago. Type I is shallow native copper either observed or has been demonstrated to be connected to in place bedrock native copper. Type I has not been carried in the glacial ice (see *Great Sand Bay lake copper* in Section 5.4). Type I is Type E having a glaciated smoothed surface by abrasion during Pleistocene glaciation. The smoothed surface had pre-existing minerals

and copper alteration products stripped away from the surface. Thus, the current alteration products on these smoothed surfaces were formed in the last 10 ka after glacial retreat. Type I was submerged under Lake Superior and predecessor glacial lake waters for the last 10 ka. The corrosion of Type I native copper is a result of oxidative chemical reactions between infiltrating ground waters and native copper over the last 10 ka. See Table 9 in Appendix 1 for sample availability and references.

6.10 Analogue Type J. Lake Superior Native Copper Gravel (Great Sand Bay lake copper nuggets)

Analogue Type J is native copper gravel on the bottomlands of Lake Superior in Great Sand Bay (see *Great Sand Bay lake copper nuggets* in Section 5.4). Fragments of native copper were released from the bedrock by erosion. Glaciofluvial processes moved and smoothed the fragments and deposited many of them in bedrock cracks and crevasses. These fragments were likely carried over a very short distance but sufficient to smooth and round the frag-

ments which often removed previous native copper corrosion products resetting the copper corrosion clock to zero. Some fragments still have remnants of associated minerals on the surface of the native copper. The native copper corrosion products on smoothed and rounded surfaces are the result of chemical reaction with lake waters over the last 10 ka. See Table 10 in Appendix 1 for sample availability and references.

6.11 Analogue Type K. Glacial Native Copper (“Float Copper”)

Analogue Type K is native copper recovered from unconsolidated sediments such as glacial debris and surface soil. Native copper masses were plucked from the bedrock, deformed and abraded within a glacier, and transported by glaciers. These fragments are here called “float copper” as they were transported by “flotation” in glacial ice. Glacial transportation process partially led to completely smoothed and rounded the fragments. The smoothed and rounded surfaces were cleaned of other minerals and pre-existing native copper corrosion products resetting the copper corrosion clock to zero. These masses were deposited with glacial sediments on or very near the surface during the

retreat of the glaciers 10 ka ago. It may be difficult in all cases to be certain that the surface corrosion clock has been fully reset to zero and minerals. In pockets within glaciated float native copper masses or on irregular surfaces it is likely that previous copper corrosion products have not been cleaned off of the native copper and thus, represent an unknown time of exposure in different environments. Hence, these particular samples should be avoided for study due to uncertain geologic context. Native copper masses range in size from pebbles to many tons. See Table 11 in Appendix 1 for sample availability and references.

6.12 Analogue Type L. Native Copper Chisel Chips

Analogue Type L is native copper chiseled underground from large masses of native copper for easier transport to the surface. Chiseling resulted in chips with fresh native copper at their corrugated surface. The corrosion clock was reset to zero on these surfaces. Hand chiseling was common during the late 1800s and some of the chisel chips

were discarded with poor rock into surface rock piles. The corrugated native copper surfaces were corroded over the past 125 to 150 years by oxalic precipitation in the zone of aeration within the poor rock piles. See Table 12 in Appendix 1 for sample availability and references.

6.13 Native copper in clay (Type M)

Analogue Type M was identified during the MICA Phase I field excursion to Keweenaw Peninsula. Observations of clay filled fault and fracture systems were made at the Adventure and Quincy mines. Based on observations in the field it seems possible that native copper can be found within or near clays related to faults and fractures. These clays may have formed by the same hydrothermal processes that formed the native copper and the clays

would have inhibited fluid access to the native copper since soon after its precipitation. Careful sampling would be required from undisturbed zones, e.g., overcoring or block removal. Type D analogue with both copper and clay, or Type M, could potentially be analogues for the copper within engineered bentonite-based barriers. Analogue Type M sample availability is not discussed in Appendix 1

6.14 Other Analogues related to human activity

Other analogues related to human activity in the Keweenaw Peninsula could be recognized. These analogues include native copper used by indigenous peoples to make items such as spear and arrow points, fishhooks, and beads. For most of these, the copper corrosion clock was reset to by human activity such as manual abrasion and deformation. The cumulative corrosion of these items depends

on several factors such as physical location, water composition, and exposure times since indigenous peoples first occupied the Keweenaw Peninsula about 7 000 years ago after glacial retreat. We have chosen to not study these samples since we cannot be certain of the corrosion exposure times. Thus, these samples are avoided to study here.

7 ANALYTICAL METHODS UNDER CONSIDERATION FOR PHASE II

Representative key samples will be selected for full characterization from a combination of the Types described above. A potential Phase II of MICA will first focus on collecting a suite of samples with well described geologic setting and context. The samples to be studied in detail will be prioritized based on contributing to our understanding of natural corrosion of native copper under a variety of environmental settings. The prioritized samples will be systematically and progressively studied using analytical methods described and assessed

in Appendices 2 and 3. The analytical methods to be used may include others not listed since the list only includes state-of-the-art methods available at GTK.

Appendices 2 and 3 describe the analytical methods and provide preliminary analytical data to demonstrate the feasibility of using these techniques as part of Phase II. No conclusions regarding copper corrosion can be drawn from these data. They are provided to demonstrate GTK analytical capabilities to carry out MICA Phase II research.

7.1 Metallurgical properties

Native copper has precipitated in bedrock where physical conditions, fluid flow rate, temperature and pressure likely affected the growth of copper grains. For example, slow cooling allows copper crystals to grow coarser. Crystal structure is not readily seen on metal surfaces without etching, but zoning has been observed on some cross sections of Type K float copper (detailed study beyond scope of Phase I MICA).

Structural characteristics of native copper samples can be used to:

- a. compare the native copper with canister metal to assess their textural similarities and differences;
- b. assess if there is an effect on corrosion; and
- c. assess there is an effect on mechanical integrity of copper.

Physical metallurgy studies crystallography, material characterization, mechanical metallurgy, and phase transformations require special expertise and methods, which GTK does not have, but are available in universities.

7.2 Supporting geological investigations related to copper samples

Native copper samples are the focus of MICA. The collection of research material is extensive, and it provides an excellent possibility to launch many kinds of studies. Depending on the scope of Phase II, supporting investigations may be needed, especially in case in situ samples can be accessed. These may include:

- Detailed study of the geological context
- Assessing the hydrogeological context (relevant to all sample types)
- Groundwater/surface water chemistry (relevant to all sample types)

- Assessing regional low temperature hydrothermal fluids after native copper precipitation
- Geochemical profiling surrounding the samples, (e.g., second-hand information from Type K float copper prospectors indicates that the float copper masses are surrounded by a greenish halo in the soil (Ken Flood, pers. comm.))
- Fracture mineral studies (in case of drill core samples)

GTK has extensive experience in investigating the geological and environmental context of geological samples.

8 DISCUSSION AND RECOMMENDATIONS

Overall, based on the recent safety cases, native copper is stable in anoxic conditions but sulfidation can result in significant corrosion of copper in some future scenarios (e.g., Posiva 2021a). Copper is not stable in oxic conditions but oxic alteration is expected to take place only during short a period of time during the storage and emplacement of the copper canisters. Analogues discussed above demonstrate that despite oxic conditions, native copper alteration is limited by surface alteration products themselves (passivation).

The salinity range of interest in safety cases can cover all conditions from fresh water to brine depending on the site. The existing known analogues described in detail so far (see Section 2.2) are from sites with fresh groundwater compositions (Finnish sites) or where the chemistry of the system has not been very clearly defined (Littleham cove). The salinity range of interest can be covered from the various types of Keweenaw Peninsula analogues. So far, the statements of copper stability in safety case assessments based on using a Keweenaw Peninsula analogue have been quite general, such as copper is stable in an environment that exhibited a moderate, near-neutral pH, low level of dissolved solids and low redox potential (as low as -0.25 VSHE) (Crisman & Jacobs 1982).

Recently, King (2021) published a thorough review on the copper analogues and their use in the safety case focused on the NWMO concept (see Section 3.2.3). King's recommendations are incorporated into this report. However, in addition to direct safety case use for NWMO, the main aspect to be considered in MICA is related to producing data to describe the native copper occurrences and related corrosion rates (or conditions for no corrosion). The copper corrosion rates are needed for overall process understanding that complements mass balance approaches taken in safety cases. Analogues are often considered for safety cases as an alternative line of evidence. In addition, topics of interest for new studies may arise from other concepts or designs (e.g., potential topics related to mechanical integrity of copper as well as deformation). It is possible to estimate corrosion rates for various settings (see Chapter 6). In addition to corrosion, passivation of native copper corrosion by corrosion minerals themselves can be examined. In safety cases, passivation due to corrosion

is considered as a negative feature as it may lead to enhanced pitting corrosion (see King et al. 2012 and Section 2.2). This phenomenon has not yet been described via natural analogues, but overall oxic alteration minerals are known to passivate native copper from extensive alteration.

One of the biggest design differences in the repository concepts considered in this project is the overall thickness of the copper in the waste packaging. While NWMO's concept has 3 mm layer of copper, SKB KBS-3 design relies of 5 cm of copper in the canister design. Keweenaw Peninsula native copper occurrences provide samples that are relevant for both thicknesses.

MICA Phase I has identified and described the environmental conditions of a set of natural analogues applicable to copper corrosion of canisters used to isolate high-level nuclear waste from the environment. Phase I has also demonstrated that samples are available that can be used to study copper corrosion. Carefully selected and representative samples subjected to the various environmental conditions will be obtained at the outset of MICA Phase II.

The corrosion of native copper will be described and analyzed during Phase II. The results of these studies will help to better understand the processes, the environmental conditions, and the rates of copper corrosion. The inventory of analogues and available samples (Chapter 6 and Appendix 1 demonstrates the potential for useful Phase II results.

This report is supplemented with preliminary analytical work reported in Appendix 2 and 3. No conclusions regarding copper corrosion can be drawn from these data. These data are provided to demonstrate GTK analytical capabilities to carry out MICA Phase II research.

The proposal for the Phase II will focus on analogue investigations utilizing the samples that

- have good potential to increase our understanding of the big picture and therefore provide a better set of natural analogue data for an alternative line of evidence supplementing the quantitative safety case;
- cover the most obvious gaps in safety case knowledge; and
- are relevant to the safety case and repository design (and design optimization).

In this report, no Phase II budgetary restrictions have been considered. This is to be done in separately after defining the final objectives and

tasks of Phase II. In Table 7 preliminary scoring of the potential analogues for the Phase II studies is presented.

Table 7. Preliminary scoring of the potential analogue types for Phase II studies.

Type	Description	Scoring (1-3)*
*1=RECOMMENDED FOR PHASE II, 2=POTENTIALLY RELEVANT, 3=NOT SAFETY CASE RELEVANT		
A	Long and Varied History of Keweenaw Peninsula Bedrock Native Copper in the Subsurface	1
B	Keweenaw Peninsula Deep Bedrock Native Copper – Long and Varied Native Copper History, Likely Less Exposed to Oxidic Conditions.	1
C	White Pine Mine Bedrock Native Copper – Long and Varied Native Copper History, Likely Less Exposed to Oxidic Conditions.	2
D	Keweenaw Peninsula Shallow Bedrock Native Copper - Long and Varied Native Copper History, Likely More Exposed to Oxidic Conditions.	1
E	Lake Superior Shallow Bedrock Native Copper	1
F	Keweenaw Peninsula Bedrock Native Copper Exposed to Supergene Weathering	3
G	Keweenaw Peninsula Bedrock Native Copper Exposed to Hydrothermal Sulfur	1
H	White Pine Mine – Bedrock Native Copper in Contact with Sulfide minerals	2
I	Lake Superior Shallow Native Copper with Glaciated Surface (Great Sand Bay Lake Copper)	3
J	Lake Superior Native Copper Gravel (Great Sand Bay Lake Copper Nuggets)	1
K	Glacial Native Copper ("Float Copper")	1
L	Native Copper Chisel Chips	2
M	Native Copper in Clay	1

9 CONCLUSIONS

This report has reviewed the relevant literature regarding the background for the project including detailed description of the geological history of the potential analogues providing a context for future work.

Thirteen types of analogues have been identified and described. For each analogue, the availability of samples for copper corrosion research has been assessed. Samples are available from all the analogues. There is a wealth of established geological context useful for Phase II.

From safety case perspective, the potential analogues identified allow corrosion studies (with rate estimates) on sites where conditions are repository relevant (expected evolution of the repository), but

also for settings that have more extreme conditions (relevant to disturbance scenarios). In addition, there are several process topics of interest that may provide specific input for the safety case (e.g., deformation of native copper being studied by NWMO).

This report provides a starting point for the MICA Phase II.

The preliminary analysis of samples (Appendix 3) shows good capability regarding physical, mineralogical, geochemical, and isotopic analyses for the future investigation phases. Additional methods may be considered.

REFERENCES

- Abrajano, T. A. & Pasteris, J. D. 1989.** Zambales ophiolite, Philippines II. Sulfide petrology of the critical zone of the Acoje Massif. *Contributions to Mineralogy and Petrology*, v. 103, 64–77.
- Akbarpour, A., Gholami, N., Azizi, H. & Torab, F. 2012.** Cluster and R-mode factor analyses on soil geochemical data of Masjed-Daghi exploration area, north-western Iran. *Arabian Journal of Geosciences* 6. Available at: <https://doi.org/10.1007/s12517-012-0596-4>
- Alexander, W. R., Reijonen, H. M. & McKinley, I. 2015.** Natural analogues: studies of geological processes relevant to radioactive waste disposal in deep geological repositories. *Swiss Journal of Geosciences* 108, 75–100.
- Alireza, R., Bakhsh, A. & Sohrabi, G. 2019.** Copper Man-to-type Mineralization in the Mejdar Volcanic Rocks, Southeast of Ardabil. Conference paper. The 10th National Geological Conference of Payame Noor University, University of Tabriz.
- Barkov, A. Y., Tarkian, M., Laajoki, K. V. O. & Gehör, S. A. 1998.** Primary platinum-bearing copper from the Lesnaya Varaka ultramafic alkaline complex, Kola Peninsula, northwestern Russia. *Mineralogy and Petrology*, v. 62, 61–72.
- Bebber, M. & Key, A. 2022.** Optimal Linear Estimation (OLE) Modeling Supports Early Holocene (9000–8000 RCYBP) Copper Tool Production in North America. *American Antiquity*, 1–17. Available at: <https://doi.org/10.1017/aaq.2021.121>
- Bell, J., Burkin, J. & Dick, L. 2020.** ARCTIC RIFT COPPER Part of world's newest metallogenic province: Kif-faanngissuseq. Available at: <https://doi.org/10.13140/RG.2.2.18610.84161>
- Bevins, R. E., Rowbotham, G. & Robinson, D. 1991.** Zeolite to Prehnite-pumpellyite Facies Metamorphism of the Late Proterozoic Zig-Zag Dal Basalt Formation, Eastern North Greenland. *Elsevier, Lithos*, v. 27, 155–165. Available at: [https://doi.org/10.1016/0024-4937\(91\)90010-I](https://doi.org/10.1016/0024-4937(91)90010-I)
- Białowolska, A., Bakun-Czubarow, N. & Fedoryshyn, Y. 2002.** Neoproterozoic flood basalts of the upper beds of the Volhynian Series (East European craton). *Geological Quarterly*, v. 46, 37–57.
- Bodden, T. J. 2019.** Spatial and Temporal Distribution of Hydrothermal Minerals and Sources of Hydrothermal Minerals Inferred from Light Stable Isotopes, Keweenaw Peninsula Native Copper District, Michigan. Master's Thesis, Michigan Technological University, 1–87.
- Bodden, T. J., Bornhorst, T. J., Bégué, F. & Deering, C. 2022.** Sources of Hydrothermal Fluids Inferred from Oxygen and Carbon Isotope Composition of Calcite, Keweenaw Peninsula Native Copper District, Michigan, USA. *Minerals* 2022, v. 12, p. 474. Available at: <https://doi.org/10.3390/min12040474>
- Bornhorst, T. J. 1997.** Tectonic context of native copper deposits of the North American Midcontinent Rift system. *Geol. Soc. Am. Spec. Pap.* 1997, v. 312, 127–136.
- Bornhorst, T. J. 2017.** Float copper, Keweenaw Peninsula, Michigan. A. E. Seaman Mineral Museum, Web Publication, v. 3, p. 4.
- Bornhorst, T. J. & Barron, R. J. 2011.** Copper deposits of the western Upper Peninsula of Michigan. *Geological Society of America*. Available at: [http://doi.org/10.1130/2011.0024\(05\)](http://doi.org/10.1130/2011.0024(05))
- Bornhorst, T. J. & Barron, R. J. 2017.** Discovery and geology of the Guinness world record Lake Copper, Lake Superior, Michigan. A. E. Seaman Mineral Museum, Web Publication, v. 2, p. 8.
- Bornhorst, T. J. & Lankton, L. D. 2009.** Copper mining: A billion years of geologic and human history. In: Schaetzl, R., Darden, J. & Brandt, D. (eds) *Michigan Geography and Geology*. New York: Pearson Custom Publishing, 150–173.
- Bornhorst, T. J. & Mathur, R. 2017.** Copper Isotope Constraints on the Genesis of the Keweenaw Peninsula Native Copper District, Michigan, USA. *Minerals* 2017, v. 7, 185.
- Bornhorst, T. J. & Mathur, R. 2018.** Copper isotope constraints on the genesis of the Keweenaw Peninsula Native Copper District, Michigan, USA. *Reply. Minerals* 2018, v. 8, p. 508.
- Bornhorst, T. J. & McDowell, S. D. 1992.** Michigan Tech Earth Science Laboratory and Experimental Mine connecting with the Quincy Native Copper Mine, Michigan. *Society of Economic Geologists Guidebook Series*, v. 13, 100–104.
- Bornhorst, T. J. & Robinson, G. W. 2004.** Precambrian aged supergene alteration of native copper deposits in the Keweenaw Peninsula: Michigan. *Institute on Lake Superior Geology Proceedings and Abstracts*, v. 50, no. part 1, 40–41.
- Bornhorst, T. J. & Woodruff, L. G. 1997.** Native copper precipitation by fluid-mixing Keweenaw Peninsula, Michigan. *Inst. Lake Super. Geol. Proc.* 1997, 4 Pt 1, 9–10.
- Bornhorst, T. J., Paces, J. B., Grant, N. K., Obradovich, J. D. & Huber, N. K. 1988.** Age of native copper mineralization, Keweenaw Peninsula, Michigan. *Economic Geology*, v. 83, 619–625.
- Boyle, C. H. & Meguid, S. A. 2015.** Mechanical performance of integrally bonded copper coatings for the long term disposal of used nuclear fuel. *Nuclear Engineering and Design*, v. 293, 403–412. Available at: <https://doi.org/10.1016/j.nucengdes.2015.08.011>
- Britannica 2020.** The Editors of Encyclopaedia. “Copper”. *Encyclopedia Britannica*, 28 Oct. 2020. Available at: <https://www.britannica.com/science/copper>. [Accessed 2 March 2021]
- Brown, A. C. 1971.** Zoning in the White Pine Copper deposit, Ontonagon County, Michigan. *Economic Geology*, v. 66, 543–573.
- Brown, A. C. 2006.** Genesis of native copper lodes in the Keweenaw Peninsula, northern Michigan. A hybrid evolved meteoric and metamorphogenic model. *Economic Geology* 2006, v. 101, 1437–1444.
- Brown, A. C. 2008.** District-scale concentration of native copper lodes from a tectonically induced thermal plume of ore fluids on the Keweenaw Peninsula, Northern Michigan. *Economic Geology*, v. 103, 1691–1694.
- Bumgarner, E. L. 1980.** The geology of the Portage Lake Volcanics in the M.T.U. mining laboratory, Hancock, Michigan. M.S. Thesis, Michigan Technological University. 138 p.
- Butler, B. S. & Burbank, W. S. 1929.** The Copper Deposits of Michigan. U.S. Geological Survey, Professional Paper 144.
- Catacosinos, P. A., Harrison, W. B., Reynolds, R. F., Westjohn, D. B. & Wollensak, M. S. 2001.** Stratigraphic Lexicon for Michigan. Michigan Department of Environmental Quality, Geologic Survey Division Bulletin 8.
- Chamberlain, J. A., MacLeod, G. R., Trail, J. & Lachance, G. R. 1965.** Native metals in the Muskox intrusion. *Can. J. Earth Sci.* 2 (1965), 188–215

- Cohen, K. M., Finney, S. C., Gibbard, P. L. & Fan, J.-X. 2013. updated 2020. The ICS International Chronostratigraphic Chart. Episodes 36, 199–204.
- Cook, S. S. 1988. Supergene Copper Mineralization at the Lakeshore Mine, Pinal County, Arizona. *Economic Geology*, v. 83, 297–309
- Côme, B. & Chapman, N. A. 1987. Natural Analogues in Radioactive Waste Disposal. United Kingdom. 492 p. Available at: <https://doi.org/10.1007/978-94-009-3465-8>
- Cornwall, H. R. 1956. A summary of ideas on the origin of native copper deposits. *Economic Geology* (1956) 51 (7), 615–631. Available at: <https://doi.org/10.2113/gsecongeo.51.7.615>
- Crisman, D. P. & Jacobs, G. K. 1982. Native copper deposits of the Portage Lake volcanics, Michigan: their implications with respect to canister stability for nuclear waste isolation in the Columbia River basalts beneath Hanford Site, Washington. Rockwell International report for the U.S. Department of Energy RHO-BW-ST-26 P.
- Diomidis, N., Johnson, L., Bastid, P. & Allen, C. 2017. Design development of a copper-coated canister for the disposal of spent fuel in a deep geological repository in Opalinus Clay. *Corrosion Engineering, Science and Technology*, v. 52, 31–39. Available at: <https://doi.org/10.1080/1478422X.2017.1292200>
- Emetz, A. V., Zagnitko, V. M. & Prykhod'ko, V. L. 2005. Mineral compositions and genesis of the ore bodies of the Zhyrychi Cu deposit (North-Western Ukraine). *Mineralogical Journal (Ukraine)*, v. 27, 77–91.
- Hall, D. S., Behazin, M., Binns, W. J. & Keech, P. G. 2021. An evaluation of corrosion processes affecting copper-coated nuclear waste containers in a deep geological repository. *Progress in Materials Science*, v. 118, 100766. Available at: <https://doi.org/10.1016/j.pmatsci.2020.100766>
- Hekinian, R. 1974. Petrology of igneous rocks from Leg 22 in the Northeastern Indian Ocean. Initial Reports of the Deep Sea Drilling Project, v. 22, 413–447.
- Hoffman, P. F., Kaufman, A. J., Halverson, G. P. & Schrag, D. P. 1998. A Neoproterozoic snowball Earth. *Science*, v. 281, 1342–1346. Available at: <https://doi.org/10.1126/science.281.5381.1342>
- Hofmeister, A. M. & Rossman, G. R. 1985. Exsolution of metallic copper from Lake County labradorite. *Geology*, v. 13, 644–647. Available at: [https://doi.org/10.1130/00917613\(1985\)13<644:EOMCFL>2.0.CO;2](https://doi.org/10.1130/00917613(1985)13<644:EOMCFL>2.0.CO;2)
- Houghton, D. 1841. [Fourth] annual report of the State Geologist. Michigan House of Representatives [Doc.] no. 27. 184 p.
- IAEA (International Atomic Energy Agency) 1989. Natural Analogues in Performance Assessments for the Disposal of Long Lived Radioactive Wastes. IAEA, Technical Reports Series No. 304.
- IAEA (International Atomic Energy Agency) 1999. Use of natural analogues to support radionuclide transport models for deep geological repositories for long lived radioactive wastes. IAEA, IAEA-TECDOC-1109.
- Ikehata, K. & Hirata, T. 2012. Copper isotope characteristics of copper-rich minerals from the Horoman peridotite complex, Hokkaido, northern Japan. *Economic Geology*, v. 107, 1489–1497.
- Ikehata, K., Chida, K., Tsunogae, T. & Bornhorst, T. 2016. Hydrothermal native copper in Ocean Island Alkali basalt from the Mineoka Belt, Boso Peninsula, Central Japan. *Economic Geology*, v. 111, 783–794. Available at: <https://doi.org/10.2113/econgeo.111.3.783>
- Jackson, C. P., Jefferies, N. L., Alexander, R., Smith, J., Friege, B., Gauss, I., Vomvoris, S., Metcalfe, R. & Marsden, R. 2014. Sealing deep site investigation boreholes. Phase 1 report. RWMS/03/042. Radioactive Waste Management Ltd. 200 p.
- Johnson, C. M., Beard, B. L. & Roden, E. E. 2008. The iron isotope fingerprints of redox and biogeochemical cycling in modern and ancient Earth. *Annu. Rev. Earth Planet. Sci.*, v. 36, 457–493.
- Jolly, W. T. 1974. Behavior of Cu, Zn, and Ni during prehnite–pumpellyite rank metamorphism of the Keweenaw basalts, northern Michigan. *Econ. Geol.*, v. 69, 1118–1125.
- Kelly, D. 2020. Fluid inclusion study of selected calcite associated with native copper, Quincy mine, Keweenaw Peninsula, Michigan. Open Access Master's Report, Michigan Technological University. 65 p.
- Kelly, D., Bornhorst, T. J. & Deering, C. 2022. Fluid inclusions in euhedral calcite crystals from the Quincy Mine, Keweenaw Peninsula native copper district, Michigan. In: Easton, R. M. (ed.) *Institute on Lake Superior Geology Proceedings, 68th Annual Meeting*, Sudbury, Ontario, Part 1 – Abstracts and Proceedings, v. 68, part 1, 35–36.
- Kelly, W. C., Rye, R. O. & Livnat, A. 1986. Saline minewaters of the Keweenaw Peninsula, northern Michigan. Their nature, origin, and relation to similar deep waters in Precambrian crystalline rocks of the Canadian Shield. *American Journal of Science*, v. 286, 281–308.
- King, F. 2021. Natural Analogues and their Use in Supporting the Prediction of the Long-Term Corrosion Behaviour of Copper-coated UFC. NWMO TR-2021-19. Toronto, Ontario. 207 p.
- King, F., Ahonen, L., Taxén, C., Vuorinen, U. & Werme, L. 2001. Copper corrosion under expected conditions in a deep geologic repository. *Svensk Kärnbränslehantering AB, SKB TR-01-23*.
- King, F., Lilja, C., Pedersen, K., Pitkänen, P. & Vähänen, M. 2012. An update of the state-of-the-art report on the corrosion of copper under expected conditions in a deep geologic repository. Posiva Oy, Posiva 2011-01. (Also published as SKB TR-10-67.)
- King, F., Puigdomenech, I. & Lilja, C. 2021. Effect of high groundwater chloride concentration on the corrosion of copper canisters. Posiva Oy, Working Report 2021-10.
- Kitakaze, A. 1998. Sulfide minerals from the Horoman peridotite, Hokkaido, Japan. *Journal of Mineralogy, Petrology and Economic Geology*, v. 93, 369–379.
- Kitakaze, A., Ito, H. & Komatsu, R. 2011. Horomanite, (Fe, Ni, Co, Cu)₉S₈, and samaniite, Cu₂(Fe, Ni)₇S₈, new mineral species from the Horoman peridotite massif, Hokkaido, Japan. *Journal of Mineralogical and Petrological Sciences*, v. 106, 204–210.
- Klasner, J. S., Cannon, W. F. & Van Schmus, W. R. 1982. The pre-Keweenaw tectonic history of southern Canadian Shield and its influence on formation of the Midcontinent Rift. In: Wold, R. J. & Hinze, W. J. *Geology and Tectonics of the Lake Superior Basin*.
- Kojima, S., Trista-Aguilera, D. & Hayashi, K. 2009. Genetic Aspects of the Manto-type Copper Deposits Based on Geochemical Studies of North Chilean Deposits. *Resource Geology*, v. 59, 87–98. Available at: <https://doi.org/10.1111/j.1751-3928.2008.00081.x>
- Lane, A. C. 1911. The Keweenaw series of Michigan. Michigan Geol. and Biol. Survey, pub. 6, Geol. set. 4, 2 vols. 983 p.
- Lankton, L. D. & Hyde, C. K. 1982. Old Reliable – an illustrated history of the Quincy Mining Company. Hancock: The Quincy Mine Hoist Association. 159 p.
- Larson, P. B., Maher, K., Ramos, F. C., Chang, Z., Gaspar, M. & Meinert, L. D. 2003. Copper isotope ratios in magmatic and hydrothermal ore-forming environments. *Chemical Geology*, v. 201(3–4), 337–350.

- LeHuray, A. P. 1989.** Native copper in ODP site 642 tholeiites. Proceedings of the Ocean Drilling Program, Scientific Results, v. 104, 411–417.
- Lilja, C., King, F., Puigdomenech, I. & Pastina, B. 2020.** Speciation of copper in high chloride concentrations, in the context of corrosion of copper canisters. Materials and Corrosion, 72 (1–2), 293–299.
- Livnat, A. 1983.** Metamorphism and Copper Mineralization of the Portage Lake Lava Series, Northern Michigan. Ann Arbor: University of Michigan, 1–292. (Ph.D. Dissertation)
- Lorand, J. P. 1987.** Cu-Fe-Ni-S mineral assemblages in upper-mantle peridotites from the Table Mountain and Blow-Me-Down Mountain ophiolite massifs (Bay of Islands area, Newfoundland). Their relationships with fluids and silicate melts. Lithos, v. 20, 59–76.
- MacLennan, S. A., Eddy, M. P., Mersch, A. J., Mehra, A. K., Crockford, P. W., Maloof, A. C., Southworth, C. S. & Schoene, B. 2020.** Geologic evidence for an icehouse Earth before the Sturtian global glaciation. Science Advances, v. 6 (24), p. 6647
- Marcos, N. 1989.** Occurrences of Native Copper as the Natural Analogue of Copper Canisters (Barrier of Nuclear Waste). Master's thesis, Helsinki University of Technology. 85 p.
- Marcos, N. 2002.** Lessons from nature. The behaviour of technical and natural barriers in the geological disposal of spent nuclear fuel. Finnish Academy of Technology, Acta Polytechnica Scandinavica, Civil Engineering and Building Construction Series No. 124.
- Marcos, N. & Ahonen, L. 1999.** New data on the Hyrkkölä U-Cu mineralization. The behaviour of native copper in a natural environment. Posiva Oy, Posiva Report 99-23. 68 p.
- Markl, G., Lahaye, Y. & Schwinn, G. 2006.** Copper isotopes as monitors of redox processes in hydrothermal mineralization. Geochimica et Cosmochimica Acta 70(16), 4215–4228.
- Martin, S. R. (ed.) 1993.** 20KE20: Excavations at a Prehistoric. Copper Workshop. Michigan Archaeologist, v. 39 (3–4), 127–193.
- Mathur, R. & Wang, D. 2019.** Transition metal isotopes applied to exploration geochemistry. Insights from Fe, Cu, and Zn. Ore Deposits. Origin, Exploration, and Exploitation, 163–183.
- Mauk, J. L. & Hancock, R. G. V. 1998.** Trace element geochemistry of native copper from the White Pine mine, Michigan, U.S.A.: implications for sourcing artifacts. Archaeometry, v. 40, 97–107. Available at: <https://doi.org/10.1111/j.1475-4754.1998.tb00826.x>
- Mauk, J. L., Kelly, W. C., van der Pluijm, B. A. & Sear, R. W. 1992.** Relations between deformation and sediment-hosted copper mineralization. Evidence from the White Pine portion of the Midcontinent Rift system. Geology, v. 20, 427–430.
- McKay, C. P. 2000.** Thickness of tropical ice and photosynthesis on a Snowball Earth. Geophysical Research Letters 27, 2153–2156. Available at: <https://doi.org/10.1029/2000GL008525>
- Miller, W. M., Alexander, W. R., Chapman, N. A., McKinley, I. G. & Smellie, J. A. T. 2000.** The geological disposal of radioactive wastes and natural analogues. Lessons from nature and archaeology. Waste management series, v. 2. Oxford: Elsevier Science Ltd. Pergamon. 332 p.
- Milodowski, A. E., Styles M. T., Horstwood, M. S. A. & Kemp, S. J. 2002.** Alteration of uraniferous and native copper concretions in the Permian mudrocks of south Devon, United Kingdom. Swedish Nuclear Fuel and Waste Management Company (SKB), SKB Technical Report TR-02-09.
- Mindat.org. 2021.** Copper. Hudson Institute of Mineralogy. Available at: www.mindat.org/show.php?id=1209. [Accessed 2 March 2021]
- Muñoz, J. O. 1975.** On stratiform copper deposits of Chile. Annales de la Société Géologique de Belgique, T. 98, 17–21.
- Murr, L. E. 2015.** A Brief History of Metals. In: Handbook of Materials Structures, Properties, Processing and Performance. Cham: Springer. Available at: https://doi.org/10.1007/978-3-319-01815-7_1
- Nagle, F., Fink, L. K., Boström, K. & Stipp, J. J. 1973.** Copper in pillow basalts from La Désirade, Lesser Antilles island arc. Earth and Planetary Science Letters, v. 19, 193–197.
- Nanni 1750 BC.** A Complaint to Ea-nasir. (In: Akkadian cuneiform. Translated by Figulla, H. H. & Martin, W. J. (eds) 1953. Letters and Business Documents of the Old Babylonian Period. Ur Excavations: Texts. V. London: British Museum Press.)
- NEA 2019.** International Features, Events and Processes (IFEP). List for the Deep Geological Disposal of Radioactive Waste. Version 3.0. NEA/RWM/R(2019)1. Paris: OECD/Nuclear Energy Agency (NEA). Available at: https://www.oecd-neo.org/jcms/pl_19906. [Accessed 1 April 2021]
- NEA 2000.** Geologic Disposal of Radioactive Waste in Perspective. General Information. Paris: OECD/Nuclear Energy Agency (NEA).
- Neumann, H. 1944.** Native Copper and Silver Ore Deposits in Dalane, Norway. Norsk Geologisk Tidsskrift, v. 23, 214–219.
- Nezafati, N., Momenzadeh, M. & Pernicka, E. 2005.** Darband copper occurrence. An example of Michigan-type native copper deposits in central Iran. In: Mao, J. & Bierlein F. P. (eds) Mineral Deposit Research: Meeting the Global Challenge. Berlin, Heidelberg: Springer. Available at: https://doi.org/10.1007/3-540-27946-6_43
- NWMO 2011.** Geosynthesis. Report NWMO DGR-TR2011-11 R000, March, Toronto, Canada.
- Pinto, V. M., Hartmann, L. A. & Wildner, W. 2011.** Epigenetic hydrothermal origin of native copper and supergene enrichment in the Vista Alegre district, Paraná basaltic province, southernmost Brazil. International Geology Review, v. 53–(10), 1163–1179. Available at: <https://doi.org/10.1080/00206810903464547>
- Pompeani, D., Steinman, B., Abbott, M., Pompeani, K., Reardon, W., DePasqual, S. & Mueller, R. 2021.** On the timing of the Old Copper Complex in North America. A comparison of radiocarbon dates from different archaeological contexts. Radiocarbon, v. 63(2), 513–531. Available at: <https://doi.org/10.1017/RDC.2021.7>
- Posiva 2012.** Safety case for the disposal of spent nuclear fuel at Olkiluoto – Complementary Considerations 2012. Posiva Oy, POSIVA 2012-11. 262 p.
- Posiva 2021a.** Canister evolution. Posiva Oy, Posiva working report WR 2021-06. 351 p.
- Posiva 2021b.** Safety Case for the Operating Licence Application – Performance Assessment and Formulation of Scenarios (PAFOS). Posiva Oy, POSIVA 2021-06.
- Posiva 2021c.** Olkiluoto Site Description 2018. Posiva Oy, POSIVA 2021-10.
- Posiva SKB 2017.** Safety functions, performance targets and technical design requirements for a KBS-3V repository. Conclusions and recommendations from a joint SKB and Posiva working group. Posiva SKB, Report 01. 116 p.
- Pu, J. P., Bowring, S. A., Ramezani, J., Myrow, P., Raub, T. D., Landing, E., Mills, A., Hodgins, E. & Macdonald, F. A. 2016.** Dodging snowballs. Geochronology of the

- Gaskiers glaciation and the first appearance of the Ediacaran biota. *Geology*, v. 44, 955–958.
- Räisänen, E. 1986.** Uraniferous granitic veins in the Svecofennian schist belt in Nummi–Pusula, Southern Finland. Technical Committee Meeting on Uranium Deposits In Magmatic and Metamorphic rocks. Report IAEA-TC-521, 37–44.
- Rapp, G., Allert, J., Vitali, V., Jing, Z. & Henrickson, E. 2000.** Determining geologic sources of artifact copper – Source characterization using trace element patterns. University Press of America. 156 p.
- Reijonen, H., Alexander, W. R., Marcos, N. & Lehtinen, A. 2015.** Complementary considerations in the safety case for the deep repository at Olkiluoto, Finland: support from natural analogues. *Swiss Journal of Geosciences*, v. 108(1), 111–120.
- Rosemeyer, T. 2002.** News from the Keweenaw: Part 2. Recent Mineral finds in Michigan’s Copper Country. Seventh in a series of articles on the mines and minerals of Michigan’s Copper Country. *Rocks & Minerals*, v. 77, no. 6, 378–394.
- Rosemeyer, T. 2009.** A 2008 Lake Superior Bonanza of Copper Crystals Keweenaw Co. MI. *Rocks & Minerals*, v. 84, no. 1, 32–41.
- Rosemeyer, T. & Carlson, S. M. 2000.** Mineralogy of Point Prospect, Keweenaw County, Michigan. *Rocks & Minerals*, v. 75, no. 4, 222–228.
- Ruiz, C. 1965.** *Geología y Yacimientos Metalíferos de Chile*. Inst. Invest. Geológicas Santiago. 305 p.
- RWM 2016.** Geological Disposal Technical Background to the generic Disposal System Safety Case. NDA Report no. DSSC/421/01.
- Salonen, V.-P. 1986.** Glacial transport distance distributions of surface boulders in Finland. Geological Survey of Finland, Bulletin 338. 57 p. Available at: https://tupa.gtk.fi/julkaisu/bulletin/bt_338.pdf
- Schleiss, W. A. 1986.** A study of vein mineralization and wall rock alteration at the Delaware Mine, Keweenaw County, Michigan. M.S. Thesis, Michigan Technological University. 86 p.
- Sikka, D. B., Petruk, W., Nehru, C. E. & Zhang, Z. 1991.** Geochemistry of secondary copper minerals from Proterozoic porphyry copper deposit, Malanjkhand, India. *Ore Geology Reviews*, v. 6, 257–290.
- SKB 2006.** Long-term safety for KBS-3 repositories at Forsmark and Laxemar – a first evaluation Main Report of the SR-Can project. Solna: Svensk Kärnbränslehantering AB. 620 p.
- SKB 2008.** Site description of Forsmark at completion of the site investigation phase. SDM-Site Forsmark. Svensk Kärnbränslehantering AB, SKB TR-08-05.
- SKB 2010a.** Design and production of the KBS-3 repository. Svensk Kärnbränslehantering AB, Technical Report TR-10-12. 60 p.
- SKB 2010b.** Design, production and initial state of the canister. Svensk Kärnbränslehantering AB, Technical Report TR-10-14. 110 p.
- SKB 2011.** Long-term safety for the final repository for spent nuclear fuel at Forsmark – Main report of the SR-Site project. Svensk Kärnbränslehantering AB, Technical Report TR-11-01. 552 p.
- Stacey, J. T. & Kramers, J. D. 1975.** Approximation of terrestrial lead isotope evolution by a two-stage model. *Earth and planetary science letters*, v. 26(2), 207–221.
- Stein, C. A., Kley, J. Stein, S. Hindle, D. & Keller, G. R. 2015.** North America’s Midcontinent Rift. When rift met LIP. *Geosphere*, v. 11, 1607–1616.
- Stoiber, R. E. & Davidson, E. S. 1959.** Amygdular mineral zoning in the Portage Lake Lava Series, Michigan copper district. *Economic Geology*, v. 54, pt. I, 1250–1277, pt. II, 1444–1460.
- Swanson-Hysell, N. L. 2021.** Chapter 4 – The Precambrian paleogeography of Laurentia. In: Pesonen, L. J., Salminen, J., Elming, S.-Å., Evans, D. A. D. & Veikkolainen, T. (eds) *Ancient Supercontinents and the Paleogeography of Earth*. Elsevier, 109–153. Available at: <https://doi.org/10.1016/B978-0-12-818533-9.00009-6>
- Trüstedt, O. 1907.** Die Erzlagerstätten von Pitkaranta am Ladoga-See. Geological Survey of Finland, Bulletin 19. 333 p. Available at: https://tupa.gtk.fi/julkaisu/bulletin/bt_019.pdf
- Tullborg, E. L., Smellie, J., Nilsson, A. Ch., Gimeno, M. J., Brüchert, V. & Molinero, J. 2010.** SR-Site – sulphide content in the groundwater at Forsmark. Svensk Kärnbränslehantering AB (SKB), SKB TR-10-30. 214 p.
- Van Schmus, W. R. 1992.** Tectonic setting of the Midcontinent Rift system. *Tectonophysics* 213, 1–15. Available at: [https://doi.org/10.1016/0040-1951\(92\)90247-4](https://doi.org/10.1016/0040-1951(92)90247-4)
- Velbel, M. A. 2009.** The “Lost Interval”. Michigan Geology from the Permian to the Pliocene. In: Schaetzl, R. J., Darden, J. T. & Brandt, D. S. (eds) *Michigan Geography and Geology*. Boston: Pearson Custom Publishing, 60–68.
- Wang, C. Y., Zhou, M.-F., Qi, L., Hou, S., Gao, H., Zhang, Z. & Malpas, J. 2006.** The Zhaotong native copper deposit associated with the Permian Emeishan flood basalts, Yunnan, southwest China. *International Geology Review*, v. 48, 742–753.
- Weege, R. J. & Pollack, J. P. 1971.** Recent developments in native-copper district of Michigan. Society of Economic Geologists Field conference, September 30 to October 2, 1971, 18–43.
- White, W. S. 1968.** The native-copper deposits of Northern Michigan. In: Ridge, J. D. (ed.) *Ore deposits of the United States, 1933–1967*. New York: The American Institute of Mining, Metallurgy, and Petroleum Engineers, 303–325.
- Wilson, M. L. & Dyl II, S. J. 1992.** The Michigan Copper Country. Tucson, Arizona. *The Mineralogical Record*. 104 p.
- Woodruff, L., Schulz, K., Nicholson, S. & Dicken, C. 2020.** Mineral deposits of the Mesoproterozoic Midcontinent Rift System in the Lake Superior region – A space and time classification. *Ore Geology Reviews* 126, 103716. Available at: <https://doi.org/10.1016/j.oregeorev.2020.103716>
- World Nuclear Association 2020.** Storage and Disposal of Radioactive Waste. Updated March 2020. Available at: <https://www.world-nuclear.org>. [Accessed 3 March 2021]
- Zhang, D., Zhou, T., Yuan, F., Fiorentini, M.L., Said, N., Lu, Y. & Pirajno, F. 2013.** Geochemical and isotopic constraints on the genesis of the Jueluotage native copper mineralized basalt, eastern Tianshan, north-west China. *Journal of Asian Earth Sciences*, v. 73, 317–333.
- Zhang, Z., Mao, J., Wang, F. & Pirajno, F. 2006.** Native gold and native copper grains enclosed by olivine phenocrysts in a picrite lava of the Emeishan large igneous province, SW China. *American Mineralogist*, v. 91, 1178–1183. Available at: <https://doi.org/10.2138/am.2006.1888>
- Zhu, B.-Q., Hu, Y.-G., Zhang, Z.-W., Cui, X.-J., Dai, T.-M., Chen, G.-H., Peng, J.-H., Sun, Y.-G., Liu, D.-H. & Chang, X.-Y. 2007.** Geochemistry and geochronology of native copper mineralization related to the Emeishan flood basalts, Yunnan Province, China. *Ore Geology Reviews*, v. 32, 366–380.

APPENDICES

Appendix 1. Availability of samples

Appendix 2. Analytical methods tested for Phase II of MICA

Appendix 3. Methodology assessment of Keweenawan native copper and corrosion minerals

APPENDIX 1.

AVAILABILITY OF SAMPLES

Written by Theodore J. Bornhorst

Table 1. Analogue Type A – Long and Varied History of Keweenaw Peninsula Bedrock Native Copper History in the Subsurface.

Copper Crystals from Various Mines

Sample status

Copper crystal clusters grew into open spaces. They have better potential of fluid accessibility to their surfaces after they were precipitated. Copper crystal clusters are available from the A. E. Seaman Mineral Museum collection, but destructive research opportunity is limited. Specimens for study can be purchased from the collector marketplace and crystal clusters from the Laker Pocket have been acquired and saved for future MICA study.

Sample issues

While the copper crystals originally grew in open spaces, the degree of post precipitation contact with

brines or meteoric water may not be determinable and has to be assumed. Post-mining physical and/or chemical treatment is usually (but not always) determinable.

References

Chapter 5 and Bornhorst Geologic Context internal document; copper crystal clusters from various mines which are described by Butler and Burbank (1929); Michigan Copper Country issue of the Mineralogical Record, v. 23, number 2, March–April 1992 describes and has photographs of many copper crystal clusters.

Open Space Pockets (“vug fillings”) from Various Mines

Sample status

Samples from various mines have cavities into which native copper has grown during precipitation. Potential fluids have relatively easier access into these cavities and therefore to the native copper surfaces. There are many readily obtainable and collectable specimens of native copper extending into open spaces, which likely were subject to corrosion since their formation. These native copper specimens represent cumulative corrosion. Native copper encased in associated minerals has relatively limited access of fluids to native copper surfaces. Samples of native copper encased and not encased in different minerals can be found throughout the Keweenaw Peninsula and provide opportunity to compare surface corrosion lesser opportunity for corrosion with much higher opportunity for corrosion.

Sample issues

While the degree of encasement of native copper in minerals is determinable from sample observations, the degree of accessibility of native copper to contact with fluids may not be determinable and has to be assumed.

References

Chapter 5 and Bornhorst Geologic Context internal document for cumulative exposure history; nature of ore described in several publications and observable in samples and underground that provide an indication of permeability and porosity data relevant to accessibility of fluids for corrosion; publications include Butler and Burbank (1929), Stoiber and Davidson (1959) and others.

Table 2. Analogue Type B – Keweenaw Peninsula Deep Bedrock Native Copper – Long and Varied Native Copper History, likely less exposed to oxic conditions.

Documented samples from deep within specific native copper mines

Sample status

Samples are available from the A. E. Seaman Mineral Museum research collection, but the number of well documented deep samples is quite limited. It is not realistic to get new samples as mines are flooded.

Sample issues

The number of documented deep samples is quite limited. The impact of cleaning and post-extraction atmospheric corrosion is uncertain. The degree of accessibility to post-precipitation fluids may be

uncertain unless copper appears to be in a cavity or copper occurs as well-formed crystals.

References

Chapter 5 and Bornhorst Geologic Context internal document; Butler and Burbank (1929) has sections about many mines; Stoiber and Davidson (1959) has very good underground description of flow top deposits; Limited other publications exist regarding specific mines to be added for specific samples as needed/available.

Drill core from Keweenaw Peninsula with known location, depth, and angle of hole.

Sample status

Historic diamond drill cores, held by the Keweenaw National Historical Park, a unit of the U.S National Park Service, from known locations are still available as of 2022 and likely accessible for sampling. Finding cavities with native copper in the drill core is uncertain. Although future status is uncertain, it is expected to be available for at least a few years.

Sample issues

To find deep bedrock native copper in drill core it will be necessary to read historic drill logs, find a specific core section, and then check to see if the box/core is present. The historic core will require

significant labor to move. Most higher-grade core sections have already been used for previous analyses. Degree of accessibility of fluids is uncertain unless native copper occurs in an open space or copper occurs as well-formed crystals.

References

Chapter 5 and Bornhorst Geologic Context internal document; Butler and Burbank (1929) wrote about many mines; Stoiber and Davidson (1959) included very good underground description of flow top deposits; Limited other publications exist regarding specific mines to be added for specific samples as needed/available.

Native copper mine rock piles

Sample status

There are remaining rock piles that are still available for sampling. Mining depth of the samples can be roughly estimated. Many samples of native copper are readily available.

Sample issues

The mining depth, when a specimen comes from a rock pile, is, at best, a rough estimate subject to considerable error. Degree of accessibility to fluids

is uncertain unless native copper or copper occurs as well-formed crystals.

References

Chapter 5 and Bornhorst Geologic Context internal document; Butler and Burbank (1929) has sections about many mines; Stoiber and Davidson (1959) has very good underground description of flow top deposits; Limited other publications exist regarding specific mines to be added as needed.

Table 3. Analogue Type C – White Pine Mine Bedrock Native Copper – Long and Varied Native Copper History, likely less exposed to oxic conditions.

White Pine Mine

Sample status

Samples of sheet copper from underground that have not been cleaned using acid exist. Direct reporting from Richard Whiteman is that the surfaces of sheet copper samples usually looked like unaltered native copper as mining proceeded. Occasionally samples would have surface alteration minerals but Richard postulated these derived from one certain part of the mine, likely at shallow levels where oxidation potentially could have happened. Brines are notably present in the underground of the White Pine Mine.

Sample issues

Since samples were not taken in situ, exact information like location or water chemistry are missing.

References

Chapter 5 and Bornhorst Geologic Context internal document; Ensign et al. (1968), Mauk et al. (1992) and references therein describe native copper at the White Pine mine

Table 4. Analogue Type D – Keweenaw Peninsula Shallow Bedrock Native Copper – Long and Varied Native Copper History, more likely exposed to oxic conditions.

Adventure Mine

Sample status

Native copper from near surface shallow levels is readily available. Most of the underground mine workings are flooded by meteoric waters. Additional levels could be dewatered for and by this project. It is possible to do underground experiments as part of MICA project. Native copper samples are readily available in situ.

least the end of Pleistocene glaciation. Exposure to brines prior to exhumation by glacial erosion is likely as long as postulated thickness of Paleozoic rocks was sufficient. Possibility of Paleozoic rock removed during Mesozoic and Cenozoic, could have significantly increased the length of exposure to oxic meteoric groundwater.

Sample issues

Accessible levels are very shallow. These shallow levels were submerged in meteoric water since at

References

Chapter 5 and Bornhorst Geologic Context internal document; Butler and Burbank (1929) very limited specific information on the Adventure mine.

Delaware Mine

Sample status

Only first level of underground workings is above the water table. Samples can be collected from this level.

submerged in meteoric water since at least the end of Pleistocene glaciation or in the zone of aeration. Exposure to brines prior to exhumation by glacial erosion is likely as long as postulated thickness of Paleozoic rocks was sufficient. The possibility of Paleozoic rock removed during the Mesozoic and Cenozoic, could have significantly increased the length of exposure to oxic meteoric groundwater.

Sample issues

The accessible first level is at a very shallow depth of accessible levels. This shallow level was likely

References

Chapter 5 and Bornhorst Geologic Context internal document; Schleiss (1986 MS thesis at Michigan

Tech on Delaware Mine), Very limited description of Delaware Mine in Butler and Burbank (1929).

Quincy Mine

Sample status

Underground sampling of native copper is possible, especially where the horizontal adit intersects the main workings of the Quincy deposit. Obtaining additional samples at some distance from the intersection of the horizontal adit and the main shaft is possible. Underground workings below the horizontal adit level are flooded.

Sample issues

The accessible levels are at some depth below the land surface but are relatively shallow. It is likely that these shallow levels were submerged in meteoric water since at least the end of Pleistocene glaciation. Exposure to brines prior to the latest exhumation by glacial erosion is extremely likely as brines are well documented at deep levels of the Quincy Mine as long as postulated thickness

of Paleozoic rocks was sufficient. The possibility of Paleozoic rock removed during the Mesozoic and Cenozoic, could have significantly increased the length of exposure to oxic meteoric groundwater. A careful literature review may clarify the depth brines were encountered during mining since brine data exists from the Quincy Mine.

References

Chapter 5 and Bornhorst Geologic Context internal document; Butler and Burbank (1929), Bumgarner MS thesis at Michigan Tech describes adit geology as do field guides by Bornhorst et al. (1986), Bornhorst and McDowell (1992), Mining history of the Quincy Mine has been addressed by Lankton and Hyde's book Old Reliable (1982 published by the Quincy Mine Association).

Caledonia Mine

Sample status

Access to shallow levels of underground workings above the water table is uncertain because of transfer of mine ownership to a different person roughly a decade ago. If access is granted, sample collection is readily available. Bornhorst has mapped underground and has a suite of samples that could be used in lieu of new samples.

Sample issues

Accessible levels are at a very shallow depth. These shallow levels were submerged under the meteoric water table since at least the end of Pleistocene

glaciation. Exposure to brines prior to exhumation by glacial erosion is likely as long as postulated thickness of Paleozoic rocks was sufficient. Nearly springs currently expel brines on to the surface. The possibility of Paleozoic rock removed during the Mesozoic and Cenozoic could have significantly increased the duration of exposure to oxic meteoric groundwater.

References

Chapter 5 and Bornhorst Geologic Context internal document; Field guides by Bornhorst and Whiteman (1992) and Bornhorst and Whiteman et al. (2013).

Valley View Quarry, Portage Township

Sample status

Multiple samples of native copper veins in the active Valley View crushed rock quarry could be readily

provided by owner. Access to study and sample the near surface native copper veins in the quarry walls is possible. Location of samples with respect to the surface is obtainable for in situ samples.

Sample issues

The accessible native copper is nearly at the surface. At this shallow level, the native copper was likely in the zone of aeration or less likely submerged in meteoric water since at least the end of Pleistocene glaciation. Exposure to brines prior to exhumation by glacial erosion is likely as long as postulated thickness of Paleozoic rocks was sufficient. The possibility of Paleozoic rock removed during the Mesozoic and Cenozoic could have significantly

increased the length of exposure to oxic meteoric groundwater.

This is a surface prospect exposed to surficial style weathering since Pleistocene glaciation.

References

Chapter 5 and Bornhorst Geologic Context internal document; relatively new quarry lacking any geologic description.

Point Prospect

Sample status

Multiple samples from the Point Prospect are available and saved back by Bornhorst for the MICA project. More samples are possibly available from the actual surface prospect, but it is hard to access and there is a lack of even tentative permission to sample.

Sample issues

For existing samples, the surrounding minerals may have been removed from the native copper and it is uncertain if acid was used. Specimens with cuprite, malachite, or azurite on the surface would be dissolved in acid. Degree of encasement in rock/minerals is determinable for some specimens.

Exploration trench zones are close to the surface and were likely in the zone of aeration or less likely submerged by meteoric water since at least the end of Pleistocene glaciation. Exposure to brines prior to exhumation by glacial erosion is likely as long as postulated thickness of Paleozoic rocks was sufficient. The possibility of Paleozoic rock removed during the Mesozoic and Cenozoic could have significantly increased the length of exposure to oxic meteoric groundwater.

References

Chapter 5 and Bornhorst Geologic Context internal document; Rosemeyer and Carlson (2000 Rocks and Minerals)

Table 5. Analogue Type E – Lake Superior Shallow Bedrock Native Copper.

Great Sand Bay in place veins

Sample status

Only some samples are identifiable as in situ veins from bottomlands of Lake Superior in Great Sand Bay or near in place. The largest in situ sample is on exhibit in the copper pavilion of the A. E. Seaman Mineral Museum. The sample's surface shows glacial abrasion while the bottom is rough with different minerals being attached. The non-glaciated surface shows the cumulative alteration equivalent to shallow bedrock copper (Type D). Type E is only the non-glaciated surface whereas the glaciated surface is Type I.

Sample issues

Identification of already collected samples that derived directly from an underwater vein is difficult. It is also difficult to identify surfaces that have been cleaned by glacial erosion or not cleaned by glacial-related processes.

References

Chapter 5 and Bornhorst Geologic Context internal document; Bornhorst (2017, A. E. Seaman Mineral Museum open access publication, although Bornhorst mixes Lake copper gravel with Great Sand Bay in situ veins.

Great Sand Bay Laker Pocket

Sample status

There are hundreds of small branching native copper crystal specimens that came from this pocket with interior open space available. Individual copper crystals are mm to cm in size. Clusters of copper crystals are up to 10s of cm across. Bornhorst has set aside a wide variety of these specimens for the MICA project.

Sample issues

Specimens have been cleaned with water. Post glacial (< 10 ka) corrosion has occurred while sub-

merged under glacial and recent waters of Lake Superior. This corrosion over the last 10 Ka years adds to previous corrosion events over the past 1 Ga. Specimens have been exposed to lake water for at least the last 10 ka.

References

Chapter 5 and Bornhorst Geologic Context internal document; Rosemeyer (2009, Rocks and Minerals)

Gull rock (Grand Marais vein)

Sample status

Branching native copper crystals encased in calcite are available through generous donation from Bob Barron and held back by Bornhorst. Acquisition of new samples by MICA team is possible by boat rental and diver.

Sample issues

Native copper is encased in calcite which limits access of water to the native copper surfaces. Need

to find fractures within calcite where water can readily penetrate to the native copper surface and has evidence of penetration by water. Postglacial corrosion adds to previous corrosion events over the past 1 Ga. Must avoid specimens cleaned with acid.

References

Chapter 5 and Bornhorst Geologic Context internal document; Rosemeyer (2002, Rocks and Minerals)

Table 6. Analogue Type F – Keweenaw Peninsula Bedrock Native Copper Exposed to Supergene Weathering.

Allouez Mine

Sample status

Only samples from surface rock piles are available for MICA study. The best rock pile at Bumbletown and will likely be entirely crushed for economic reasons (decorative crushed stone) before Phase II of the MICA project. Some samples have been obtained by Bornhorst for study.

Sample issues

While it is geologically reasonable that the supergene weathering is a result of Precambrian

weathering, it is possible that unusual conditions facilitated supergene weathering during the Mesozoic to Cenozoic or Pleistocene.

References

Chapter 5 and Bornhorst Geologic Context internal document; Very limited published information in Butler and Burbank (1929).

Algoma Mine

Sample status

Only samples from surface rock piles are available for MICA study. Access to surface rock pile likely but not confirmed.

Sample issues

While it is geologically reasonable that the supergene weathering is a result of Precambrian weather-

ing, it is possible that unusual conditions facilitated supergene weathering during the Mesozoic to Cenozoic or Pleistocene.

References

Chapter 5 and Bornhorst Geologic Context internal document; Very limited published information in Butler and Burbank (1929).

Table 7. Analogue Type G – Keweenaw Peninsula Bedrock Native Copper Exposed to Hydrothermal Sulfur.

Appropriate samples may not be available or collectable. It may be difficult to definitely determine if the surface of a mass of native copper is sufficiently exposed to sulfur-bearing late-stage hydro-

thermal fluids. It may be difficult to distinguish between corrosion related to late-stage hydrothermal fluids or to later corrosion related to anoxic brines or anoxic/oxic meteoric water.

Quincy Mine

Sample status

Kelly (2020) described a transition within a few calcite crystals from main-stage native copper to late-stage hydrothermally precipitated copper sulfides. Native copper in calcite at the contact between these two stages of growth of calcite have very likely been exposed to sulfur bearing late-stage hydrothermal fluid

late-stage sulfur bearing fluids) has yet to be documented. These native copper surfaces are encased in calcite. Encasement decreases the effect of corrosion during post late-stage fluid events and hence, native copper corrosion may be almost entirely a result of sulfur-bearing fluids. The study of fluid inclusions may help unravel fluid history.

Sample issues

Native copper in contact with sulphide-bearing calcite or in contact with chalcocite (exposed to

References

Chapter 5 and Bornhorst Geologic Context internal document; Kelly (2020) Michigan Tech MS thesis research observed native copper inclusions in calcite followed by chalcocite previously not described.

Delaware Mine

Sample status

Full access is only to first level of underground workings to collect samples including the Stoutenberg vein and adjacent wall rock. The last filling of the Stoutenberg vein is sulfide mineral-bearing.

per can be obtained for which there is confidence that sulfur-bearing hydrothermal fluids were in contact with the native copper. It is uncertain if samples of native copper can be identified as not exposed to late-stage sulfur-bearing hydrothermal that can be used as background comparison to help distinguish between the effect of hydrothermal sulfur and other corrosion events.

Sample issues

It is uncertain if suitable samples of the sulfide-bearing Stoutenberg vein and adjacent native cop-

References

Chapter 5 and Bornhorst Geologic Context internal document; Schleiss (1986 MS thesis at Michigan

Tech on Delaware Mine), Very limited description of Delaware in Butler and Burbank (1929).

Baltic Mines

Sample status

In publications, Baltic Mines are known for having chalcocite-bearing veins that crosscut the native copper deposit. The MICA project has access to rock piles of the Baltic deposit at Champion and likely at the Baltic cheese factory to search for appropriate samples. There are also samples in the A. E. Seaman Mineral Museum research collection and at Keweenaw Gem and Gift to which the MICA project has access.

erals may not be found. Distinguishing between corrosion resulting from sulfur-bearing late-stage hydrothermal fluids and other corrosion events may not be possible.

References

Chapter 5 and Bornhorst Geologic Context internal document; Butler and Burbank (1929) provides limited specific information on the Baltic mines.

Sample issues

Suitable samples where native copper is in contact with late-stage sulfur-bearing hydrothermal min-

Centennial Mine

Sample status

Native copper bearing samples with crosscutting sulfide-bearing veinlets are mentioned by Butler and Burbank as more common in the Centennial mines at the north end of the C & H conglomerate deposit. Centennial mine was dewatered in the 1980s and there may be available samples. As of 2022 Centennial sample availability has not been investigated.

Sample issues

Suitable samples may not be found.

References

Chapter 5 and Bornhorst Geologic Context internal document; Butler and Burbank (1929), Weege and Pollack (1971).

Tamarack Mines

Sample status

Native copper bearing samples with crosscutting sulfide-bearing veinlets are mentioned by Butler and Burbank as more common in the northern mines of the C & H deposit. Tamarack Junior mine is one of the few C & H rock piles and on the northern end of the deposit. Access to the rock pile has been investigated but is uncertain as of 2022.

Sample issues

Suitable samples may not be found.

References

Chapter 5 and Bornhorst Geologic Context internal document; Butler and Burbank (1929).

Table 8. Analogue Type H – White Pine Mine – Bedrock Native Copper in contact with sulfide minerals.

White Pine Mine

Sample status

Multiple samples of native copper crosscutting White Pine chalcocite ore are available for MICA study. Two larger samples and several smaller samples are available from Bornhorst for the MICA project.

Sample issues

It is uncertain whether a physical contact between native copper and chalcocite can be found or a contact close enough to assure that chemical reaction between native copper and chalcocite could have readily happened. Reaction during hydrothermal

deposition of native copper in the chalcocite ore is also possible as long as native copper precipitating fluids had access to the surface of chalcocite grains. A dry contact is not expected to have significant amount of corrosion. The access of fluids to the physical contact surface is uncertain.

References

Chapter 5 and Bornhorst Geologic Context internal document, Ensign et al. (1968), Mauk et al. (1992) and references therein describe native copper at the White Pine mine; Mauk and Hancock (1998) provide trace element geochemistry of native copper from White Pine.

Table 9. Analogue Type I – Lake Superior Shallow Native Copper with Glaciated Surface (Great Sand Bay lake copper).

Great Sand Bay in place veins

Sample status

Only some samples are identifiable as in situ veins from bottomlands of Lake Superior in Great Sand Bay or near in place. The largest in situ sample is on exhibit in the copper pavilion of the A. E. Seaman Mineral Museum. The surface and therefore potential secondary minerals were abraded by glacier(s), exposing the fresh native copper surface to glacial lake water; the corrosion clock on the glaciated surface was partially or fully reset. Most vein samples are not smoothed. This lack of a glaciated surface indicates that the corrosion clock has not been reset so postglacial corrosion adds to previous corrosion events over the past one billion years. Only the glaciated surfaces are Type I.

Sample issues

Identification of already collected samples that were directly from an underwater vein and with a glaci-

ated surface is difficult. Only the Lake Copper on display at the A. E. Seaman Mineral Museum has documented provenance and a glaciated surface. It is also difficult to identify surfaces that have been abraded by glacial erosion to ensure that the corrosion clock was fully reset to zero. It may be desirable to avoid this analogue type and instead work with analogue Type J.

References

Chapter 5 and Bornhorst Geologic Context internal document; Bornhorst (2017, A. E. Seaman Mineral Museum open access publication, although Bornhorst mixes Lake copper gravel with Great Sand Bay in place veins.

Table 10. Analogue Type J – Lake Superior Native Copper Gravel (Great Sand Bay lake copper nuggets).

Great Sand Bay Lake Copper Gravel

Sample status

A wide variety of Lake Copper gravel samples from the bottomlands of Lake Superior in Great Sand Bay are available from Bornhorst for the MICA project. Acquiring new samples from the extensively sampled lake ground by a diver is difficult.

Sample issues

Resetting of the corrosion clock is uncertain in some specimens. The native copper pebbles have

been cleaned by a pressure washer. Some samples were treated with acids but are generally easy to identify and avoid.

References

Chapter 5 and Bornhorst Geologic Context internal document; Bornhorst (2017, A. E. Seaman Mineral Museum open access publication) although mixes Lake copper gravel with Great Sand Bay underwater vein.

Table 11. Analogue Type K – Glacial Native Copper (“Float” copper).

Unknown specific localities from western Upper Peninsula

Sample status

Many samples of float copper are readily available on the marketplace from slices to complete samples.

Sample issues

Certainty about a resetting of the corrosion clock is uncertain in some specimens. Many masses of native copper have been cleaned by a pressure washer. There are many slices of float copper for observation and analysis, but the evolutionary context is missing, as the sample is fragmentary.

Cutting solid masses of native copper requires special consideration since ductile copper inhibits cutting. Ken Flood at Keweenaw Gem and Gift is a local expert on cutting float copper. The geologic context of these samples is unknown. Pockets or fractures with copper corrosion products should be avoided as these lack geologic context.

References

Chapter 5 and Bornhorst Geologic Context internal document; Bornhorst (2017, A. E. Seaman Mineral Museum open access publication).

Specific locality of in place float copper from western Upper Peninsula

Sample status

No in situ float copper samples are available at this time. It is likely to be able to get locality information for in situ float copper from float copper hunters with financial incentive.

Sample issues

It may be difficult to be certain that the corrosion clock has been reset to zero. Pockets or fractures

with copper corrosion products should be avoided as these lack geological context.

References

Chapter 5 and Bornhorst Geologic Context internal document; Bornhorst (2017, A. E. Seaman Mineral Museum open access publication).

Superior Sand and Gravel float copper

Sample status

Many float copper samples are recovered from near the surface soil and/or unconsolidated glacial sediment. Some are recovered from multiple meters below the surface surrounded by unconsolidated glacial sediment, but such information is usually unavailable. These particular float copper samples come from a sand and gravel pit. Since they are not from the surface, they are not surrounded by organic surface soil although downward percolating water could introduce surface organic products. Native copper in this setting was exposed to oxic groundwater, most likely in the zone of aeration, for the last 10 ka. Bornhorst has a few samples from this local sand and gravel pit available for study by MICA. More samples can readily be acquired but it is highly unlikely to get in situ samples.

Sample issues

Resetting of the corrosion clock is uncertain in some specimens. The detailed context of in situ samples is mostly unknown although general setting is better known than for most float copper samples. Not likely to get an in situ sample. Pockets or fractures with copper corrosion products should be avoided as these lack geologic context.

References

Chapter 5 and Bornhorst Geologic Context internal document; Bornhorst (2017, A. E. Seaman Mineral Museum open access publication).

Table 12. Analogue Type L – Native copper chisel chips.

Central and Cliff Mines

Sample status

Samples from the Central and Cliff Mines are available from Bornhorst for MICA project. Additional samples from specific locations are obtainable and perhaps collectable.

Sample issues

Samples have been cleaned with water and perhaps by a pressure washer, which could have removed

some corrosion products from specimens not specifically collected for the MICA project. Sampling of chisel chips is difficult. Corrosion time during storage in a rock pile can only be estimated.

References

Chapter 5 and Bornhorst Geologic Context internal document; No specific reference identified for chisel chips.

APPENDIX 2.

ANALYTICAL METHODS TESTED FOR PHASE II OF MICA

Written by Timo Ruskeeniemi and Xuan Liu

This appendix provides a concise overview of analytical methods that can be applied in analogue studies. It is not meant to be exhaustive but focused on the most relevant and most widely-used methods.

1 MORPHOLOGICAL, TEXTURAL AND MINERALOGICAL ANALYSIS

1.1 X-ray computed tomography

Copper corrosion layers can be thin and mineralogically complex. To select the most effective analytical methods, it is important to know and assess possible complications. Detailed 2D and 3D imaging can provide valuable information about geometries of corrosion zones and the contact relation with surrounding minerals. X-ray computed tomography (XCT) is a useful tool to initiate the studies (see Appendix 3).

XCT produces 3D models of the sample based on composition and density contrasts of different components (See examples in Section 5.1 of Appendix 3). The high density of copper limits the penetration depth of X-rays, preventing internal scanning deeper than a couple of centimeters, but it may reveal some internal textures close to the surface. The method is particularly useful for studying features such as surface topography of the copper, mineral layering, and porosity of the alteration crust at a micron-resolution. For detailed studies, the resolution can be extended to nano-scale. Also other methods are available for higher resolution.

Because the technique is non-destructive, it guides sample selection and preparation in general and allows studies on delicate samples that would be prone to be deformed during traditional cutting methods.

The main aims of the XCT scans are:

- a) Scanning of the alteration crust to observe its thickness, internal layering and other textures generated by mineral growth. The data allows to measure different parameters, such as singular volumes and orientation of the phases. Mineralogical and analytical tools can then be used to characterize and date the minerals. In the best case, the method helps to answer if the textures in the alteration crust are indicative of one or several events.
- b) The surface of the copper under the alteration crust tells something about the life cycle of the sample. For example, scratches on the surface indicate mechanical wearing and potential glacial transport. Further, the surface morphology may reveal how the alteration/corrosion has advanced, i.e., pitting, intergranular or some other type.
- c) Sample selection and guidance for preparation is required for detailed investigations. It is important and cost-efficient to start these studies with a method that does not need sample preparation. XCT helps to select samples for more cleverly devised metallurgical methods and other studies.

1.2 Petrography

Conventional thin and polished thick sections are still the method of choice for petrographic analysis. If the samples are coated with thin alteration

crusts, polished slabs are favored. Oil should be used in sample preparation and alcohol for polishing (See Appendix 3).

1.3 Micro X-ray diffraction

Micro X-ray diffraction (XRD) provides definite recognition of the crystalline minerals but requires subsampling of the phases of interest (See Sections 4.4 and 5.2 of the Appendix 3 for examples). Although the required amount can be a single crystal, the need for subsampling can limit its applicability in very detailed studies. However, it works well for most of the mineralogical needs of this project. If sampling limitations occur, micro-XRD is applied. It uses a very narrow X-ray beam and collects information from an area of few tens of

µm. Crystallinity index (CI) is a measure of crystallinity. It can be defined from XRD and some other spectra and is widely used for clay mineralogy. Higher CI values indicates higher ordering in the mineral lattice and higher formation temperature of the mineral.

Low-temperature supergene alteration can include phases that are poorly crystalline. In this case, the mineral identification is based solely on chemical information and as such remains semiquantitative.

2 CHEMICAL CHARACTERISTICS

The chemical composition of native copper has several important aspects relevant for the goals of the MICA project, including at least:

- a) Unravelling the chemical similarities/differences between MICA native copper and canister-building copper;
- b) Understanding potential influences of the chemical differences on corrosion resistance;
- c) Understanding how the chemical composition of native copper varies within the selected locations and within individual samples.

The mineralogy, isotopic signatures and fluid inclusions can provide information about the pres-

sure and temperature conditions during formation.

In addition to native copper, information on mineral chemistry is required:

- a) to identify and obtain chemical composition of the Cu phases involved in the alteration/corrosion crust;
- b) to find mineral species which contain sufficient element contents for age determination (e.g., U-Pb, Rb-Sr, etc.);
- c) to find chemical signatures which may give insight to the water-rock interaction processes (surface or groundwater).

2.1 X-ray spectroscopies

X-ray spectroscopy (XRF) is the emission of characteristic secondary X-rays (or fluorescent) from a material that is irradiated with high-energy X-rays. Characteristic X-rays are produced by removing electrons in the inner shell of atoms, leaving a vacancy that promotes electronic transition from a higher-shell electron. The transition yields photon energy in the form of an X-ray characteristic for the element's energy gap. With this method, most elements can be detected and quantified except for

light elements (atomic weight less than 16 amu). Data is typically acquired at µm scale.

Electron probe microanalysis (EPMA) is a non-destructive technique to determine the chemical composition of small amounts of solid materials, operating with a similar mechanism as XRF except the incident electron beam. The electron microprobe uses wavelength dispersive spectroscopy (WDS) for precise quantitation. For precise analysis, suitable standards of known composition should

be analyzed along with the sample's measurement conditions. The activation volume excited by the beam is typically on the order of 2 µm, even though the beam itself is less than 1 µm.

Energy dispersive spectroscopy (EDS), operating with similar working principle, uses a focused

beam of high-energy electrons to generate several signals, including characteristic X-rays, at the surface of solid specimens. The X-rays can be used for qualitative and semi-quantitative analysis.

2.2 Atomic spectroscopy and spectrometry

Atomic absorption spectroscopy (AAS) is a spectroscopic technique for the quantitative determination of chemical elements using the absorption of optical radiation (light) by free atoms in the gaseous state. This technique is based on absorption of light by free metallic ions. Test results provide concentrations of trace to major compositional elements.

Inductively-coupled plasma optical emission spectroscopy (ICP-OES) is a type of emission spectroscopy that uses inductively coupled plasma to produce excited atoms and ions that emit electromagnetic radiation at wavelengths characteristic of a particular element. The intensity of the emissions from various wavelengths of light are proportional to the concentrations of the elements within the sample. Most elements can be measured down to ppb level.

Apart from AAS and ICP-OES, several techniques are available for analyzing element compositions down to ppt levels. The most used one is a combination of mass spectrometry and ICP (ICP-MS). It uses ICP as the source of ions, where samples aerosols are converted to positively-charged ions

that are separated and detected based on mass-to-charge ratios. It can be operated in solution mode and laser ablation (LA) mode. The former can offer much lower detection limits with higher precision and accuracy, but it requires labor-intensive and time-consuming sample preparation. In contrast, LA can offer rapid and high throughput measurement with minimal sample preparation.

Alternatively, laser induced breakdown spectroscopy (LIBS) has also been widely used for trace element analysis of metals. It is a type of atomic emission spectroscopy, which uses a highly energetic laser pulse as the excitation source. The laser forms a plasma, which atomizes and excites samples. The formation of the plasma begins when the focused laser achieves a certain threshold for optical breakdown, which generally depends on the environment and the target material.

Please refer to Appendix 3 for preliminary analyses utilizing SEM-EDS, micro-XCT, micro-XRF, XRD and laser ablation-inductively coupled plasma-mass spectrometry (LA-ICP-MS).

3 ISOTOPE GEOCHEMISTRY

3.1 Native copper

ICP-MS with single collector (SC) and multiple collectors (MC) are the most effective way to measure isotope compositions. SC-ICP-MS is widely used for determining U-Pb ages, while MC-ICP-MS is the best choice for isotope ratio measurement. MC-ICP-MS works similarly to a SC-ICP-MS except that it detects ion beams of different masses simultaneously, so analyses generally have a high precision and accuracy. Both instruments can be operated with aspirated solutions and solids sampled by laser ablation.

Native copper cannot be dated directly due to a lack of radionuclides such as K, Rb, Sm, U and Th. Most dating work done with respect to formation

age of native copper has used gangue minerals that are intergrown with copper (e.g., Rb-Sr dating for Keweenaw Peninsula copper, Bornhorst et al. 1988). However, it might be possible to obtain common Pb model ages based on common lead growth models (Stacey & Kramers 1975).

However, stable isotopes could be very useful complimentary targets. The most widely studied and used one is the Cu isotope systematic (e.g., Larson et al. 2003, Mathur & Wang 2019). The method is often used in archaeology together with Pb isotopes for provenancing of Cu artefacts (e.g., Klein et al. 2009), and the same method could be

used in provenancing e.g., the float type samples. The prominent merit of Cu isotopes lies in the fact that Cu is a multi-valent element. Its valence state varies from 0 in reducing condition to +1 and +2 in oxidizing conditions. During redox reactions, Cu isotopes (^{63}Cu and ^{65}Cu) tend to fractionate with ^{63}Cu preferentially entering into reduced phases

and ^{65}Cu into oxidized phases (Markl et al. 2006). The magnitude of fractionation, thus, provides a proxy for studying redox processes. In addition, Cu isotopes can also fractionate in several other processes involving liquid–vapor phase separation, multi-step equilibrium processes, and organism-related processes (Markl et al. 2006).

3.2 Other minerals

Constraining the timing of copper corrosion events is important for MICA.

Isotope geochemistry is an important continuation of the other mineralogical investigations. Many common minerals contain elements (H, O, C, Sr, U etc.), which have stable or radioactive isotopes.

Environmental isotopes are widely used as tracers for formation conditions, identification of source areas or mineralogical processes. Isotope signatures (e.g., $^{87}\text{Sr}/^{86}\text{Sr}$ ratio) can be directly used for classification of the analyzed minerals or for source area identification. Isotopes tend to fractionate in geological processes due to the small differences in their mass. The heavy isotope of oxygen (^{18}O) incorporates preferentially to the solid phase during mineral precipitation, while the light isotope (^{16}O) is enriched in the residual fluid. Temperature driven fractionations occur also in water at phase changes (water–vapor–water). Light isotopes are preferably added to the vapor phase, and the signature of the water is getting heavier.

When the controls and rates of fractionation are known, isotope data can be used to assess hydrogeological conditions. If isotope information of the fluid phase is available or can be inferred from other sources, it is possible to calculate the fractionation/formation temperature for the mineral. This is a widely used application for carbonates, especially for calcite, which is one of the most common minerals in the geological record.

Radioactive isotopes are extensively used for dating purposes. At best, they give an ‘exact’ date for the mineral. Depending on the decay rate, different radiometric systems can be used for a range of age determination. For radiocarbon (^{14}C) the upper limit is 60 ka, while U–Pb dating is applicable for several hundred thousand years to billions of years (See Section 5.4 of the Appendix 3 for examples). Uranium series elements provide numerous dating options from days upwards (e.g., ^{234}U – ^{230}Th can date samples up to 450 ka). Use of any radiometric method requires consideration if the system has been closed or open. An open system allows import and export of elements, which may result in depletion of mobile daughter isotopes and incorrect dates.

The selection of a dating method depends on the available minerals. At the moment it is not clear how far the mineralogical investigations and isotope geochemistry can be used to study the secondary mineral species. However, there is a potential for valuable information and the described methodology will be tested. Oxygen and C isotopes on copper carbonate (malachite) crust for example may reveal if this type of alteration has taken place in a single or multiple events, temperature levels and water species involved. Proposed mineralogical studies will show if there are other options for this approach.

4 FLUID INCLUSIONS STUDIES

Studies on primary fluid inclusions provide information about the fluid composition of the parent fluid. The method is particularly useful for high-temperature environments. In the Keweenaw Peninsula calcites which have crystallized simultaneously with the native copper are available for these studies. Fluid inclusions (FI) are commonly

trapped in crystal defects and fractures, and thus less likely to occur in minerals that formed at low and slow crystallization.

The study of FIs is a special technique in mineralogy. Although FIs are not solid, they have a direct link to the formation of minerals. Primary FIs are samples of the parent fluid from which the

mineral has formed. Additionally, depending on the formation conditions, they may contain gas bubbles and mineral crystals. Fluid inclusions are relatively common in minerals. Most inclusions are smaller than 20 µm. Geothermometric analysis of fluid inclusion can yield data under the microscope

by heating and freezing to yield homogenization precipitation temperature, trapping pressure, and density Geochemical data on fluid composition can be obtained from FIs by Laser Raman Spectrometry or by LA-ICP-MS

APPENDIX 3.

METHODOLOGY ASSESSMENT OF KEWEENAWAN
NATIVE COPPER AND CORROSION MINERALS

Written by Xuan Liu

1 INTRODUCTION

The Phase I of the project has obtained an inventory of a few samples for preliminary analysis presented in this Appendix. The objectives of this test study were to 1) evaluate the limits of analytical capability and 2) to assess methodological feasibility. A methodology framework has been developed to streamline the required knowledge and analytical capacity for achieving these objectives. The framework consists of three constituent blocks termed as Objectives, Knowledge, and Technologies (Fig. 1). The “Objectives” block shows the overall objectives and is connected to and supported by

the “Knowledge” block that requires knowledge of mineralogical, geochemical, geochronological, and structural properties of the samples. The “Technology” block shows analytical techniques and instruments required for the knowledge. The Knowledge block is linked to three analytical technologies that could benefit the planning of the next phases of the project, i.e., electron microprobe, laser ablation ICP mass spectrometry, and micro-X-ray tomography.

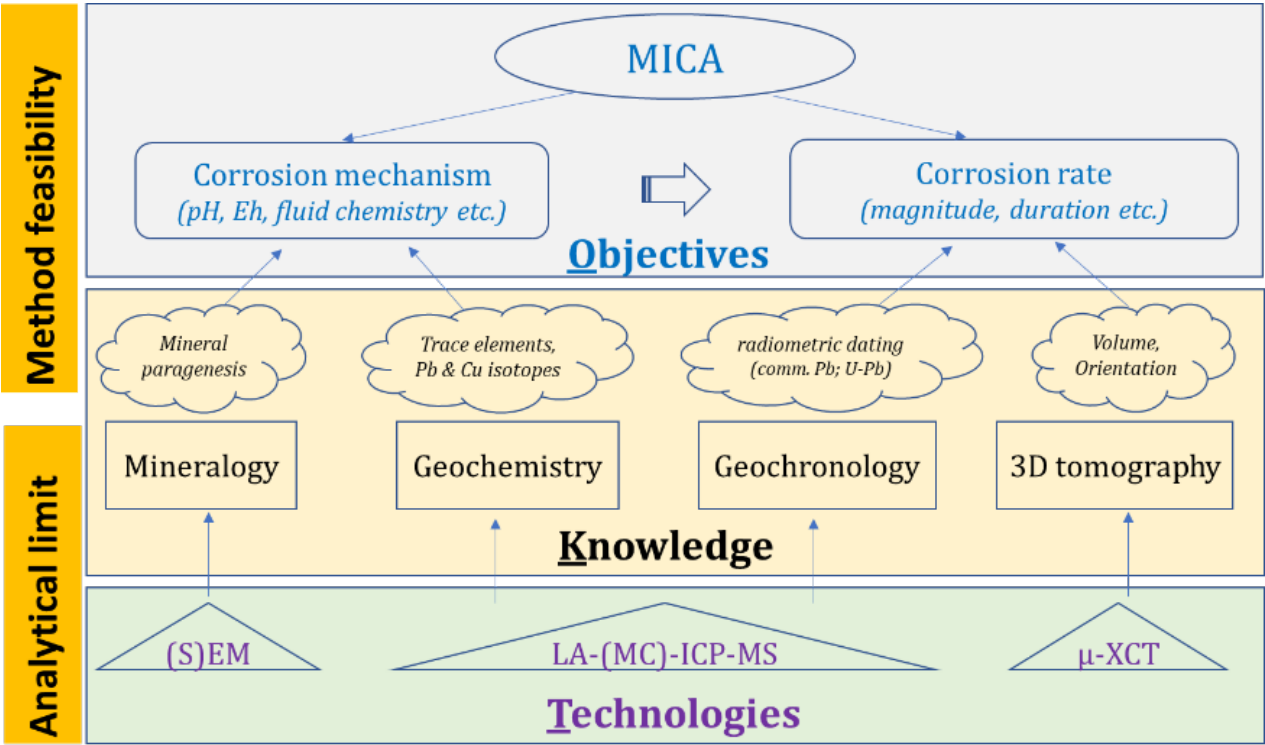


Fig. 1. A schematic diagram showing the technical methodology of this test study. SEM: scanning electron microscopy, (S)EM: (scanning) electron microprobe, LA-(MC)-ICP-MS: laser ablation (multi-collector) inductively-coupled plasma spectrometry (LA-ICP-MS), μ-XCT: micro- X-ray tomography.

2 SAMPLES

A total of 10 samples were selected from an existing sample inventory (Table 1). This selection is not exhaustive but represents different types of samples and hence various types of analytical challenges. It should be clarified that no efforts have been made to link these samples to the sample types defined in the Chapter 6 of the main report since that context information of these samples are subject to uncertainty.

Petrographic descriptions of the selected hand specimens along with other available information are given in Table 1. It should be noted that the table was prepared before mineralogical studies, and consequently, mineral phases were primarily described based on optical properties.

Some modifications were made to the original analytical plan during the work. Table 2 summarizes the type and number of analyses, compared with the original plan. All modifications made are justified and further described below.

Overall, the planned work was fully accomplished, with 85% of the intended analyses completed and extra work of μ -XRF and XRD being

added. Specifically, six types of analyses were fully done, including microscopy, SEM, XCT, laser-situ trace element, laser-situ U-Pb dating, and in-situ Cu isotopes. Thirteen solution trace element analyses have not been undertaken, but two additional samples were analyzed for trace element composition by laser ablation. Copper isotope analyses were predominantly conducted by laser ablation (additional 7 samples) instead of solution method (2 of planned 13). The reasons why solution work was largely omitted are threefold. The laser ablation has a higher throughput (5–10 samples per day vs. 5–10 samples per week), spatial resolution (down to 40 μ m vs several cm), and in-situ capabilities compared to solution method. These advantages are prominent when very localized analyses are needed, for instance, to test study elemental and isotopic variation adjacent to a corrosion layer and thin films of corruptions.

To complement the deficiency of intended analyses, μ -XRF and XRD were utilized for 3 samples. These additional analyses proved useful in distinguishing Cu oxides and malachite.

Table 1. Petrographic descriptions and general introduction of the selected samples.





Sample No.	Petrography	Image
MICA1	Float copper with uneven surface covered by at least two types of alteration minerals. The bottom alteration layer is a mixture of metallic gray and reddish minerals, overlain by greenish malachite.	
MICA2	A float copper with rock fragments. The Cu is largely uncorroded, but some areas show metallic gray and reddish alterations.	
MICA3	A float sample with generally thin alteration edges. This sample also contains well-developed "cob-web" alterations, which comprise several layers, starting from metallic gray, transitioning to reddish layer, and a malachite layers. It also contains carbonate inclusions.	
MICA4	A sample consisting of native copper and quartz. The quartz is fractured and filled/cemented with Cu veinlets. On the edge of Cu, there are small pinch-outs. These textures might indicate Cu forming later than the quartz. Sample was assigned as float (found as one) but represents bedrock copper.	

Table 1. Cont.







Sample No.	Petrography	Image
MICA5	A float copper, largely covered by malachite, which is in turn covered by consolidated dirt. The malachite surface shows "sponge"-like texture.	
MICA6	A chisel chip Cu, assumed to be chopped off in 1860-1880, and collected in 2013 from a rock pile. It is native Cu, coated by layered alteration of metallic gray minerals and malachite.	
MICA7	A conglomerate, consisting of at least two types of clasts. It has a reddish appearance with apachite cementations.	
MICA8	A sample with large, euhedral calcite crystals, growing on native Cu. The large calcite contains Cu and malachite inclusions. Native copper is covered by reddish alteration or malachite.	
MICA9	A dendritic lake copper consisting of small, euhedral crystals of native copper. The surface of crystals is largely tanned with reddish color, locally covered by yellowish materials.	
MICA10	A native copper vein crosscutting disseminated Cu sulfides. The voluminous sulfides in the host rock may provide potential environment for sulfidation of the copper vein.	

Table 2. A summary of the intended analyses, and the actually performed analyses.

Sample	Object	Intended analysis																Added analysis	
		Microscopy		SEM (2D)		XCT (3D)		Trace element				(U)-Pb		Cu Isotopes					
								LA		Sol.		LA		Sol.		LA		XRF	XRD
MICA1	corr.	x	✓	x	✓	x	✓		✓✓	x	×		✓✓	x	×		✓✓		
	Cu									x	×			x	×				
MICA2	Cu	x	✓					x	✓	x	×			x	✓		✓✓		
MICA3	corr.	x	✓	x	✓	x	✓	x	✓	x	×	x	✓	x	×	x	✓	✓✓	✓✓
	Cu							x	✓	x	x			x	✓		✓✓	✓✓	✓✓
MICA4	Cu	x	✓	x	✓	x	✓	x	✓	x	×			x	×		✓✓		
MICA5	corr.	x	✓			x	✓		✓✓	x	×		✓✓	x	x		✓✓		✓✓
MICA6	corr.	x	✓	x	✓		✓			x	×			x	×		✓✓		
	Cu	x	✓					x	×	x	×	x	×	x	×	x	✓		
MICA7	corr.	x	✓	x	✓	x	✓		✓✓	x	×		✓✓	x	×		✓✓		
MICA8	both	x	✓			x	✓			x	×			x	×				
MICA9	both	x	✓			x	✓			x	×			x	×				
MICA10	both	x	✓	x	✓	x	×	x	✓✓	x	×	x		x	×	x	✓		

corr.: corrosion products

"x" denotes intended analysis; "x" denotes undone analysis.

"✓" denotes finished analysis.

"✓" denotes added analysis.

3 SAMPLE PREPARATION

Depending on the analysis type, samples were cut, crushed, and polished. Sample contamination (mainly oxidation) were fully considered and avoided as much as possible during sample preparation (see Section 3.2). The presence of surface oxidation is exemplified by Figure 2, comparing

the sample MICA3 before and after polishing with mineral separates extracted from the same sample (considered as fresh). The surface oxidation was likely induced due to exposure to air and moisture during storage and transport.

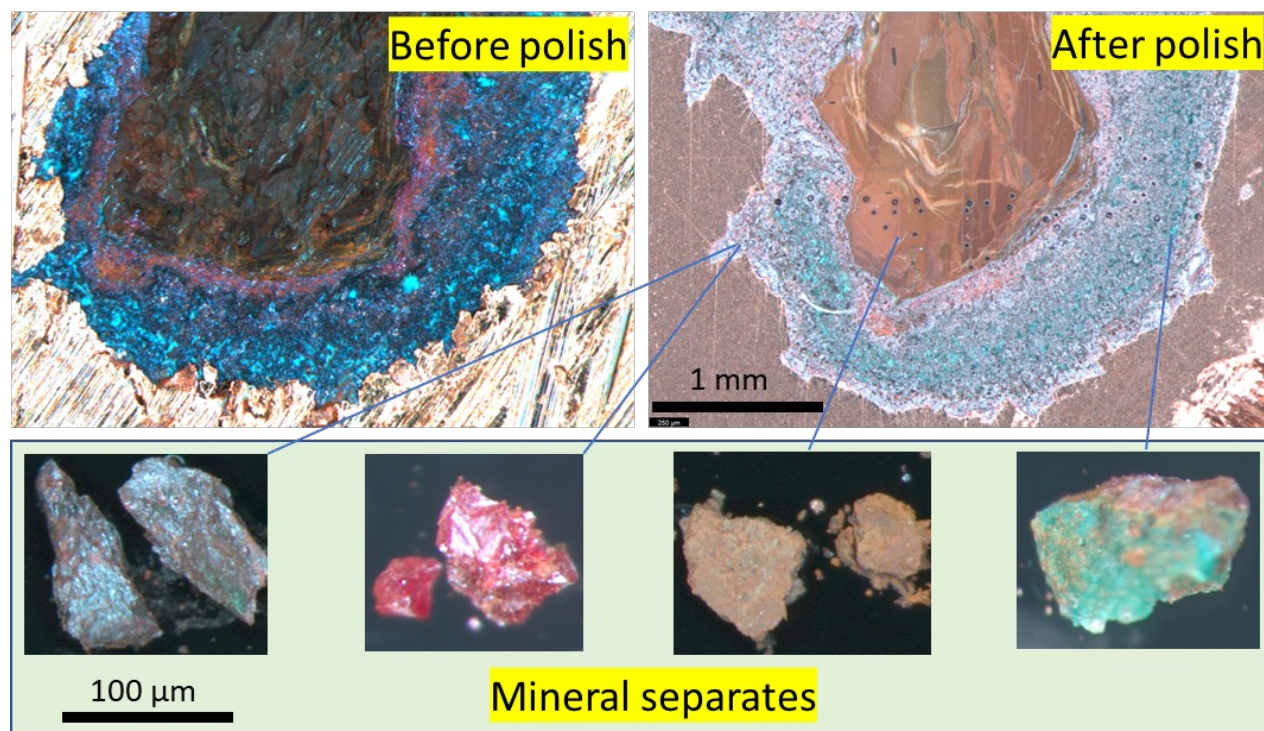


Fig. 2. Comparison of colors for MICA3 before and after polishing treatment (upper panel) with mineral separates (lower panel). It is evident that the surface color after polishing is notably different from that before polishing, and polishing reveals true colors and thus reflects true mineralogy of the sample. The images in the lower panel show mineral separates corresponding to observations from polished sample, from left to right, cuprite (mixed color of metallic gray and red), cuprite (red), nano Cu silicate (earthy brown), and malachite (green) (analyzed by XRD in Section 5.2).

Cutting the sample to a suitable size for loading in SEM and laser ablation cell is essential. The conventional method of using a diamond blade to saw involves cooling by water. However, water could be a source of oxidation that may affect mineral stability, for instance conversion of cuprite (Cu_2O) to tenorite (CuO). Hence, sample cutting was performed in two ways to avoid the use of water as coolant: hand-sawing and oil-cooled cutting with a diamond blade. Both methods have negligible effect on the samples since no significant amounts of oxidants and little heat are introduced. The latter one is much faster whereas the former one has the advantage of preserving powders derived from cutting, which can be used for subsequent chemical analyses upon handpicking. Surface polishing was

done by using alcohol-based polishing material.

Copper isotope measurements were made on native coppers of the MICA2 and MICA3 using fractions micro-drilling. The drilling work was performed with a conventional rotary drill mounted with a 1 mm diameter HSS steel drill bit (WÜRTH Spiralbohrer).

Part of the MICA3 sample containing corrosion minerals was crushed and hand-picked. Crushing was done with an iron crusher, which later turned out to scrape off iron splinters from the crusher. The scratching is probably related to the existence of silicate minerals (mainly quartz and feldspar as shown by XRD). A more proper crusher would have been agate mortar to avoid additional washing of the samples due to potential iron contamination.

4 METHODS

4.1 Optical microscopy

The prepared sample slabs were first examined and imaged with a binocular microscope and petrographic microscope with reflected light at the Espoo Research Lab of GTK. The microscopic images were

then used as a guide for subsequent imaging and analyses. Samples after polishing and laser ablation were imaged again with microscopes.

4.2 μ -XCT imaging

Micro-X-ray computed tomography (μ -XCT) imaging was conducted with a GE phoenix v|tome|x s at the Espoo Research Lab of GTK prior to other analyses. The samples were scanned using the 240 kV microfocus tube. At each angle, the detector waited for a single exposure time and then took

an average over three exposures. No ring artifact reduction was used in reconstruction, except for sample MICA5. The settings are listed in Table 3. The Thermo Fisher Pergeos 2020.2 software was used to process and visualize the images.

Table 3. Scan settings used for the samples. ACC = accelerating voltage, CUR = tube current, POW = tube power, FILT = beam filter (copper), RES = image resolution, EXP = single exposure time, #PRO = number of projections, TOT = total scan time, BHC = beam hardening correction (range 0–10).

Sample	MICA1	MICA3	MICA4	MICA5	MICA6	MICA7	MICA8	MICA9
ACC / kV	220	220	220	220	150	220	200	200
CUR / μ A	900	510	182	100	50	900	175	120
POW / W	198	112.2	40.04	22	7.5	198	35	24
FILT / mm	1.5	2.0	2.0	1.0	1.0	2.0	0.5	0.5
RES / μ m	100.04	71.88	33.55	20	7.39	100	30.3	23
EXP / ms	131	333	1000	1000	2000	200	500	500
#PRO	1500	2500	2500	2500	2300	2000	2500	2200
TOT / min	13	56	167	167	307	27	83	73
BHC	8	8	6	6	6	6	6	0

4.3 μ -XRF mapping

The X-ray fluorescence (μ -XRF) imaging was performed on MICA3 to test study elemental patterns of major to minor elements in the native copper and the corrosion layers. The used instrument was a Bruker M4 Tornado plus housed at the Espoo Research Lab of GTK. The system has an Rh X-ray 30-Watt anode target, two simultaneously operating 30mm² XFlash® silicon drift detectors (SDD) with an energy resolution of <145 eV at 275 kcps (measured on MnK α) via beryllium windows and poly-capillary optics that can focus a beam spot size down to 20 μ m. Scanning and sample navigation is carried out via a motorized stage which moves the sample beneath the static X-ray beam.

All data acquisition was then performed in separate runs using an accelerating voltage of 50 kV

with a beam current of around 200 μ A. The X-ray beam was focused on a 20 μ m spot of the sample surface, which was sitting under 2 mbar vacuum within sample chamber. The pixel dwell time was 3 ms/pixel to maximize the signal (which was 275 kcps maximum).

The qualitative background-subtracted maps were generated using the Bruker M4 software. The elemental mapping produces 2-dimensional compositional maps by collecting an entire X-ray spectrum for each pixel in a grid. For a given element displayed on a map, the pixel intensity is proportional to the intensity of the X-ray spectrum in the selected region of interest. By default, an element's region of interest is centered on the elemental peak with the highest intensity at K α line.

4.4 SEM imaging and EDS mineral chemistry

Scanning electron microscope (SEM) was used for backscattered electrons imaging (BSE) and to analyze mineral chemistry by energy-dispersive spectrometer (EDS). The instrument is a Hitachi SU3900 SEM equipped with an Oxford Instruments EDS-spectrometer X-Max 20 mm² (SDD) housed at the Espoo Research Lab of GTK. The instrument normally runs at a 20 kV acceleration voltage that produces 1 nA electron beam current with a dimension of around 1–3 μm . Low vacuum mode was used.

INCA software was used to determine the chemical composition of the samples. The quality of the EDS analyses is quantitated by normalization to 100%. It should be noted that the results are semi-quantitative. The phase identification is based on the numerical elemental composition. Exact identification of phases is not always possible based on the EDS data. Especially phases/minerals which contain C, OH- or H₂O-groups, Be or lighter elements are difficult to reliably identify.

4.5 XRD crystallography

X-ray diffraction (XRD) analyses were performed with a Bruker D8 Discover (A25) powder diffractometer, equipped with LYNXEYE XE-T detector (semiconductor silicon strip in 1-D mode) at the Espoo Research Lab of GTK. X-ray tube (line focus) anode material is copper, and the utilized wavelengths are Cu K α 1 = 1.5406 Å, Cu K α 2 = 1.5444 Å, (Cu K α average = 1.5418 Å), Cu K β contamination = 1.3922 Å.

The samples were handpicked mineral particles less than 1 mm in diameter. For XRD phase identification measurements, a few particles of each sample, less than 0.5 mg in total, were placed on sample preparation glass and crushed directly on the glass in ethanol suspension using a small agate pestle, and dried.

The X-ray powder diffractograms were measured for 0.5 hours from the 2 θ range from 4 to 110° 2 θ (CuK α) in continuous measurement mode 0.06° 2 θ /s angular velocity, which divided into 6914 steps corresponds to 0.015° 2 θ -steps with the measurement time of 0.25 s/step. Primary optical path automatic diverges slits of 15 mm sample length and 2.5° soller slit. Secondary optical path contains a 2.5° soller slit and no filters.

Goniometer radius is 280 mm, motorized beam knife lifts from the sample surface during the measurement to prevent beam scattering by air at low 2 θ angles and to prevent beam shadowing by the knife at high 2 θ angles. The sample spinner was on, and the generator settings were 40 kV/40 mA.

The relative humidity of the instrument cabin was recorded at the beginning of the measurements, being 34% for all samples. The humidity of the sample somewhat affects the diffraction peak

positions of hydrous phases like swelling clays. The room temperature was 22 °C.

The phase identification (qualitative analysis) was done using Bruker EVA 6.0 software and ICDD (International Centre for Diffraction Data, Powder Diffraction File) PDF-4 Minerals 2021 database that contains only naturally occurring inorganic crystalline phases (minerals). The diffraction data was treated using 1) background fitting and 2) slit simulation to fixed slits to compensate the enhanced peak intensities towards higher 2 θ angles by the automatic slit measurement.

Diffractograms provide information on the crystal structure of the sample material phases but not directly about their chemical composition. Because of this, substances with similar chemical composition but different structures can be distinguished, such as cuprite and tenorite. Furthermore, samples containing light elements such as carbon that are undetectable by electron microprobes can be identified robustly.

Diffraction peak broadening can be caused by very fine particle size (nm-scale, crystallite size), poor crystalline order (too fast or difficult crystal growth or metamict substance), or varying chemical composition (solid solution series, isomorphism) due to non-equilibrium conditions of crystallization. Amorphous components cannot be identified, but their presence is visible in an increased background noise typically in d-spacing range 6–2.4 Å (maximum at ~4Å). In these samples, the amount of powdered material was very low, the amorphous background “hump” of the underlying preparation glass is very distinct. It does not prevent the phase identification of the diffraction peaks that appear on top of the high amorphous background.

4.6 LA-ICP-MS trace elements

Trace element analyses of native copper, cuprite, nano Cu silicate, and malachite were performed using laser ablation inductively-coupled mass spectrometry (LA-ICP-MS). The instrument is a sector field single collector ICP-MS (AttoM, Nu Instruments Ltd., Wrexham, UK) coupled with an Excite 193nm ArF excimer laser-ablation system (Photon Machines, San Diego, USA) housed at the Espoo Research Lab of GTK. Samples were ablated in He gas (gas flows = 0.4 and 0.1 l/min) within a HelEx two-volume ablation cell. The He aerosol was mixed with Ar (gas flow= 0.85–0.95 l/min) prior entering the ICP. The gas mixture was optimized daily for maximum sensitivity. Copper metal and corrosion phases (oxides, Cu silicate, and malachite) react distinctively with laser beam. Consequently, different analytical conditions and calibration strategies were used to maximize the signal for optimal precision and accuracy.

For copper metals, a series of experiments were done to select optimal laser parameters. In those experiments, a standard material ERM-EB75B (a manufactured electrolytic copper doped with known contents of trace elements) were used for calibrating the unknowns. In total, 60 spot analyses were conducted with different laser fluence (from 2.17 J/cm² to 5.79 J/cm²), repetition rate (5 Hz, 10 Hz, 15 Hz), and number of shots (200 shots, 400 shots, and 600 shots). The data has been presented in the 2022 Nordic Geological Winter Meeting (Liu et al. 2022). The laser conditions were tested against ablation pit morphology, ablation yield, lowest detection limit, analytical precision, and analytical accuracy. The general conclusion was that the higher fluence and repetition rate the better the results. The ablation at fluence lower than 4.35 J/cm² turned out to be quite poor, which were consistent with previous studies (e.g., Bogaerts et al. 2003). Even though 5.79 J/cm² produced the best results, the laser gas degraded much faster with this high fluence, which precluded automated analyses with long sequences. Instead, 4.35 J/cm² offered a good compromise between data

quality and laser gas lifetime. Therefore, the MICA native copper samples were measured with the following parameters: the laser energy was set to 60% of total 5 mJ and was focused on a 40 µm- circular spot, yielding a fluence of 4.35 J/cm². The laser was run at a pulse frequency of 10 Hz for 400 shots, which gave a 40 s signal which was preceded with baseline measurement for 20 s. Standard material ERM-EB75B was used to tune the instrument. With the laser conditions described above, ²⁰⁸Pb generated about 2500 cps at 4.8 ppm Pb. During each analytical run, standard-sample-standard (SSB) technique was employed. ERM-EB75 was used for external calibration and also quality check. Data reduction was done with GLITTER 4.4.4 software, and ⁶⁵Cu was used as the Internal Standard, assuming 99.99 wt.%. The analytical precision (standard error) was 1–5% for transition metals, 10–30% for non-metals; analytical accuracy was 10–15% for transition metals, and 50–80% for non-metals.

For trace element measurements in cuprite, Cu silicates, and malachite, lower laser energy was used, 30% of total 5 mJ and a fluence of 2.17 J/cm². The laser was run at a pulse frequency of 5 Hz for 200 shots. Each measurement was initiated with a 20 second baseline measurement followed by switching on the laser for 40 seconds for signal acquisition. Analyses were made using time resolved analysis (TRA) with continuous acquisition of data for each point (generally following the scheme of primary standard, quality control standards, 10–20 unknowns). Data reduction was performed with GLITTER 4.4.4 software. NIST-610 was used as primary reference material, and NIST-612 were used as quality control. The ⁶⁵Cu isotope was used as the internal standard assuming a stoichiometric value for cuprite, apachite, and malachite. For nano Cu silicate, ²⁹Si was used as the internal standard, and values were measured by SEM-EDS. The analytical precision and accuracy were better than 10%.

4.7 LA-ICP-MS U-Pb dating

Determination of U-Pb and common Pb ages of cuprite, Cu silicate, and malachite were attempted to be analyzed by laser ablation inductively-coupled mass spectrometry (LA-ICP-MS). The same analytical setup at the Espoo Research Lab of GTK was

used. The laser was operated with 30% of 5 mJ, a beam diameter of 25 µm, a pulse frequency of 5 Hz, and a beam energy density of 2.17 J/cm² was used. Each measurement included a short pre-ablation, 20 s of He flushing, 10 s of on-mass background

measurement, followed by 40 s of ablation with a stationary beam. The ^{235}U isotope was calculated from the signal at mass 238 using a natural $^{238}\text{U}/^{235}\text{U}=137.88$. Mass number 204 was used as a monitor for common ^{204}Pb . The contribution of ^{204}Hg from the plasma was eliminated by on-mass background measurement prior to each analysis. In an ICP-MS analysis, ^{204}Hg mainly originates from the He supply. The observed background counting-rate on mass 204 was 200–300 cps and has been stable at that level over the last years.

Calibration standard GJ-1 (609 ± 1 Ma; Belousova et al. 2006), in-house reference samples A382 (1877 ± 2 Ma, Huhma et al. 2012), and A1772 (2712 ± 2 Ma, Huhma et al. 2012) were run at the beginning and end of each analytical session, and at regular intervals during sessions. Raw data were corrected for the machine background, laser induced

elemental fractionation, mass discrimination and drift in ion counter gains and reduced to U-Pb isotope ratios by calibration to concordant reference zircons, using the GLITTER 4.4.4 software (Van Achterbergh et al. 2001). Further data reduction including common Pb lead correction and error propagation was performed using in-house Excel spreadsheets. Errors include measured within-run errors (SD) and quadratic addition of reproducibility of standard (SE). Estimated errors in the calibration standard GJ1 were: 0.2% for $^{207}\text{Pb}/^{206}\text{Pb}$, and 2% for both $^{206}\text{Pb}/^{238}\text{U}$ and $^{207}\text{Pb}/^{235}\text{U}$. To minimize the effects of laser-induced down-hole elemental fractionation, the depth-to-diameter ratio of the ablation pit was kept low, and isotopically homogeneous segments of the time-resolved traces were calibrated against the corresponding time interval for each mass in the reference zircon.

4.8 MC-ICP-MS Cu isotopes by solution and laser ablation

Cu isotopes in copper metal in the samples MICA2 and MICA3 were measured by multi-collector (MC)-ICP-MS with both solution mode and/or laser ablation mode. The cuprite, Cu silicate, and malachite were measured by MC-ICP-MS with laser ablation.

For solution analysis, about 1–10 mg drilled-out copper metal per sample was weighed (~ 0.4 – 12 mg) to 3 ml Teflon beaker. Samples were cleaned with pure alcohol (~ 0.7 ml) in ultrasonic bath for 15 min. After cleaning, alcohol was evaporated to dryness on hotplate at 120°C . Sample was then dissolved in ultra clean $\text{HCl}:\text{HNO}_3$ 3:1 mixture (1 ml). Cap was closed and sample was dissolved on a hotplate at 120°C for 1–2 hours. Sample was evaporated at 120°C to dryness and dissolved in ultra clean 2% HNO_3 (2 ml). Before the MC-ICP analysis, samples were further diluted with ultra clean 2% HNO_3 to have Cu at 1 ppm. The first 2 ml solution were diluted 200–3000 times. All vessels and pipettes were acid cleaned.

Cu isotope analyses were performed at low resolution and in static mode using a Nu Plasma HR MC-ICP-MS at the Espoo Research Lab of GTK. The standard solution NIST SRM 976 ($^{65}\text{Cu}/^{63}\text{Cu}=0.4746$) was used as the calibration standard and was reported using δ notation against this standard solution; ERM-AE647 ($^{65}\text{Cu}/^{63}\text{Cu}=0.4456$; $\delta^{65}\text{Cu}_{\text{NIST976}}=0.2\text{‰}$) was used as a quality control; standard nickel isotope solution NIST SRM 986 was aspirated into the ICP simultaneously as an internal standard. Under these conditions, after a 90 s

baseline, 240 s of sample acquisition the internal precision is $^{65}\text{Cu}/^{63}\text{Cu} \leq \pm 0.02\text{‰}$ (1 SE).

For laser ablation analysis, Cu isotopes were measured using the same MC-ICP-MS coupled with a Photon Machine Analyte G2 laser microprobe. Samples were ablated in He gas (gas flows = 0.4 and 0.1 l/min) within a HelEx ablation cell (Müller et al. 2009). Cu isotopes were analyzed at low resolution. During the ablation, the data were collected in static mode (^{63}Cu , ^{65}Cu). Again, different laser parameters were used for copper metal and other minerals.

For copper metal, the optimal laser conditions were selected based on optimization experiments described in Section 4.5. The measurements were done manually, so no compromise was needed for automation. The laser was run with line mode at 90% of 5 mJ and 25-micron spot size, 6.5 J/cm² fluence, and 10 Hz repetition rate. ERM-EB75 (the $^{65}\text{Cu}/^{63}\text{Cu}$ ratio is determined by solution MC-ICP-MS to be $\delta^{65}\text{Cu}_{\text{NIST976}}=-0.1 \pm 0.1\text{‰}$, unpublished data) was used as an external standard; ERM-EB74 (the $^{65}\text{Cu}/^{63}\text{Cu}$ ratio is determined by solution MC-ICP-MS to be $\delta^{65}\text{Cu}_{\text{NIST976}}=-0.2 \pm 0.1\text{‰}$, unpublished data) was used as a quality control; standard nickel solution NIST SRM 986 was aspirated into the ICP simultaneously as an internal standard. Results are reported as δ value compared to the NIST SRM 976 value.

For Cu oxide, silicate and malachite, a lower laser energy was used to achieve best ablation. The laser

was run at 20% of 5 mJ, a fluence of 1.45 J/cm² and 25 µm. The total Cu signal obtained for standards and samples was typically 1.0–1.5V. The CPY1 standard was used for external standard bracketing and CPY2 for quality control (Lazarov & Horn 2015). Standard nickel solution NIST SRM 986 was aspirated into the ICP simultaneously as an internal stand-

ard. Under these conditions, after a 20 s baseline, 60–80 seconds of ablation was needed to obtain an internal precision of $^{65}\text{Cu}/^{63}\text{Cu} \leq \pm 0.00002$ (1 SE). For the quality control standard CPY2 our measured $\delta^{65}\text{Cu}_{\text{NIST976}}(\text{‰})$ value is $+0.25 \pm 0.2$ (n=18, 2σ) against the average value of $+0.17 \pm 0.02$ (‰) from Lazarov and Horn (2015).

5 MAIN FINDINGS AND LIMITATIONS

5.1 2D and 3D geometry of corrosion

Knowledge of how corrosion phases and native copper are spatially related is useful for planning sample preparation, analytical locations as well as for understanding corrosion processes. In this test study, the geometry of the corrosions was investigated in two- and three- dimensions. 2D observations were made primarily by reflected light microscope; 3D observations were made using µ-XCT.

The sample MICA3 (Fig. 3), which is a cut slab of a float copper piece (cut in a random direction) and has a peculiar corrosion pattern that is much more pervasive than on the other edges of

the float sample, was investigated for the corrosion minerals in detail. Reflected light microscopy (note that the surface in this sample is unpolished) revealed complex geometry and internal structure of the corrosion zones. Viewed from 2D plan, the corrosion products formed two types of apparent geometries. Since the original float copper is not available, little conclusion can be made of the 3D geometry of the original strongly corroded area. Both emanating from the sample edge, the upper part of corrosion products is interconnected to form a “cob-web” geometry, with irregular “islands” of copper metal, whereas the lower part ones occur

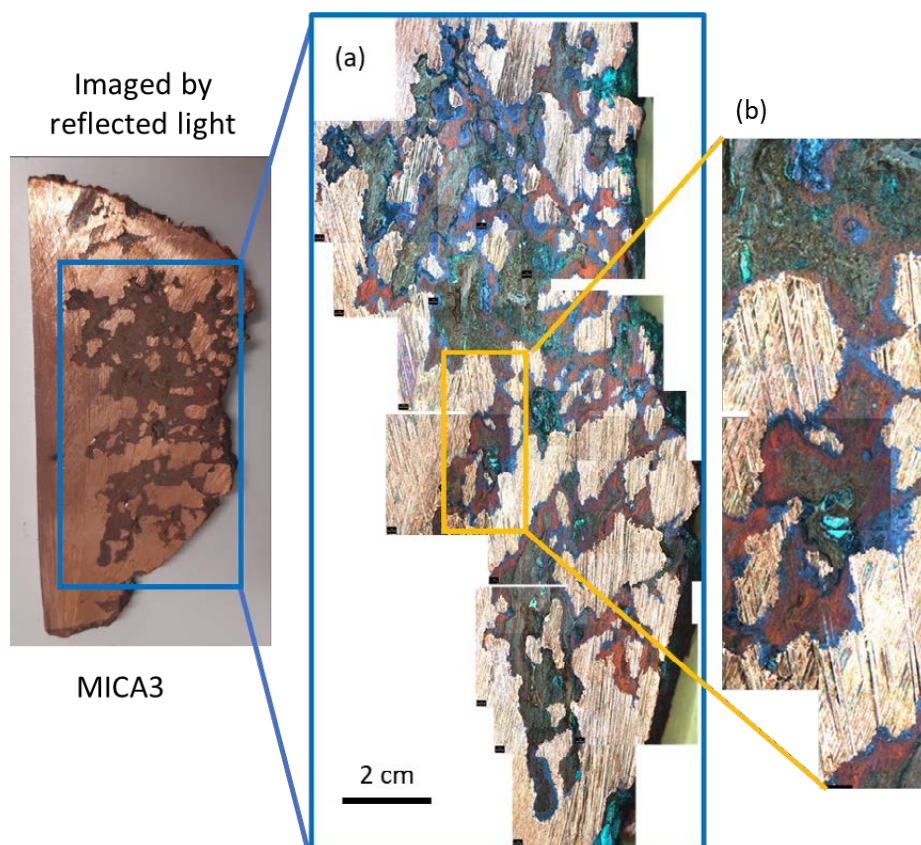


Fig. 3. Corrosion geometry viewed by reflected light microscope for one cross-section (as received in the sample).

as discrete elongated channels and display less interconnectivity (Fig. 3a). Internally, these corrosion zones display layer structures, transitioning from metallic blue cuprite next to copper metal, to reddish cuprite. These Cu oxide zones are best preserved in the channel structures (Fig. 3b) and are commonly disrupted by brownish nano-scale mixture of cuprite and clinoclhorite in the “cob-web” structure. Detailed mineralogy is described in the Section 5.2.

The observed structure is likely formed during a complex process of fluids interacting with native copper (likely prior to the float formation since the other surfaces of the sample show no pervasive alteration). However, the analysis shows that in 2D we can distinguish minerals and relevant patterns for further assessment of the corrosion processes. The sample MICA3 is an important sample for recording the 3D setting of the sub-samples in any future sampling. However, MICA3 has a thickness of about 1 cm, providing opportunity to look at corrosion geometry in a 3-D space, even if limited, comparing to the original float copper (Fig. 4). XCT 3D imaging revealed a generally similar pattern as seen on the sample surface, but noticeable differences have been observed at different depths (along the y-axis) as exemplified by the yellow boxes in Figure 4.

The main objective of the examination was to see what type of structures can be observed via XCT and if mineral phases are distinguishable. Similar imaging has been done for the other 7 samples as shown in the Figure 5 and Figure 6. Key observations for each sample are outlined below.

For MICA1 (Fig. 5a.1), silver grains are clearly distinguished from cuprite on the 3D surface (Fig. 5a.3) and from copper host on the 2D section (Fig. 5a.2) by their higher brightness. Similarly, thin layers of cuprite (<1 mm in thickness) coating on native copper are recognizable in the 2D section). Unfortunately, malachite, although optically seen in Figure 5a, did not show up properly in the XCT images due to the presence of beam hardening artefact and high background.

For MICA4, a primary copper pinch-out structure (Fig. 5b.1) is vividly revealed in the 3D image (Fig. 5b.2). Copper metal is clearly distinguished

from surrounding quartz fragments in the 2D section (Fig. 5b, right). Some fake responses exist in the center of the copper block. Irregular boundary between copper and quartz is very clear.

For MICA5 (Fig. 5c.1), 3D imaging shows the topography of the sample, with a small degree of artefact (Fig. 5c.2). Similar to MICA1, cuprite is clearly distinguished from copper host, but its boundary with malachite is ambiguous due to fake responses and background.

For MICA6 (Fig. 6a.1), 3D imaging shows the topography of the sample, clearly revealing the distinction between the corrosion crust and underlying native copper (Fig. 6a.2). The 2D section also shows low-density features (grains or voids) in the sample and provides a good tool for observing their orientation in the sample.

For MICA7 (Fig. 6b.1), 3D imaging shows the topography of the sample, clearly revealing the distinction between the green apachite and surrounding red sedimentary clasts (Fig. 6b.2). The 2D section clearly shows apachite filling the interstitial space of the conglomerate (Fig. 6b.3). It also seems to indicate the presence of other phases (brightness higher than the host but lower than apachite), but this observation needs further confirmation due to presence of fake responses.

For MICA8 (Fig. 6c.1), 3D imaging shows the topography of the sample, and the distinction between malachite and copper, but it is not possible to clearly tell calcite apart from malachite (Fig. 6c.2). However, the 2D section clearly shows calcite and surrounding copper can be distinguished, but malachite not (Fig. 6c.3).

For MICA9 (Fig. 6d.1), 3D imaging shows the topography of the sample, with some amounts of noises (Fig. 6d.3).

Clearly, the combination of 2D microscopic and 3D XCT techniques are a useful tool for describing the geometry of copper corrosion minerals. Nonetheless, the peculiar nature of corrosion samples in terms of varieties of mineral phases, and very thin corrosion layers can be a challenge using XCT. This is especially true for low-density minerals like malachite. However, as a non-destructive method, XCT is seen useful to be used prior to applying destructive sub-sampling.

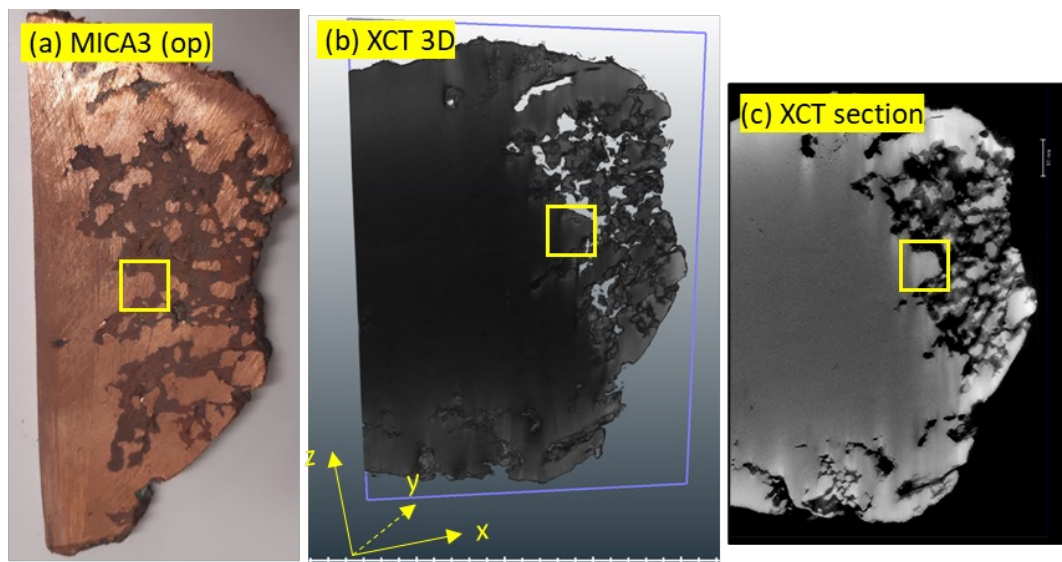


Fig. 4. XCT 3D imaging (b, c) compared to an optical image (a) of the MICA3 sample. In the XCT 3D image (b), topography of native copper is clearly visible, and the areas with corrosion minerals are shown as “pits” and “holes”; the large batch of dark in the copper host is a result of beam hardening artefact and does not represent real density contrast. The XCT section (c) is a cross-section plan as denoted by the blue square in the 3D image. In this image, the corrosion minerals are represented by lower brightness than the copper host. Cuprite (gray) and Cu silicate (black) are also clearly distinguished.

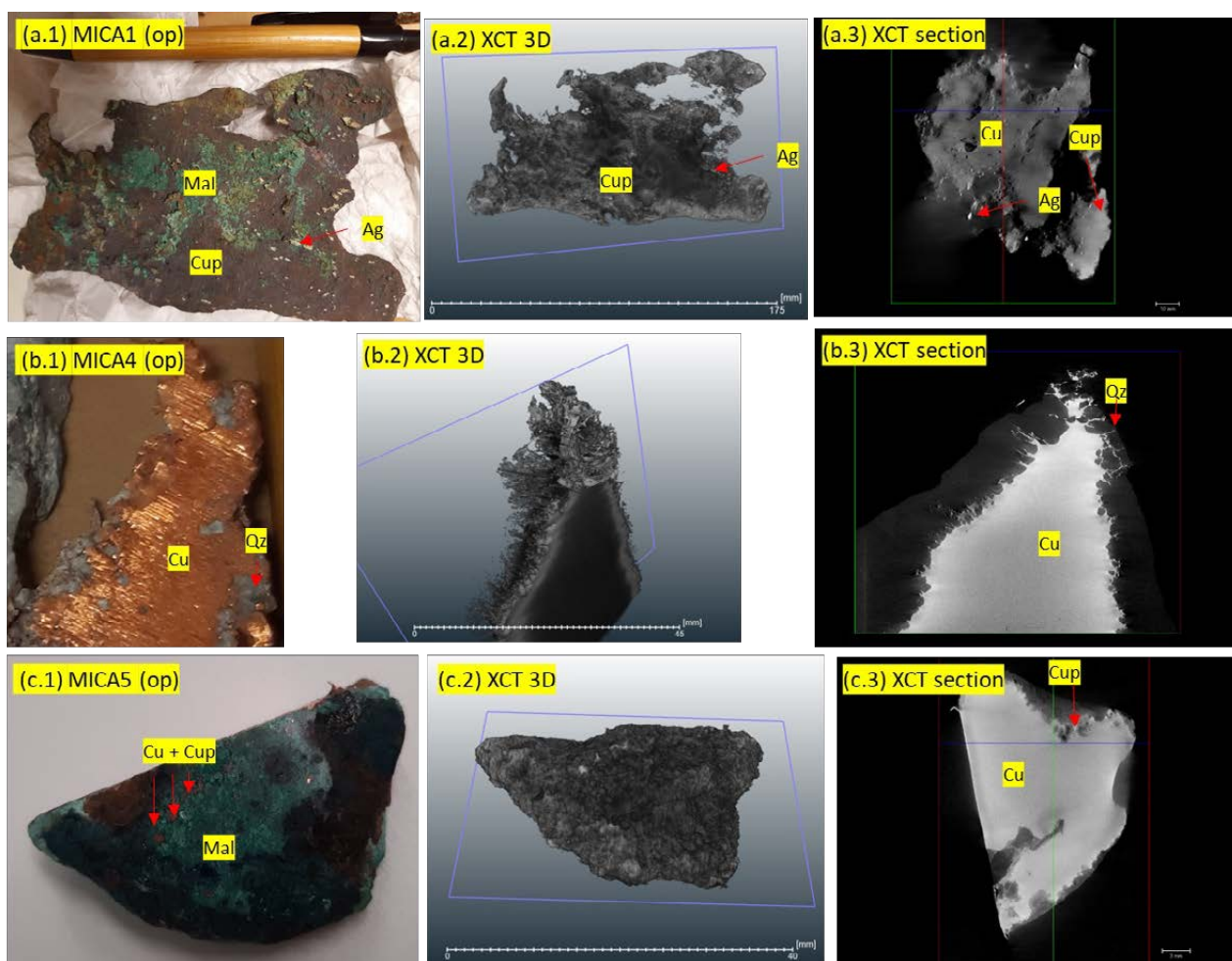


Fig. 5. A compilation of photographs for the samples MICA1 (a. 1–3), MICA 4 (b. 1–3) and MICA 5 (c. 1–3) imaged by XCT. The images include an optical image, a 3D, and 2D cross section from XCT. Some detailed descriptions are provided in the main body of text. APc: apachite; Cc: calcite; Cu: native copper; Cup: cuprite; Mal: malachite; Qz: quartz; op: optical; XCT: X-ray computed tomography.

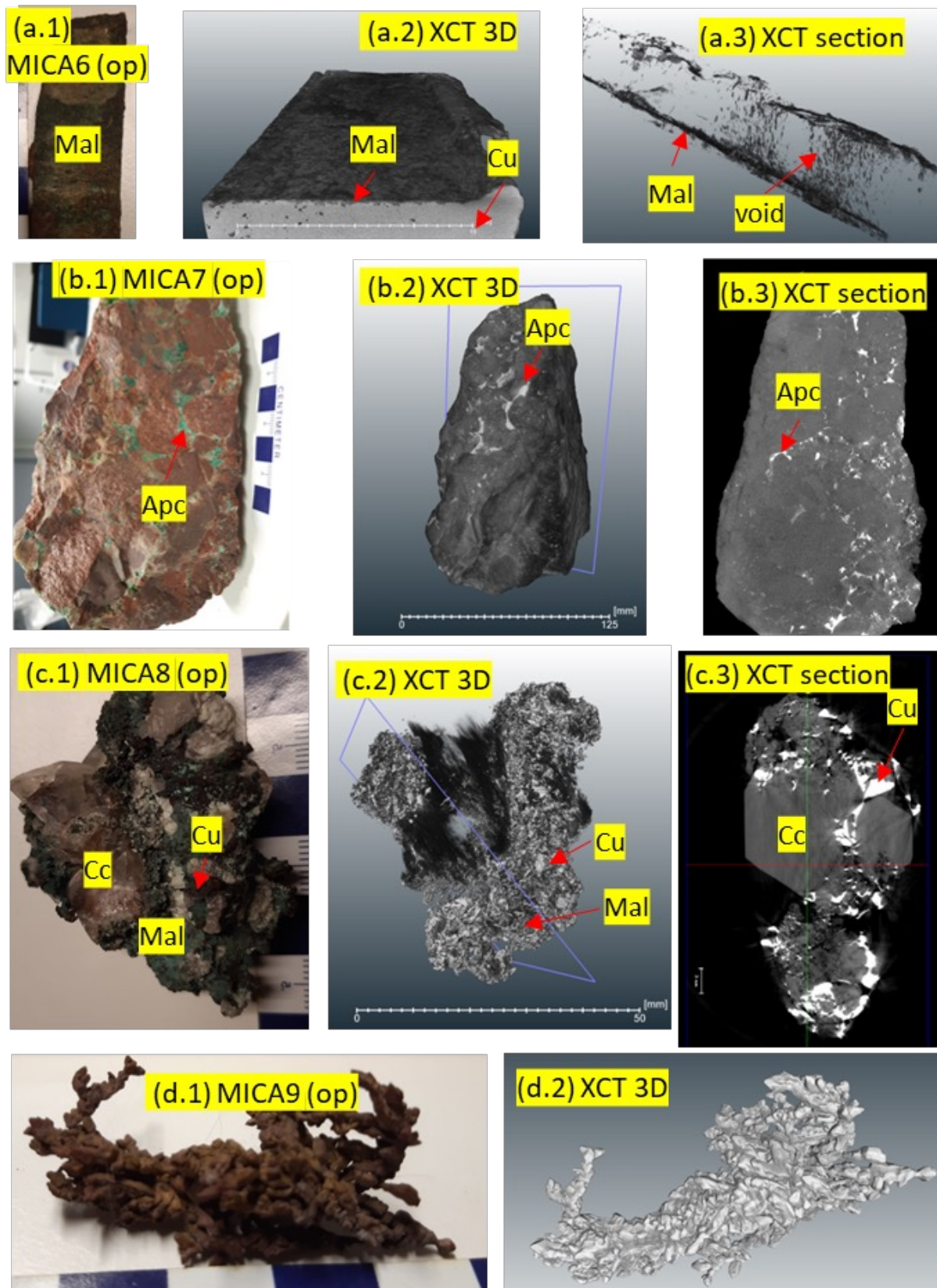


Fig. 6. A compilation of photographs for the samples MICA 6 (a), MICA 7 (b), MICA 8 (c) and MICA 9 (d) imaged by XCT. The images include an optical image, a 3D, and 2D cross section from XCT. Some detailed descriptions are provided in the main body of text. APC: apachite; Cc: calcite; Cu: native copper; Cup: cuprite; Mal: malachite; Qz: quartz; op: optical; XCT: X-ray computed tomography.

5.2 Mineralogy

In this test study, mineral phases related to native copper corrosion were first studied based on reflected light microscopy and SEM-EDS. This integrated technique is effective for obtaining a rough idea about mineral species including native copper, native silver, copper oxides, and copper carbonate, but appears insufficient to distinguish between different species of copper oxides and sometimes telling apart carbonates from silicates. This insufficiency stems from limitations of the instrument used. For instance, EDS spectroscopy is relatively insensitive to elements lighter than Na, including carbon and oxygen that are the major constituents of oxides and carbonates. Consequently, XRD was utilized as a complementary tool. The XRD results

for malachite are later confirmed by LA-ICP-MS analyses.

Following the format from previous section, MICA3 is used as an example. As described in the Section 5.1, corrosion in the MICA3 exhibit four colors under reflected light. Metallic gray and reddish colored grains occur in the corrosion channels/volumes and “cob-webs” sitting in the native copper host (Fig. 7). Within these, brownish corrosion minerals are observed, which show internal banding of dark and bright brown. The contact between metallic gray-reddish zone and brownish zone is transitional with respect to color and banding (Fig. 7c). Both zones have also bright green corrosion products that appear younger than the

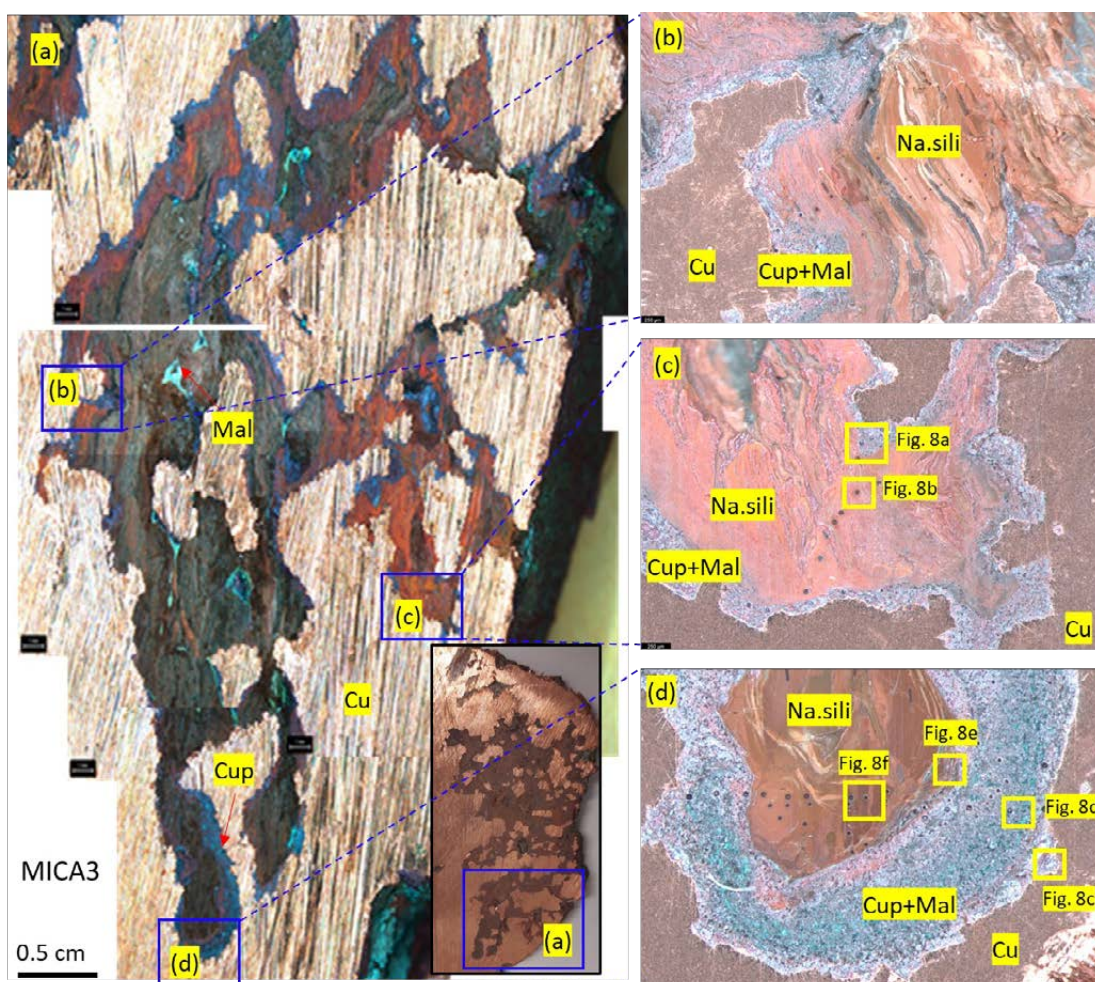


Fig. 7. Microphotographs of the MICA3, showing structure, texture, optical properties of corrosion minerals. (a) A close-up view of hand specimen; (b) A close-up image showing mineralogical transition from Cu oxides (reddish and metallic gray) to banded Cu oxides (red) and banded brown corrosion; (c) A close-up view showing similar phenomenon to with (b) less brown corruptions; (d) A close-up view showing malachite invading the older two corruptions. It should be noted that Figure 8a was taken before polishing, the blueish color was tenorite formed via surface oxidation of cuprite. After polishing, the blueish color disappeared and turned into mixed metallic gray and green (also see elaborations in Section 3.1). Cu: native copper; Cup: cuprite; Mal: malachite; Na. sili: nano-mixture of cuprite and clinocllore.

others two generations aforementioned (Fig. 7d). Based on these optical properties, these minerals were initially identified as cuprite (reddish), tenorite (metallic gray), and malachite (brownish and green).

The aforementioned mineralogical interpretation was tested with SEM-EDS for a semi-quantitation of chemical composition for the minerals of interest. In total, 149 spot analyses were made within the two areas shown in Figures 7c, 7d, and Table 4 (14 for copper, 27 for cuprite, 66 for nano Cu silicate, 42 for malachite). EDS analyses suggest that

the copper was nearly pure Cu, with no other elements being detected in the spectra. Even though no reliable information about the limit of detection (LOD) is available, it is safe to conclude no other elements were at content higher than 1 wt.%. It is worth mentioning that C and O was always present in the EDS spectra due to presence of small amount of air in the sample chamber. To reliably exclude these two elements, copper standard ERM-EB75b, which contains no C and O, was analyzed at the same time, which gave quite similar peak areas (150–200 for C) as copper in MICA3.

Table 4. Examples of major elements (in wt.%) in native copper in MICA3 and EB75 copper standard analyzed by SEM-EDS.

Sample	Spectrum	C	O	Cu	Total
MICA3	Figure 7a 1	6.15	3.43	90	100
	Figure 7c 1	3.03	0.720	96	100
ERM-EB75B	1	6.86	b.d.l.	93	100
	2	10.4	1.43	88	100
	3	8.24	b.d.l.	92	100

b.d.l.: below detection limit. Note that the data selected here are for illustrative purpose.

Under BSE imagery, cuprite shows lower brightness than copper (Fig. 8a,c,d,e). After excluding C signal, EDS spot analyses of cuprite yielded an average of 84 ± 6 wt.% (1sd; n=27) of Cu and 16 ± 7 wt.% (1sd; n=27) of O. This chemical composition only slightly deviated from stoichiometric values (89 wt.% for Cu; 11 wt.% for O) but is apparently higher than tenorite (80 wt.% for Cu; 20 wt.% for O). These chemical analyses support the possibility of using EDS to identify cuprite, but it is recommended that other features (mineral color, XRD spectrum) should be combined to be fully conclusive.

Under BSE imagery, the unzoned reddish phases exhibit slightly lower brightness than cuprite (Fig. 8a). EDS analyses show an average of 60 ± 10 wt.% (1sd; n=24) of Cu and 29 ± 8 wt.% (1sd; n=24) of O, with about 5 wt.% Si, 3 wt.% Fe, 1 wt.% Al, and minor amounts of Mg, K, Ti. Chemical analyses alone cannot identify this mineral species.

Under BSE imagery, the banded brownish phases (Fig. 7a,c) appeared as dark (Fig. 8a,b,e,f). EDS analyses indicate that they contain an average of 12 ± 8 wt.% (1sd; n=39) of Cu, 14 ± 3 wt.% (1sd; n=39) of Si, 12 ± 9 wt.% (1sd; n=39) of Fe, 4 ± 1 wt.% (1sd; n=39) of Al, 1.3 ± 0.7 wt.% (1sd; n=39) of K, 1.2 ± 0.9 wt.% (1sd; n=39) of Mg, and minor amounts of Ti. Within these phases, there exist heterogeneous bands differing in BSE brightness (Fig. 8f). Both phases show similar Cu content (about 12 wt.%) but differ in Fe–Mg and Si–Al–K contents. The brighter zone contains higher Fe (26 wt.% vs. 18 wt.%) and Mg (1.3 wt.% vs. 1.0 wt.%), but lower Si (11 wt.% vs. 16 wt.%), Al (2.8 wt.% vs. 3.8 wt.%), and K (0.7 wt.% vs. 1.7 wt.%). Similar to the reddish phase, it was not possible to assign this chemical composition to any known mineral species. However, XRD showed that this phase is not a single mineral but rather a nano-scale mixture of cuprite and clinocllore.

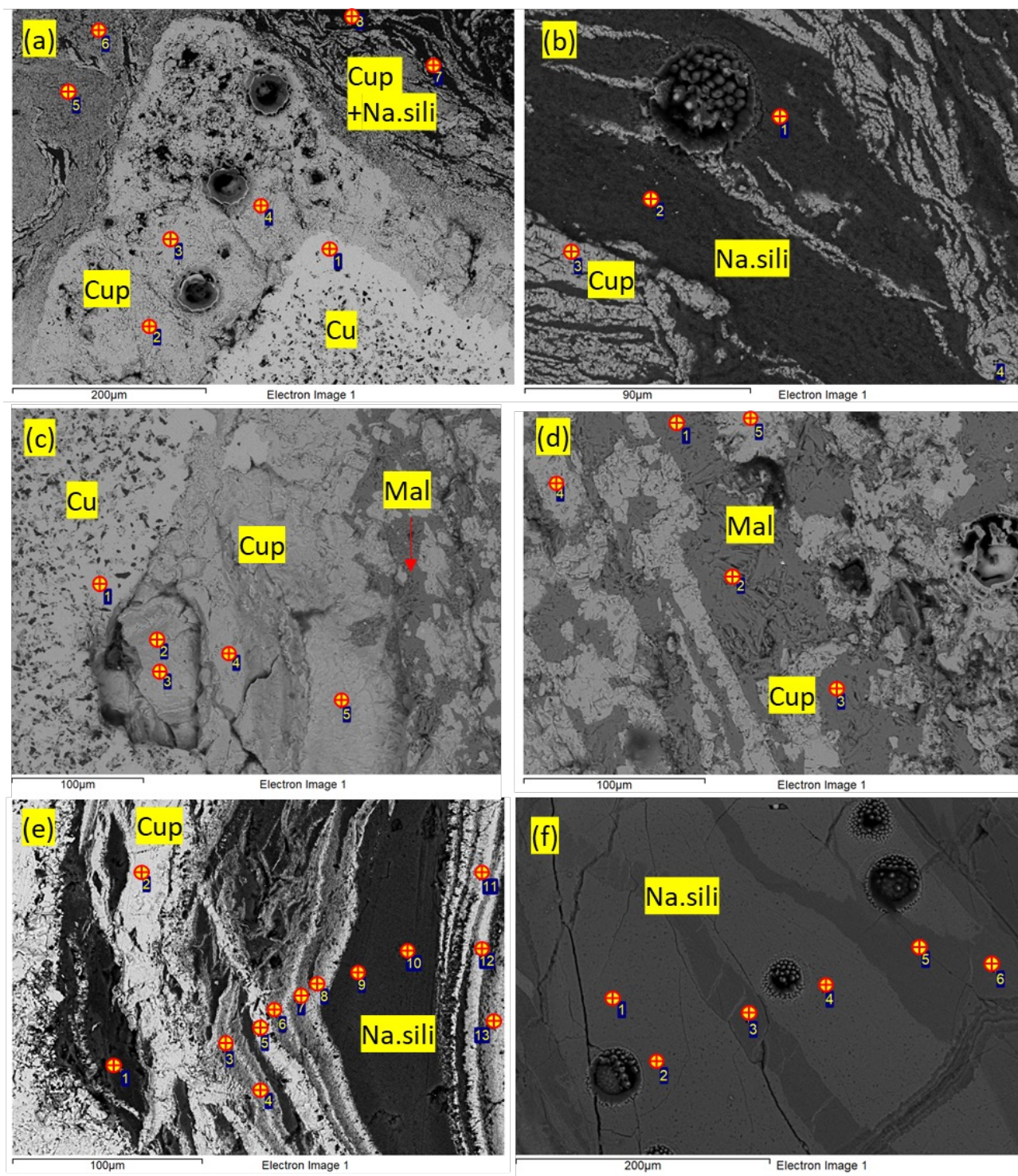


Fig. 8. BSE images of the MICA3. Areas of imaging are shown in Figure 8. The circled crosses represent locations of EDS spot analysis; the numbering beside can be found in the annexed original data file. Analyses on native copper (a.1 and c.1) are specifically shown in the Table 4. The holes in the images are laser ablation pits for trace element and U-Pb dating. Details about BSE feature, mineral species discussion and EDS chemical results are described in the relevant texts. Please note that the size of the circled crosses is much larger than the electron beam size (1–3 µm). Cu: native copper; Cup: cuprite; Mal: malachite; Na. sili: nano-mixture of cuprite and clinocllore.

The greenish minerals (Figs. 7d, 8d) are characterized by increased signal of carbon compared to other mineral phases. Considering the low sensitivity of EDS on C, elemental quantification is not used for further discussion. In the EDS spectrum, Cu was detected as a major component subordinated by Si, C, and O. XRD analyses detected malachite as the only possible candidate for this mineral.

These chemical patterns observed in EDS point analysis were further confirmed by μ -XRF element

mapping (Fig. 9). Furthermore, μ -XRF scanning suggested that these local patterns consistently showed up in a larger scale. This means that EDS and μ -XRF are complementary with the respect of capability of spatial coverage. μ -XRF should be considered as a tool for an initial quick screening of samples.

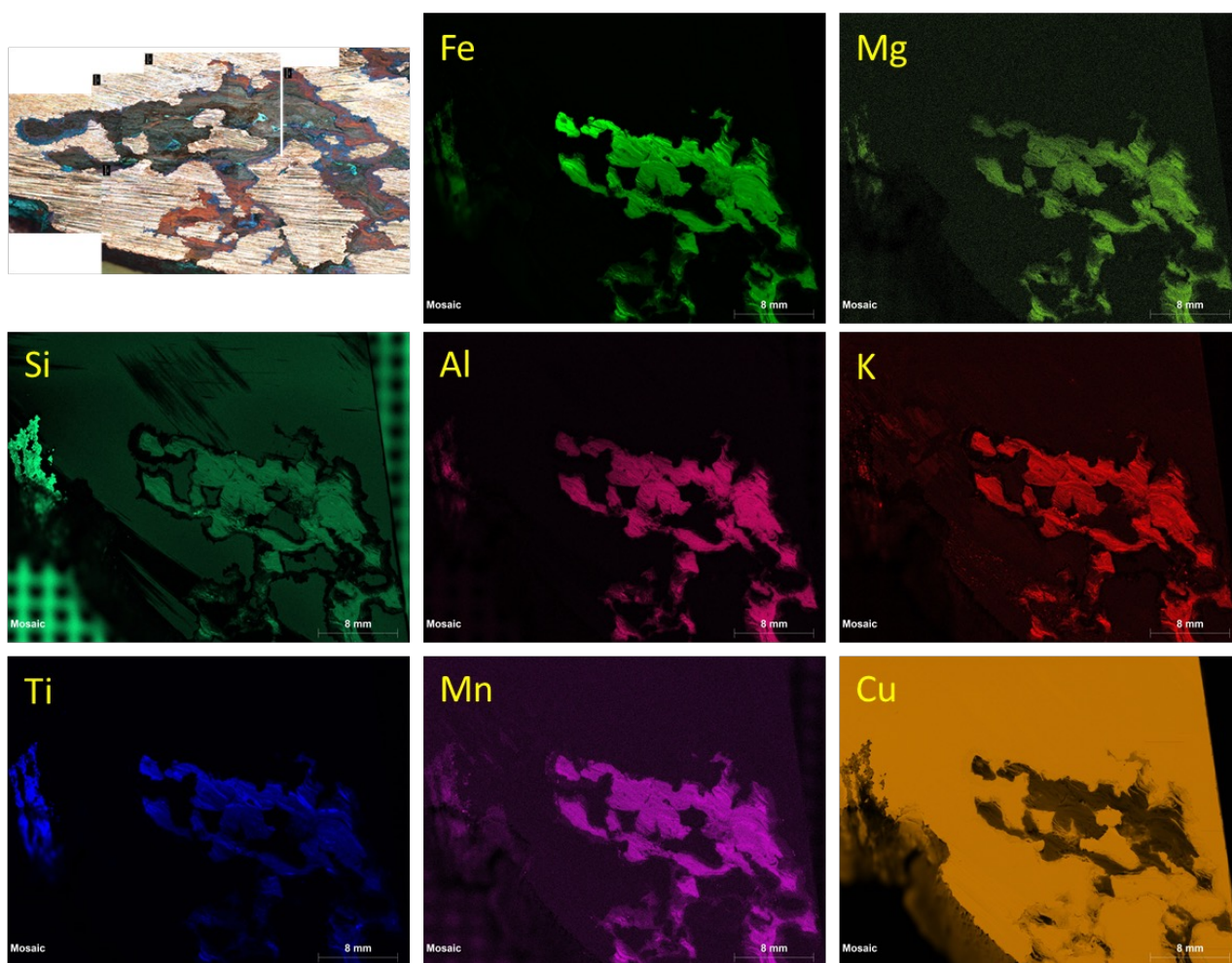


Fig. 9. μ -XRF imaging of the MICA3. The image in the upper left corner was taken with reflected light, and the remaining ones are elemental maps based on sample's fluorescence response to X-ray radiation. In general, the elemental patterns are consistent with what have been revealed by EDS analyses, but μ -XRF is capable of scanning larger areas in a much shorter time.

Mineral phases in the MICA3 were further investigated by XRD, especially the reddish and brown phases whose chemical compositions do not point to any known mineral species. About 100 grams of fragment were cut from the sample, followed by crushing and hand-picking. The hand-picking was done in an exhaustive way to recover all types of minerals based on their optical properties such as

color, luster, transparency, and crystalline habit. In total, four types of minerals were recovered as shown in the Figures 2 and 10.

The results suggest that both the metallic gray and reddish phases are cuprite, with a small amount of malachite present in the metallic gray grains (Fig. 10a). No tenorite peaks have been identified, and thus they may not be present in the samples.

The reddish phases containing 50–60 wt.% Cu do not represent unknown minerals, but rather represent mixtures of cuprite and another phase. The presence of Si, Fe, and Al suggests that this phase is most likely a cuprite–clinochlore nano-mixture.

Regarding the brown phases, XRD analyses suggest that they do not represent unknown mineral, either. Instead, the peaks in the XRD spectrum (Fig.

10a) correspond to a mixture of cuprite and clinochlore. Since the analyzed grains were powdered down to μm -size, it is sensible to infer that the mixtures were at nm-scale. This interpretation can explain the chemical compositions revealed by EDS and μ -XRF.

Lastly, the green phases are confirmed by XRD to be malachite.

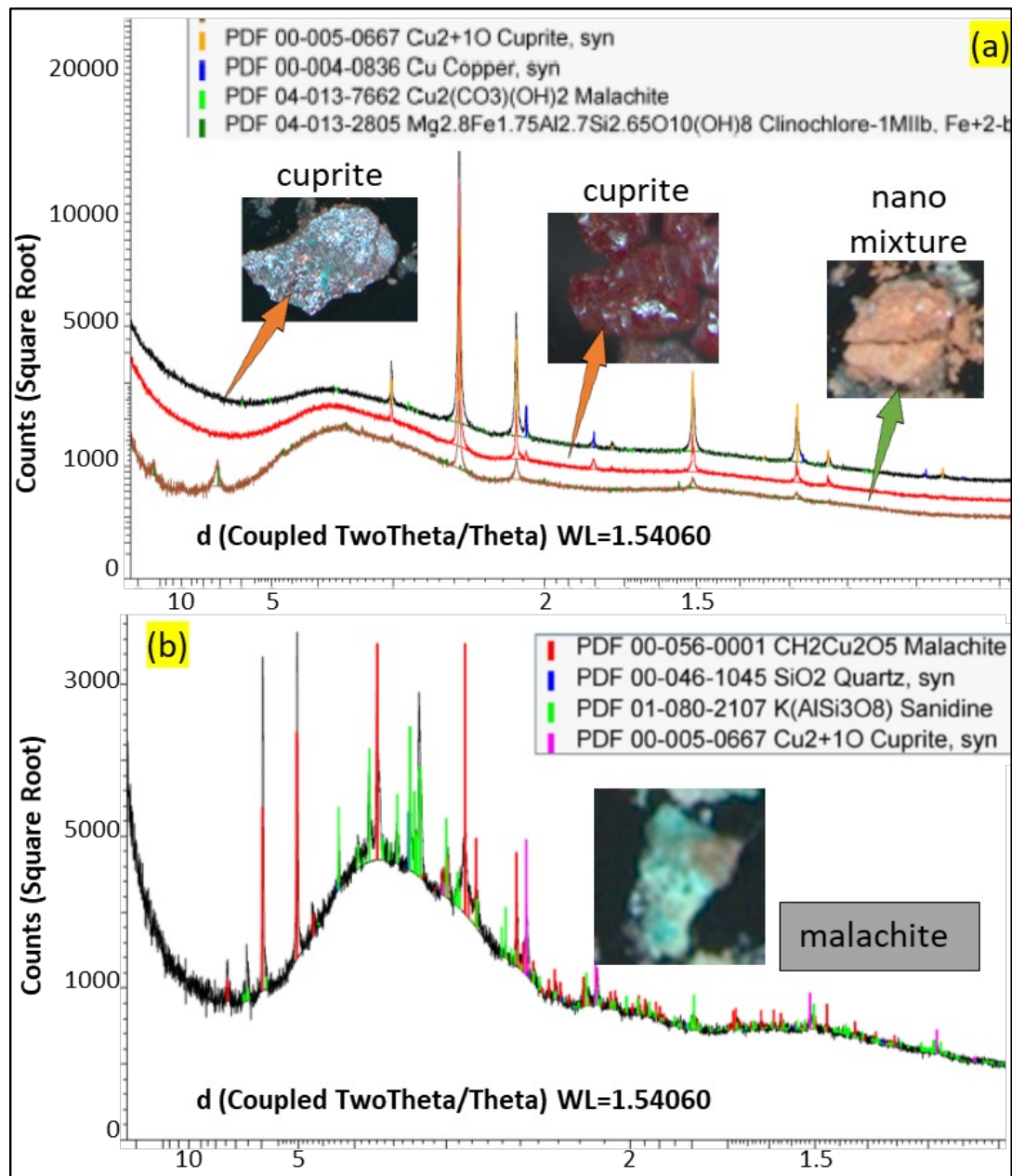


Fig. 10. XRD spectra for mineral separates from the MICA3 sample. (a) Three spectra obtained on metallic gray, red, and brown phases; (b) One spectrum obtained on green phase. Peaks of the spectrum gives the crystallographic information pointing to specific mineral. In (a), the metallic gray particle produced peaks that are indicative of cuprite, native copper, and malachite; the red phase produced peaks of cuprite; the brown phase produce peaks that are designated to cuprite and clinochlore. In (b), the green phase produced various peaks that correspond to malachite, quartz, sanidine, and cuprite. The inset images are the four types of minerals hand-picked from the sample. They are believed to represent the whole mineral species presented in the sample. More details about the sample petrography and elaborations of the XRD results are described in the main text.

Another five samples were studied with the same methodology. The main findings are described below.

In MICA11, 50 spot SEM-EDS analyses have been made. The chemical results have revealed three types of minerals, including native silver, cuprite, and malachite. These minerals are identifiable with hand specimen and microscope (Fig. 11a,b). Under

BSE, native silvers showed the highest brightness (Fig. 11c), and EDS analyses indicate that they contain around 94 ± 2 wt.% Ag (1sd; n=15) with 6 ± 2 wt.% Cu. Cuprite showed lower brightness (Fig. 11d) and contained 81 ± 4 wt.% Cu (1sd; n=28). Malachite showed up dark in BSE images (Fig. 11d), and EDS picked up deviated Cu contents (45–60 wt.%) due to inefficiency in analyzing carbon.

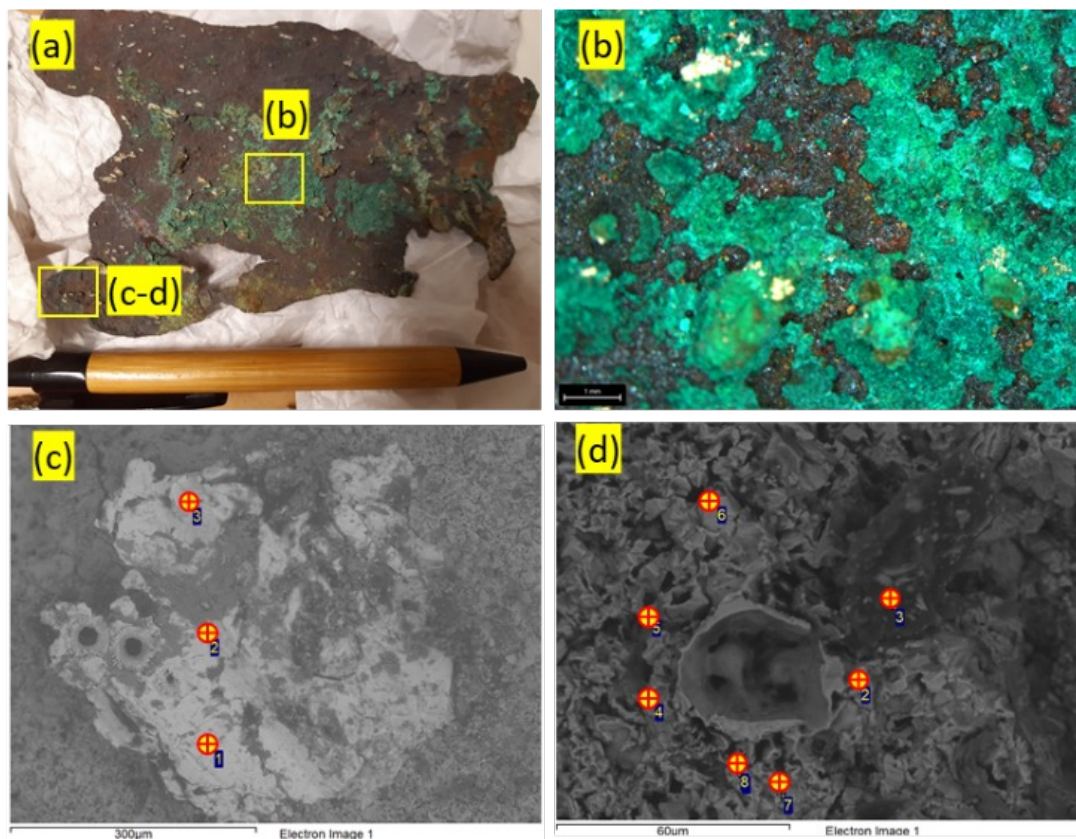


Fig. 11. Images of MICA11 taken with optical camera (a), a reflected microscope (b) and SEM (c-d). Malachite is seen overlying cuprite, and silver pinches out from the sample surface. These minerals are confirmed by EDS analyses.

The MICA5 was fully covered by a greenish crust (Fig. 12a). Optical observation on polished surface implied that there existed another layer of cuprite in contact to native copper (Fig. 12b,c). The greenish crust was tested with XRD, showing spectra corresponding to malachite (Fig. 12d).

In MICA6, 84 spot SEM-EDS analyses have been made. The green minerals on the surface showed intermediate brightness under BSE (Fig. 13b,c),

and EDS analysis revealed chemical compositions close to malachite, with 40–50 wt.% Cu, 10–20 wt.% C, and 30–50 wt.% O. The reddish minerals underneath malachite showed high brightness under BSE (Fig. 13b,c), and EDS analyses yielded chemical composition similar to cuprite (90 wt.% Cu; 10 wt.% O). Apart from these, quartz has been identified as well, showing a dark BSE (Fig. 13c).

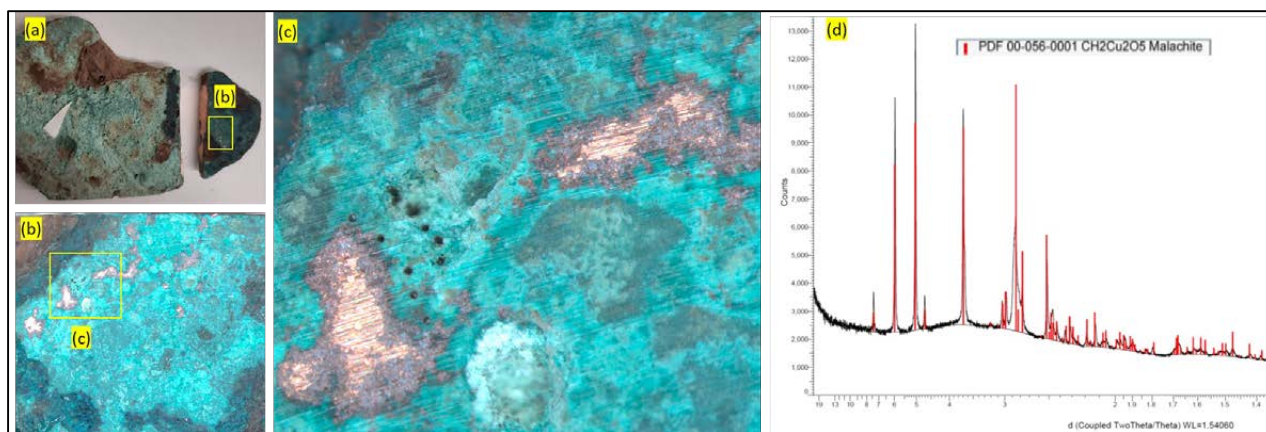


Fig. 12. Images of MICA5 taken with optical camera (a), reflected light microscopes (b, c), and XRD (d).

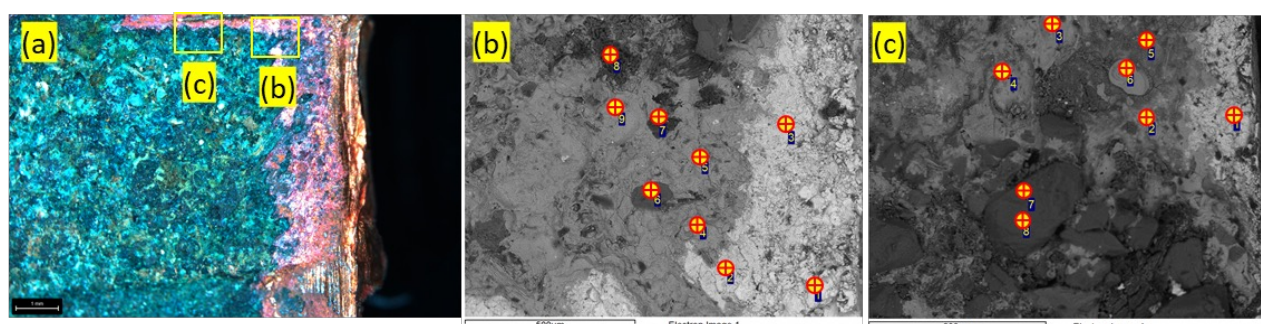


Fig. 13. Images of MICA6 taken with reflected light microscope (a) and SEM-BSE (b-c). Malachite is seen overlying cuprite, and silver pinches out from the sample surface through the alteration layer. These minerals are confirmed by EDS analyses. Quartz is identified.

In MICA7, a blue mineral grows in the interstitial space between conglomerate clasts (Fig. 14a,b). SEM-EDS analyses revealed highly consistent Cu, Si and slightly variable Al. Sixteen analyses revealed 31 ± 2 wt.% (1sd) Cu, 21 ± 0.4 wt.% (1sd) Si, 47 ± 3 wt.% (1sd) O, and variable Al (0–0.6 wt.%). The

composition is most close to that of apachite (37.8 wt.% Cu; 18.5 wt.% Si; 42.2 wt.% O; 1.5 wt.% H). Chrysocolla (33.9 wt.% Cu; 17.1 wt.% Si; 45.1 wt.% O; 2.1 wt.% Al; 1.9 wt.% H) is less likely since Al in the sample is too low.

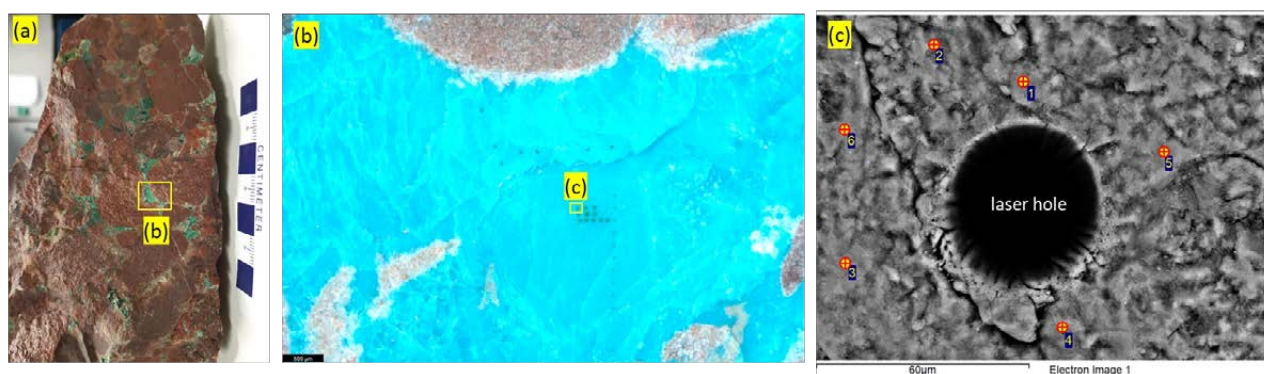


Fig. 14. Images of MICA7 taken with optical camera (a), reflected light microscope (b) and SEM-BSE (c). Apachite is suggested by SEM-EDS analyses.

MICA10 is a special sample with native copper veinlets crosscutting stratabound chalcocite (Cu_2S) hosted by black shale (Fig. 14a). It is expected that this type of sample might contain copper corrosion

involving sulfidation. Under reflected light microscope, most native copper remains optically unaltered (Fig. 15b) except in several smaller veinlets Cu oxides can be seen (Fig. 15c).

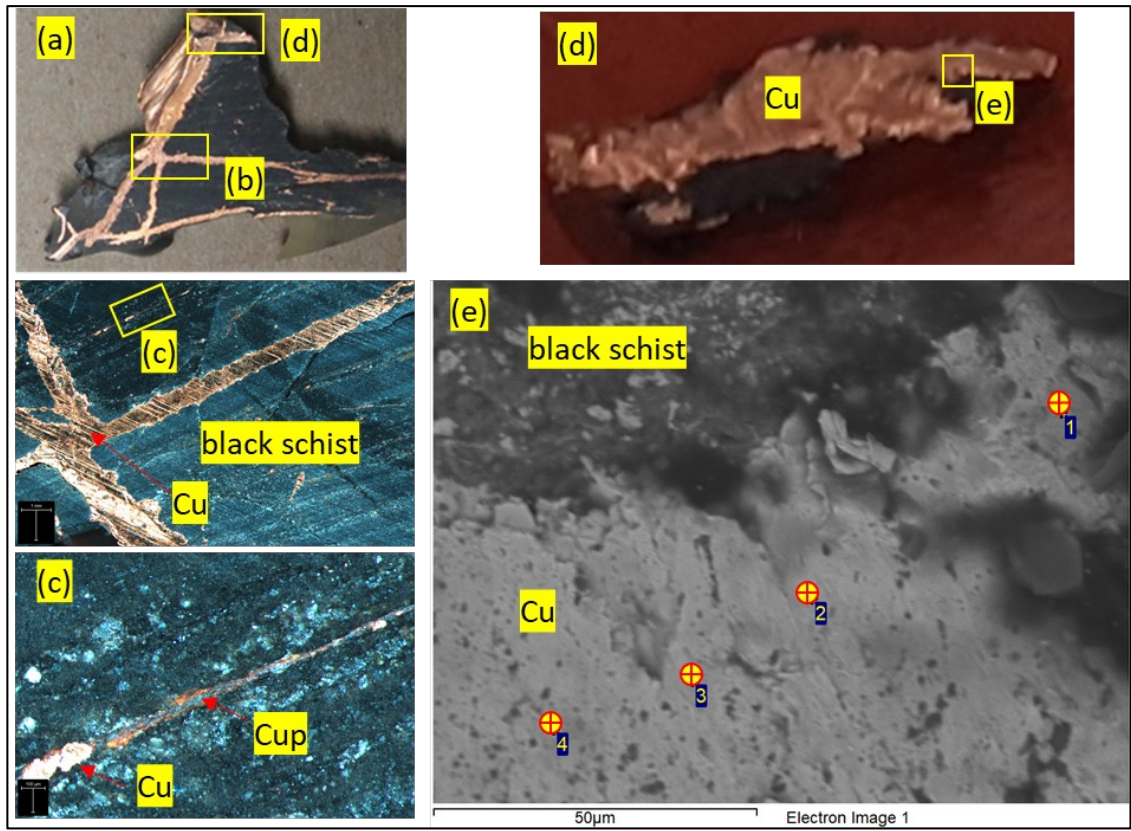


Fig. 15. Images of MICA10 taken with optical camera (a, d), reflected light microscope (b–c), and SEM–BSE (e). Optically, the sample contained Cu oxides hosted in chalcocite stratabounds (c); EDS analyses revealed sulfur in the copper, but the sulfur state is unknown.

Eighteen SEM–BSE–EDS analyses on native copper suggest the presence of sulfur. Under BSE, the copper displayed patchy texture (Fig. 15e). Compared to bright part that is nearly pure copper, EDS analyses revealed that the darker patches (Fig. 15e) may contain 5–20 wt.% sulfur in addition to Cu (80–90 wt.%) and O (5–10 wt.%) (Table 5). The O signal intensity (peak areas) were similar to

copper standard (ERM–EB75b); therefore, it is quite likely that O does not exist in significant amount in the analyzed sample. However, the composition is far from any type of Cu sulfide and sulfur bearing patches are disseminated throughout the native copper. Currently it is not possible to know the state of sulfur in this analyzed sample.

Table 5. Major elements (in wt.%) in native copper in MICA10 analyzed by SEM–EDS.

	Spectrum	O	Al	Si	S	Cu	Total
1	Figure 15e 1	7.67	b.d.l.	1.40	9.33	82	100
2	Figure 15e 2	6.57	b.d.l.	1.39	b.d.l.	92	100
3	Figure 15e 3	7.20	1.26	1.17	18.23	72	100
4	Figure 15e 4	8.77	b.d.l.	2.63	4.36	84	100

b.d.l.: below detection limit.

As to analytical methods, it can be concluded that a combination of microscopy, SEM-BSE-EDS, and XRD is effective in revealing corrosion mineralogy to the greatest extent. Nevertheless, there are still limitations, such as in X-ray spectroscopy (EDS, μ -XRF, EMPA) due to the inefficiency of detecting light elements such as C, O, H, etc., which are

common in corrosion minerals. Power XRD (this test study) can bypass the problem by probing into crystal structure, but meaningful studies could be affected by sampling bias. Inasmuch, other methods should be taken into consideration, such as LIBS, in-situ XRD, Raman, and infrared spectroscopy.

5.3 Trace element geochemistry

Understanding the trace elemental features in the native copper and various corrosion minerals are beneficial in several aspects. It provides a baseline for comparing copper host and its corrosion minerals. A good knowledge of element mobility and partitioning behavior can be helpful in studying corrosion conditions and processes. Insights into elemental patterns (content, zonation, etc.) is also essential information to adequately characterize the starting material and can potentially help decipher corrosion mechanisms, for instance, corrosion along element zonings. In addition, a good understanding of the trace elements in the corrosion mineral (and potentially copper host) can provide valuable information for subsequent isotope studies.

The following sections are devoted to describing trace element patterns within the minerals observed in this test study including native copper, cuprite, Cu silicate (nano-silicate and apachite included), and malachite.

5.3.1 Native copper

Overall, 80 measurements have been made on 5 samples, including MICA2, MICA3, MICA4, MICA5, and MICA10 (Fig. 16, Table 6). In general, these native copper samples contain detectable amounts of Si, Ti, Fe, Ni, Zn, As, Se, Ag and Pb. The contents typically vary between samples in a significant manner.

Silver is a relatively less variable element that constantly occurs at a significant level. Therefore,

it is used as a reference element in bivariate plots.

The analyzed copper samples are characterized by significant amounts of silver, which is in accordance with previous studies (see Section 4.4 in the main report). MICA2 copper has the lowest averaged Ag content (18.5 ± 24.1 ppm). MICA3 (109 ± 34 ppm), MICA4 (208 ± 24 ppm), and MICA10 (82 ± 8 ppm) have similar Ag contents, while MICA5 has the highest Ag (273 ± 41 ppm). All samples contain Ti (1–9 ppm), Fe (6–18 ppm), Ni (2–10 ppm), Zn (2–8 ppm), As (4–13 ppm), Se (1–9 ppm), and Pb (0–3 ppm) (Fig. 16b–h), which is not typically detected in Keweenaw Peninsula native copper (see Section 4.4 in the main report). It is worth noting that MICA10 contains exceptionally high As (4738 ± 2601 ppm); MICA3 contains higher Pb (10.6 ± 15.2 ppm) as generally observed in Keweenaw Peninsula native coppers, with large variations in concentrations (see Section 4.4 in the main report). On the Si–Ag and Pb–Ag plots (as an example) (Fig. 17a,b), different samples can clearly be distinguished.

An analytical traverse in MICA3 revealed variations in Ag and Pb (Fig. 18). The laser measurements are located along a traverse with increasing distance to the boundary of a corrosion rim and copper host (from #16 to #29). Results show a variation in Ag content with an increasing start, decreasing middle and a flat-out end (Fig. 18). A similar pattern is also seen in Pb. On a bivariate plot, there is a correlation between Pb and Ag with two outliers (Fig. 17).

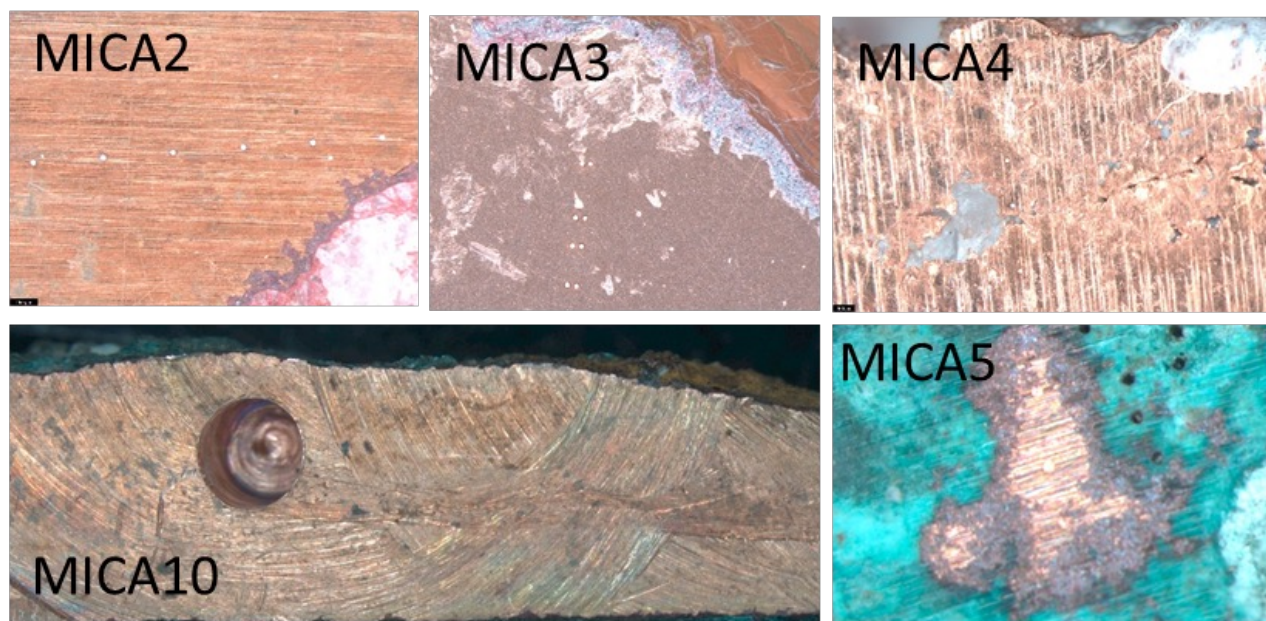


Fig. 16. Images of native copper samples analyzed for trace elements by LA-ICP-MS.

Table 6. Trace element contents (ppm) in the native copper analyzed by LA-ICP-MS.

Sample	Spot	Be	Si	S	Ti	Cr	Mn	Fe	Co	Ni	Zn	As	Se	Ag	Cd	Pb
MICA2	1	b.d.l.	28.6	53.0	6.59	5.26	b.d.l.	12.5	b.d.l.	b.d.l.	5.44	23.6	19.4		0.680	11.1
	2	0.750	0.84	b.d.l.	1.87	1.25	b.d.l.	17.1	b.d.l.	b.d.l.	1.05	8.66	b.d.l.	23.8	b.d.l.	0.137
	3	0.740	b.d.l.	b.d.l.	b.d.l.	b.d.l.	b.d.l.	10.4	1.75	0.330	3.49	b.d.l.	b.d.l.	15.6	0.256	0.0370
	4	1.75	2.84	21.0	b.d.l.	b.d.l.	1.18	4.6	b.d.l.	b.d.l.	2.98	16.7	b.d.l.	22.9	b.d.l.	0.0860
	5	1.88	b.d.l.	29.6	4.99	2.09	0.9	10.9	b.d.l.	0.760	b.d.l.	b.d.l.	b.d.l.	15.3	0.440	b.d.l.
	6	1.02	0.62	39.4	7.65	b.d.l.	b.d.l.	5.02	b.d.l.	b.d.l.	4.79	b.d.l.	b.d.l.	13.7	0.670	b.d.l.
	7	b.d.l.	b.d.l.	b.d.l.	b.d.l.	b.d.l.	b.d.l.	9.40	b.d.l.	0.240	b.d.l.	b.d.l.	b.d.l.	13.5	b.d.l.	0.155
	8	b.d.l.	1.00	38.6	b.d.l.	b.d.l.	0.42	6.04	b.d.l.	b.d.l.	2.81	11.5	5.76	16.8	b.d.l.	0.0400
	9	2.06	1.52	22.2	b.d.l.	b.d.l.	b.d.l.	13.9	0.910	3.96	3.98	b.d.l.	b.d.l.	12.0	b.d.l.	b.d.l.
	10	0.94	b.d.l.	28.2	b.d.l.	b.d.l.	b.d.l.	6.41	b.d.l.	1.10	2.45	b.d.l.	2.94	10.3	b.d.l.	b.d.l.
	11	0.610	b.d.l.	24.3	b.d.l.	0.260	b.d.l.	8.32	b.d.l.	2.39	1.53	b.d.l.	b.d.l.	11.2	b.d.l.	b.d.l.
	12	0.870	b.d.l.	26.2	b.d.l.	1.23	2.51	5.38	2.86	b.d.l.	5.17	16.8	b.d.l.	14.2	0.560	0.0430
	13	0.970	3.15	35.3	b.d.l.	1.6	b.d.l.	b.d.l.	2.80	0.0500	b.d.l.	b.d.l.	b.d.l.	18.8	b.d.l.	b.d.l.
	14	0.590	2.64	51.5	2.69	0.790	b.d.l.	6.96	b.d.l.	2.95	1.50	4.00	3.73	14.1	b.d.l.	0.0520
	15	0.770	3.08	41.4	b.d.l.	b.d.l.	b.d.l.	b.d.l.	b.d.l.	b.d.l.	3.87	6.17	1.03	12.0	b.d.l.	0.124
	16	b.d.l.	b.d.l.	32.3	4.72	0.970	1.77	7.16	2.61	2.99	5.42	4.09	4.77	10.7	0.265	0.222
	17	0.650	b.d.l.	b.d.l.	b.d.l.	1.09	1.8	4.28	50.9	0.680	b.d.l.	b.d.l.	b.d.l.	14.9	b.d.l.	b.d.l.
	18	b.d.l.	2.8	37.4	b.d.l.	b.d.l.	b.d.l.	9.86	b.d.l.	b.d.l.	b.d.l.	b.d.l.	3.51	11.7	0.530	0.0390
	19	1.28	b.d.l.	28.3	b.d.l.	1.59	b.d.l.	4.89	119	b.d.l.	6.66	20.1	b.d.l.	16.3	0.350	0.197
	20	0.420	3.89	43.9	b.d.l.	0.380	2.11	b.d.l.	b.d.l.	b.d.l.	b.d.l.	b.d.l.	b.d.l.	13.8	b.d.l.	b.d.l.
	21	0.730	2.88	23.6	b.d.l.	b.d.l.	b.d.l.	7.01	2.20	4.45	b.d.l.	b.d.l.	b.d.l.	14.7	b.d.l.	0.0940
	22	0.990	b.d.l.	3.61	b.d.l.	b.d.l.	b.d.l.	12.2	b.d.l.	b.d.l.	b.d.l.	b.d.l.	b.d.l.	15.0	b.d.l.	0.0620
	23	b.d.l.	b.d.l.	6.23	b.d.l.	b.d.l.	b.d.l.	5.32	b.d.l.	2.86	2.58	b.d.l.	b.d.l.	14.0	b.d.l.	0.444
	24	0.440	1.07	16.9	5.35	0.690	0.55	6.89	4.03	3.13	1.24	9.77	3.76	12.5	b.d.l.	0.108

Table 6. Cont.

Sample	Spot	Be	Si	S	Ti	Cr	Mn	Fe	Co	Ni	Zn	As	Se	Ag	Cd	Pb
	25	b.d.l.	2.66	b.d.l.	b.d.l.	0.370	b.d.l.	10.3	b.d.l.	b.d.l.	b.d.l.	b.d.l.	1.04	14.1	0.720	0.144
	26	b.d.l.	4.28	b.d.l.	3.05	b.d.l.	b.d.l.	5.97	2.38	5.45	b.d.l.	b.d.l.	1.56	11.0	b.d.l.	b.d.l.
	27	0.810	b.d.l.	22.8	b.d.l.	b.d.l.	3.06	3.33	b.d.l.	b.d.l.	2.97	b.d.l.	4.33	10.6	b.d.l.	0.0800
	28	b.d.l.	b.d.l.	b.d.l.	3.74	0.810	b.d.l.	8.45	b.d.l.	4.75	b.d.l.	b.d.l.	b.d.l.	12.6	b.d.l.	b.d.l.
	29	0.340	b.d.l.	b.d.l.	4.49	b.d.l.	b.d.l.	16.4	1.23	3.35	b.d.l.	b.d.l.	b.d.l.	13.7	b.d.l.	b.d.l.
	30	b.d.l.	b.d.l.	25.1	b.d.l.	b.d.l.	b.d.l.	6.72	2.47	4.48	b.d.l.	b.d.l.	b.d.l.	14.6	b.d.l.	b.d.l.
	31	0.350	b.d.l.	13.1	b.d.l.	b.d.l.	1.66	1.70	b.d.l.	2.20	0.590	b.d.l.	1.71	10.9	0.145	0.0340
MICA3	1	b.d.l.	1.72	27.5	b.d.l.	b.d.l.	0.31	9.27	1.54	b.d.l.	4.50	5.52	3.46	105	b.d.l.	16.2
	2	1.26	16.4	39.0	3.36	0.540	4.13	5.7	b.d.l.	b.d.l.	5.38	23.3	3.53	121	b.d.l.	4.72
	3	b.d.l.	17.7	8.91	4.5	0.680	3.21	11.3	b.d.l.	0.50	2.00	b.d.l.	b.d.l.	140	b.d.l.	4.20
	4	b.d.l.	17.5	28.9	6.97	b.d.l.	5.52	6.21	2.90	b.d.l.	4.14	26.8	0.420	85.5	b.d.l.	42.1
	5	b.d.l.	12.7	40.9	10.8	b.d.l.	0.57	10.1	2.60	b.d.l.	3.43	12.9	0.870	93.5	0.0890	5.79
	6	b.d.l.	22.2	11.4	4.04	b.d.l.	3.62	2.09	b.d.l.	1.19	1.03	4.83	b.d.l.	115	0.238	73.7
	7	b.d.l.	9.53	35.5	b.d.l.	b.d.l.	3.27	4.26	3.22	0.940	3.10	b.d.l.	b.d.l.	110	0.168	4.61
	8	b.d.l.	4.04	6.95	5.77	b.d.l.	2.13	10.4	0.770	b.d.l.	5.99	b.d.l.	2.41	105	b.d.l.	8.02
	9	1.16	13.5	24.8	b.d.l.	b.d.l.	2.21	9.91	b.d.l.	b.d.l.	0.980	b.d.l.	1.40	134	b.d.l.	6.24
	10	b.d.l.	7.98	36.1	4.22	b.d.l.	1.31	5.27	b.d.l.	3.66	3.80	b.d.l.	6.83	107	0.165	2.03
	11	b.d.l.	9.22	47.6	b.d.l.	1.06	1.3	1.83	1.49	b.d.l.	2.49	9.97	1.04	101	b.d.l.	2.04
	12	1.49	5.47	37.9	6.88	2.30	2.99	8.74	b.d.l.	b.d.l.	3.91	12.5	b.d.l.	121	0.290	2.72
	13	b.d.l.	8.51	23.2	b.d.l.	b.d.l.	1.95	b.d.l.	1.59	0.570	b.d.l.	b.d.l.	0.88	64.7	0.108	0.820
	14	b.d.l.	75.0	b.d.l.	b.d.l.	b.d.l.	1.58	12.9	0.730	2.74	1.45	b.d.l.	1.32	57.1	0.111	5.29
	15	0.620	12.8	26.6	3.63	0.540	3.52	4.08	2.35	0.870	8.95	b.d.l.	10.2	109	0.650	2.91
	16	0.840	33.8	7.82	6.71	b.d.l.	1.66	3.86	3.06	b.d.l.	1.40	28.2	b.d.l.	228	b.d.l.	3.68
	17	0.230	67.7	19.6	b.d.l.	1.06	0.59	2.66	0.990	b.d.l.	5.05	6.14	b.d.l.	89.2	b.d.l.	12.7
	18	b.d.l.	19.4	46.4	3.83	0.680	3.26	2.51	b.d.l.	1.87	4.21	3.65	3.01	97.5	b.d.l.	15.6
	19	b.d.l.	37.6	10.5	1.44	0.510	2.59	6.27	1.70	b.d.l.	13.8	6.46	0.610	102	0.164	3.27
	20	b.d.l.	20.0	b.d.l.	b.d.l.	1.92	1.96	30.6	8.39	2.94	b.d.l.	18.1	4.26	159	0.340	26.4
	21	b.d.l.	25.2	17.5	7.80	b.d.l.	1.77	12.6	b.d.l.	b.d.l.	4.42	18.7	5.45	152	0.510	15.7
	22	b.d.l.	21.3	7.7	b.d.l.	b.d.l.	b.d.l.	4.00	b.d.l.	0.340	3.95	26.6	7.81	55.9	b.d.l.	3.02
	23	b.d.l.	27.2	42.5	b.d.l.	b.d.l.	b.d.l.	5.06	b.d.l.	b.d.l.	b.d.l.	7.11	b.d.l.	72.4	b.d.l.	8.16
	24	b.d.l.	32.7	131	3.25	b.d.l.	b.d.l.	19.6	b.d.l.	8.37	9.12	23.6	b.d.l.	77.5	0.910	2.54
	25	b.d.l.	25.8	b.d.l.	2.21	2.43	3.63	14.3	b.d.l.	2.08	2.68	b.d.l.	b.d.l.	118	b.d.l.	2.30
	26	b.d.l.	15.8	b.d.l.	b.d.l.	2.19	b.d.l.	6.86	b.d.l.	b.d.l.	2.03	b.d.l.	b.d.l.	102	0.193	11.69
	1-1	b.d.l.	14.4	39.6	b.d.l.	1.02	2.94	5.29	b.d.l.	4.39	2.27	30.5	b.d.l.	121	b.d.l.	0.0510
	2-1	b.d.l.	13.3	b.d.l.	6.80	b.d.l.	1.47	2.41	0.94	3.40	b.d.l.	5.91	b.d.l.	121	b.d.l.	b.d.l.
MICA4	6	b.d.l.	b.d.l.	b.d.l.	0.210	b.d.l.	b.d.l.	8.72	0.800	2.53	3.06	b.d.l.	b.d.l.	449	0.360	0.0540
	7	1.28	2.01	66.8	8.88	16.7	1.49	7.87	b.d.l.	1.93	1.58	b.d.l.	2.56	133	b.d.l.	0.0750
	8	b.d.l.	b.d.l.	0.410	b.d.l.	110.98	0.71	4.04	b.d.l.	b.d.l.	1.46	b.d.l.	b.d.l.	127	b.d.l.	0.127
	9	0.860	b.d.l.	4.43	b.d.l.	b.d.l.	1.67	11.3	b.d.l.	4.24	1.72	b.d.l.	0.670	178	b.d.l.	0.0950
	10	b.d.l.	3.39	31.0	25.9	243	0.05	9.41	b.d.l.	7.62	3.02	13.7	b.d.l.	234	b.d.l.	0.134
	11	0.480	b.d.l.	b.d.l.	b.d.l.	85.6	b.d.l.	12.3	b.d.l.	30.7	3.39	b.d.l.	b.d.l.	172	b.d.l.	0.0630

Table 6. Cont.

Sample	Spot	Be	Si	S	Ti	Cr	Mn	Fe	Co	Ni	Zn	As	Se	Ag	Cd	Pb
	12	b.d.l.	b.d.l.	b.d.l.	b.d.l.	32.5	0.83	11.3	0.790	b.d.l.	2.79	b.d.l.	0.180	201	b.d.l.	0.0430
	13	b.d.l.	1.55	36.6	6.61	12.0	b.d.l.	13.6	b.d.l.	b.d.l.	0.380	0.210	b.d.l.	168	b.d.l.	0.0720
	14	b.d.l.	b.d.l.	b.d.l.	5.73	b.d.l.	b.d.l.	10.7	b.d.l.	5.02	3.55	b.d.l.	b.d.l.	181	b.d.l.	b.d.l.
	15	b.d.l.	6.72	37.5	b.d.l.	b.d.l.	1.19	3.06	b.d.l.	4.68	3.44	b.d.l.	3.21	246	b.d.l.	b.d.l.
MICA5	16	b.d.l.	0.92	18.7	b.d.l.	b.d.l.	1.47	29.3	b.d.l.	b.d.l.	3.05	b.d.l.	b.d.l.	263	b.d.l.	b.d.l.
	17	b.d.l.	1.81	b.d.l.	b.d.l.	b.d.l.	0.93	18.7	b.d.l.	11.7	2.86	b.d.l.	0.480	249	b.d.l.	b.d.l.
	18	0.780	b.d.l.	8.99	2.05	b.d.l.	b.d.l.	18.7	1.80	b.d.l.	1.89	b.d.l.	0.620	211	b.d.l.	0.0630
	21	b.d.l.	19.1	141	b.d.l.	21.7	2.02	51.5	12.9	b.d.l.	1.33	1.02	3.42	269	b.d.l.	b.d.l.
MICA10	1	b.d.l.	b.d.l.	b.d.l.	b.d.l.	b.d.l.	b.d.l.	22.1	30.1	6.56	25.9	2226	13.3	76.9	b.d.l.	2.66
	2	b.d.l.	b.d.l.	b.d.l.	b.d.l.	5.78	b.d.l.	5.59	b.d.l.	0.970	b.d.l.	3257	b.d.l.	71.9	0.259	b.d.l.
	3	b.d.l.	b.d.l.	21.7	1.46	b.d.l.	b.d.l.	4.09	b.d.l.	3.10	3.42	4433	b.d.l.	79.9	0.208	0.157
	4	b.d.l.	b.d.l.	40.9	b.d.l.	b.d.l.	b.d.l.	13.8	8.62	3.39	10.9	9036	b.d.l.	95.9	0.117	0.490
	5	1.05	b.d.l.	b.d.l.	b.d.l.	b.d.l.	b.d.l.	3.84	0.370	2.00	1.66	b.d.l.	11.0	84.2	b.d.l.	0.079

b.d.l.: below detection limit. Note that Cu was used as an Internal Standard for calibration. The value was assumed to be 99.98% according to EDS analyses.

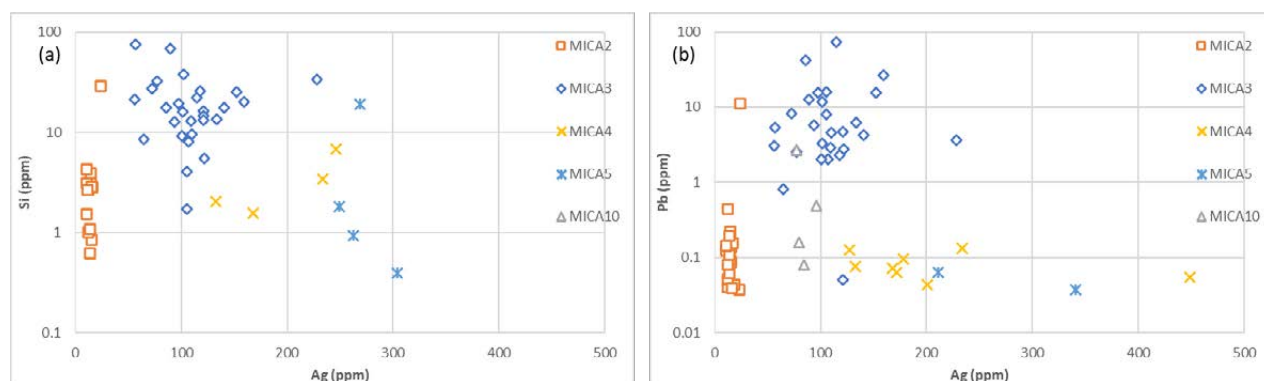


Fig. 17. Si and Pb versus Ag plots of native copper samples.

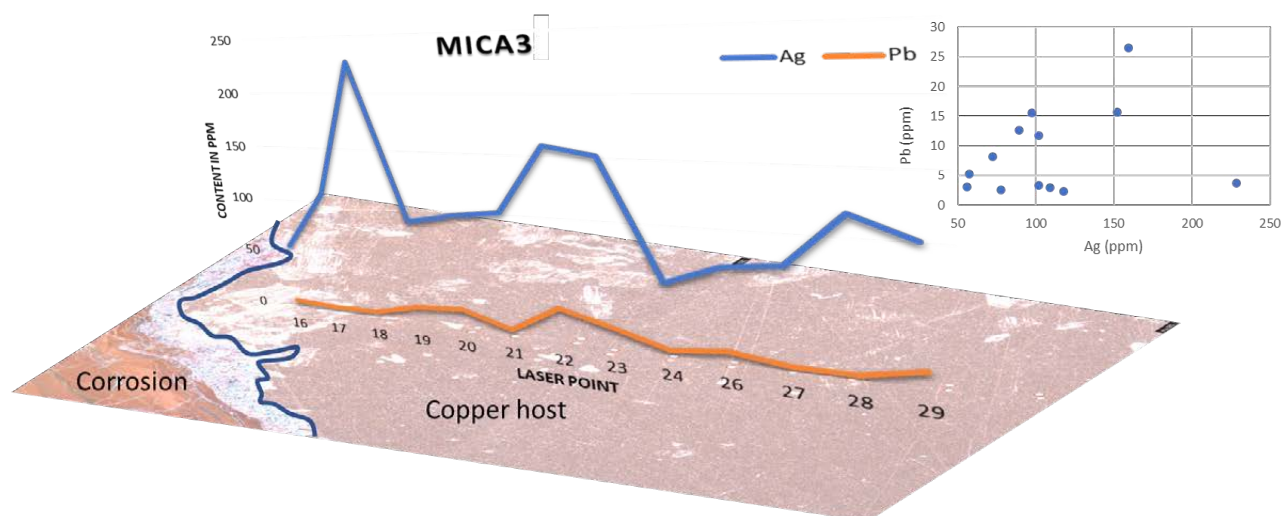


Fig. 18. A traverse of Ag and Pb in the MICA3, immediately next to a corrosion zone. See the text for description and discussion.

5.3.2 Cuprite

Overall, twenty-three spot analyses were made for three samples (Fig. 19, Table 7). With the phase change from copper metal (99.98% Cu) to cuprite, Cu decreases by about 10%, while O increases by 10%. Apart from these two elements, many other elements were detected in cuprites. Alkaline (Na, K), earth alkali (Mg), semi-metals (Al, Pb), transition metals (Ti, V, Cr, Fe, Zn), non-metals (Si, P, S, As), and actinides (Th, U) are in particularly high amounts (Fig. 20).

The most remarkable difference between cuprite and copper metal is that the former one is more enriched in all the trace elements to some extent,

particularly alkaline and alkaline earth metals (Figure). This is probably due to the change of crystal structure from metal to oxide, increasing the capacity for elemental substitution. On a bivariate plot against Si, it is apparent that alkaline and alkaline earth metals are roughly correlated to Si (Fig. 20a,b,c,d), whereas other elements are not. This likely indicates the reaction of copper with a hydrothermal fluid enriched in these elements possibly originating from the surrounding wall rocks.

By contrast, Ag seems to be stable during corrosion. Silver contents in cuprite are comparable to those of copper host. This observation indicates a higher resistance of Ag to fluids present during the corrosion.

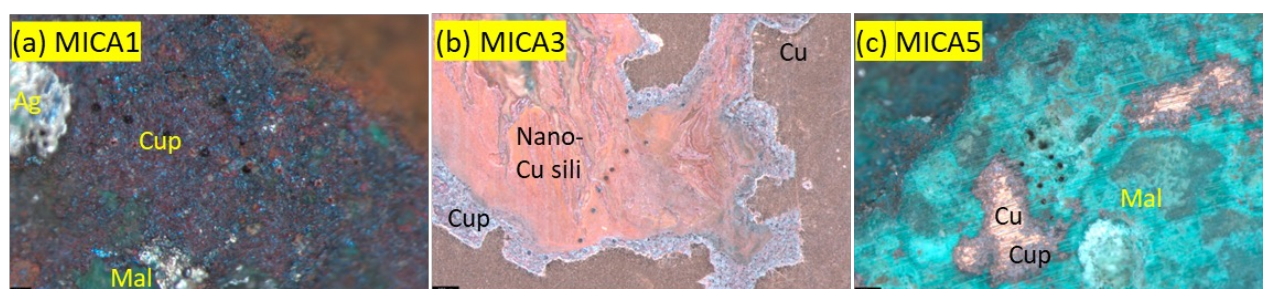


Fig. 19. Images of the samples analyzed for trace elements in cuprite by utilizing LA-ICP-MS. Laser ablation pits are also visible from the images. Cu: copper host; Cup: cuprite; Nano-Cu sili: Nano-scale mixture of cuprite and clinocllore; Mal: malachite.

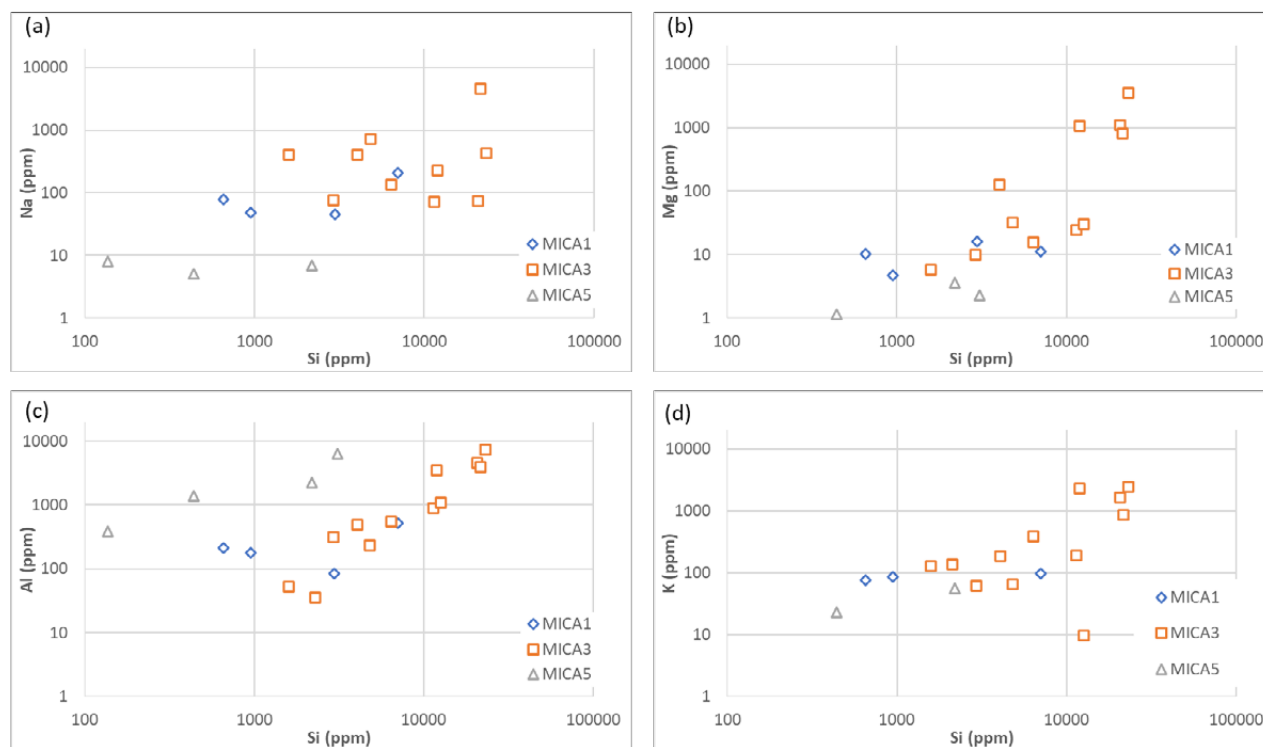


Fig. 20. Bivariate plots of elements versus Si in cuprite.

Table 7. Major and trace element contents (ppm) in the cuprite analyzed by LA-ICP-MS.

Sample	Spot	Li	Be	Na	Mg	Al	Si	P	S	K	Ti	V	Cr	Fe	Mn	Co	Ni
MICA11	1	b.d.l.	b.d.l.	208	11.2	525	7018	331	b.d.l.	96.7	b.d.l.	7.35	b.d.l.	3449	b.d.l.	b.d.l.	b.d.l.
	3	b.d.l.	b.d.l.	48.1	4.76	175	947.1	85.5	b.d.l.	85.0	b.d.l.	1.52	b.d.l.	b.d.l.	b.d.l.	b.d.l.	b.d.l.
	4	b.d.l.	b.d.l.	77.2	10.1	212	655.3	130	b.d.l.	75.4	b.d.l.	1.30	b.d.l.	2019	b.d.l.	b.d.l.	b.d.l.
	5	b.d.l.	b.d.l.	45.7	16	84.9	2965	89.8	b.d.l.	b.d.l.	b.d.l.	1.84	b.d.l.	b.d.l.	b.d.l.	b.d.l.	b.d.l.
MICA3	1	b.d.l.	0.710	76.1	9.79	311	2918	46.8	208	61.6	b.d.l.	7.45	b.d.l.	226	2.66	0.9	7.69
	2	2.07	1.64	136	15.7	544	6397	46.5	248	388	12.1	0.527	b.d.l.	269	0.770	0.81	50.4
	3	1.43	b.d.l.	70.6	24.1	898	11420	74.4	506	192	b.d.l.	0.850	10.4	113	2.64	0.18	39
	5	0.947	0.900	b.d.l.	29.7	1104	12612	144	436	9.84	32	12.0	b.d.l.	972	1.53	0.59	b.d.l.
	6	3.75	2.56	73.7	1113	4631	20698	220	261	1630	1966	55.1	22.2	13126	118	2.52	19.9
	12	b.d.l.	b.d.l.	426	3505	7292	23150	b.d.l.	b.d.l.	2468	2202	54.0	b.d.l.	7068	183	b.d.l.	b.d.l.
	13	b.d.l.	b.d.l.	405	128	485	4045	299	b.d.l.	186	125	72.0	b.d.l.	925	b.d.l.	b.d.l.	b.d.l.
	14	b.d.l.	b.d.l.	710	32.1	230	4812	234	b.d.l.	65.1	b.d.l.	134	59.0	b.d.l.	b.d.l.	b.d.l.	b.d.l.
	15	b.d.l.	b.d.l.	135	30.8	88	b.d.l.	b.d.l.	b.d.l.	b.d.l.	b.d.l.	12.2		b.d.l.	b.d.l.	b.d.l.	b.d.l.
	16	b.d.l.	b.d.l.	b.d.l.	b.d.l.	35.9	2296	208	b.d.l.	b.d.l.	b.d.l.	30.9	67.7	711	b.d.l.	b.d.l.	b.d.l.
	18	b.d.l.	b.d.l.	4631	822	3888	21519	162	b.d.l.	862	59.7	4.76	b.d.l.	855	39.2	b.d.l.	b.d.l.
	27	b.d.l.	b.d.l.	402	5.86	51.6	1587	398	b.d.l.	130	b.d.l.	4.03	b.d.l.	b.d.l.	b.d.l.	b.d.l.	b.d.l.
	27	b.d.l.	b.d.l.	227	1055	3463	11910	324	b.d.l.	2328	556	75.0	b.d.l.	b.d.l.	37.2	b.d.l.	b.d.l.
	27	b.d.l.	b.d.l.	b.d.l.	b.d.l.	b.d.l.	b.d.l.	128	b.d.l.	70.1	b.d.l.	13.9	b.d.l.	b.d.l.	b.d.l.	b.d.l.	b.d.l.
	27	b.d.l.	b.d.l.	b.d.l.	b.d.l.	b.d.l.	2130	247	b.d.l.	136	b.d.l.	6.87	51.9	3508	b.d.l.	b.d.l.	b.d.l.
MICA5	16	b.d.l.	b.d.l.	7.96	b.d.l.	386	136.2	26.5	b.d.l.	b.d.l.	b.d.l.	8.35	2.39	b.d.l.	b.d.l.	b.d.l.	b.d.l.
	18	b.d.l.	b.d.l.	6.92	3.56	2233	2185	42.3	b.d.l.	55.8	b.d.l.	39.6	8.81	715	b.d.l.	b.d.l.	b.d.l.
	19	b.d.l.	b.d.l.	5.08	1.15	1384	439.4	29.1	b.d.l.	23.3	b.d.l.	30.1	5.46	b.d.l.	b.d.l.	b.d.l.	b.d.l.
	20	b.d.l.	b.d.l.	b.d.l.	2.32	6336	3075	82.4	b.d.l.	b.d.l.	16.1	149	10.9	b.d.l.	b.d.l.	b.d.l.	b.d.l.

Table 7. Cont.

Zn	Ga	Ge	As	Se	Rb	Sr	Ag	Sb	Te	Cs	Ba	La	Ce	Sm	Pb	Th	U
	b.d.l.	b.d.l.	7105	b.d.l.	b.d.l.	1.01	959	4.14	b.d.l.	b.d.l.	b.d.l.	0.370	1.02	b.d.l.	b.d.l.	b.d.l.	b.d.l.
30.1	b.d.l.	b.d.l.	1179	b.d.l.	b.d.l.	b.d.l.	754	0.740	b.d.l.	b.d.l.	b.d.l.	b.d.l.	b.d.l.	b.d.l.	b.d.l.	b.d.l.	b.d.l.
32.8	b.d.l.	b.d.l.	1715	b.d.l.	b.d.l.	0.590	594	0.560	b.d.l.	b.d.l.	b.d.l.	b.d.l.	b.d.l.	b.d.l.	b.d.l.	b.d.l.	b.d.l.
30.3	b.d.l.	b.d.l.	1515	b.d.l.	b.d.l.	0.510	218	0.760	b.d.l.	b.d.l.	4.62	0.267	0.320	b.d.l.	b.d.l.	b.d.l.	b.d.l.
14.4	0.658	b.d.l.	1.48	6.23	0.144	0.154	190	b.d.l.	0.325	0.0819	0.735	0.502	0.249	0.537	0.804	0.0259	0.0462
19	b.d.l.	b.d.l.	1.76	b.d.l.	b.d.l.	b.d.l.	244	0.161	b.d.l.	0.213	b.d.l.	0.308	0.556	0.712	0.908	b.d.l.	0.0153
14.8	0.704	b.d.l.	1.14	0.910	0.324	0.252	270	0.284	b.d.l.	0.130	b.d.l.	0.842	1.00	0.408	0.172	0.0224	0.0252
b.d.l.	0.145	b.d.l.	1.87	1.27	0.148	0.124	300	b.d.l.	b.d.l.	b.d.l.	0.143	1.15	1.55	0.643	0.0284	0.0434	0.175
14.8	4.87	1.32	5.84	0.920	5.93	4.08	39.9	0.358	0.352	1.34	23.5	10.5	18.3	1.20	8.54	3.93	0.886
b.d.l.	7.65	b.d.l.	b.d.l.	b.d.l.	9.14	5.31	30.0	b.d.l.	b.d.l.	1.82	33.4	11.7	20.1		9.20	3.89	1.00
b.d.l.	b.d.l.	b.d.l.	b.d.l.	b.d.l.	b.d.l.	b.d.l.	44.0	b.d.l.	b.d.l.	b.d.l.	b.d.l.	b.d.l.	b.d.l.	b.d.l.	b.d.l.	b.d.l.	0.800
b.d.l.	b.d.l.	b.d.l.	b.d.l.	b.d.l.	b.d.l.	b.d.l.	234	b.d.l.	b.d.l.	b.d.l.	b.d.l.	b.d.l.	b.d.l.	b.d.l.	b.d.l.	b.d.l.	b.d.l.
b.d.l.	b.d.l.	b.d.l.	b.d.l.	b.d.l.	b.d.l.	b.d.l.	551	b.d.l.	b.d.l.	b.d.l.	b.d.l.	b.d.l.	b.d.l.	b.d.l.	b.d.l.	b.d.l.	b.d.l.
b.d.l.	b.d.l.	b.d.l.	b.d.l.	b.d.l.	b.d.l.	b.d.l.	469	b.d.l.	b.d.l.	b.d.l.	b.d.l.	b.d.l.	b.d.l.	b.d.l.	b.d.l.	b.d.l.	b.d.l.
263	9.60	b.d.l.	119	b.d.l.	1.54	4.25	80.3	39.7	b.d.l.	0.30	71.3	0.560	1.65	b.d.l.	35.07	b.d.l.	0.165

Table 7. Cont.

Zn	Ga	Ge	As	Se	Rb	Sr	Ag	Sb	Te	Cs	Ba	La	Ce	Sm	Pb	Th	U
b.d.l.	b.d.l.	b.d.l.	b.d.l.	b.d.l.	b.d.l.	b.d.l.	82.7	b.d.l.	b.d.l.	b.d.l.	b.d.l.	b.d.l.	b.d.l.	b.d.l.	b.d.l.	b.d.l.	b.d.l.
b.d.l.	4.92	b.d.l.	b.d.l.	b.d.l.	7.18	3.60	48.0	b.d.l.	b.d.l.	1.20	24.8	3.36	5.64	b.d.l.	3.40	1.53	0.88
b.d.l.	b.d.l.	b.d.l.	b.d.l.	b.d.l.	b.d.l.	b.d.l.	89.0	b.d.l.	b.d.l.	b.d.l.	b.d.l.	b.d.l.	b.d.l.	b.d.l.	b.d.l.	b.d.l.	b.d.l.
b.d.l.	b.d.l.	b.d.l.	b.d.l.	b.d.l.	b.d.l.	b.d.l.	335	b.d.l.	b.d.l.	b.d.l.	b.d.l.	b.d.l.	b.d.l.	b.d.l.	b.d.l.	b.d.l.	b.d.l.
16.0	0.350	b.d.l.	2.36	b.d.l.	b.d.l.	b.d.l.	9.91	b.d.l.	b.d.l.	b.d.l.	0.340	0.104	0.36	b.d.l.	b.d.l.	0.051	0.217
27.4	0.970	b.d.l.	12.3	b.d.l.	b.d.l.	0.240	96.4	b.d.l.	b.d.l.	b.d.l.	1.25	0.450	1.08	0.51	0.24	0.39	1.77
13.7	0.600	0.81	11.2	b.d.l.	b.d.l.	0.191	61.6	b.d.l.	b.d.l.	b.d.l.	0.770	0.638	1.86	0.51	0.088	0.205	0.817
8.97	1.45		23.7	b.d.l.	b.d.l.	0.350	26.9	b.d.l.	b.d.l.	b.d.l.	2.32	1.60	3.02	0.64	0.24	0.345	1.18

b.d.l.: below detection limit. Note that Cu was used as an Internal Standard for calibration. The values were measured by SEM-EDS.

5.3.3 Nano- Cu silicate

The nano-mixture of cuprite and clinochlore is quite unique. It appears to form by mechanical

mixing of clinochlore and cuprite (partly evidenced by the fact that there is no correlation between Cu and Si).

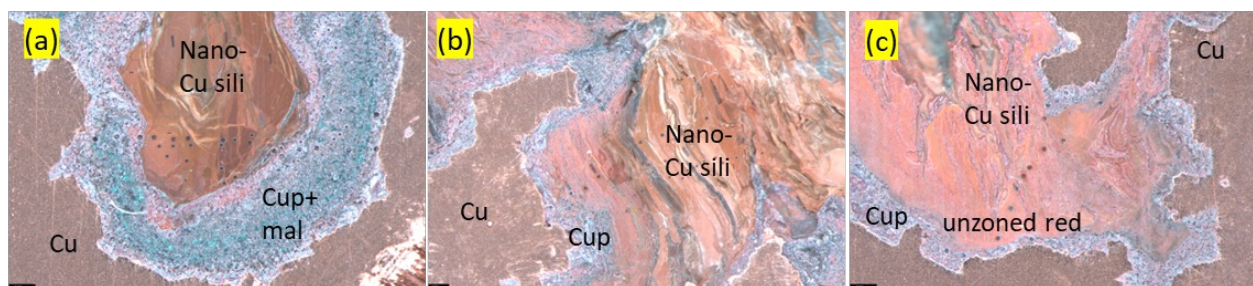


Fig. 21. Images of nano-Cu silicates in MICA3 with laser spots. Cu: copper host; Cup: cuprite; Nano-Cu sili: Nano-scale mixture of cuprite and clinochlore; unzoned red: unzoned reddish phase; Mal: malachite.

A total of fourteen measurements of trace elements were done for this mineral phase for MICA3 (Fig. 21, Table 8). The results show that they are enriched in trace elements (Fig. 22). Generally, they contain an average of 11 ± 2 wt.% Cu, 7 ± 3 wt.% Al, 5 ± 4 wt.% Fe, 3 ± 2 wt.% Mg, 1 ± 0.6 wt.% Ti; 1184 ± 649 ppm Na; 863 ± 290 ppm Mn, 519 ± 155 ppm S, 158 ± 79 ppm Zn 156 ± 53 ppm Cr, 135 ± 88 ppm V, 104 ± 74 ppm Ni; 74 ± 24 ppm Ce, 72 ± 33 ppm Rb, 50 ± 19 ppm Ga, 48 ± 26 ppm Li, 40 ± 14 ppm La, 32 ± 18 ppm Co, 27 ± 14 ppm Pb, 26 ± 9.8 ppm Sr, 13 ± 4.7 ppm Th; 8 ± 2.9 ppm As, 5 ± 1.5 ppm Sm, 3 ± 1.2 ppm Ge, 3 ± 0.9 ppm U, 0.9 ± 0.6 ppm Ag. Compared with cuprite, the lithophile elements (alkaline, alkaline earth, lanthanides, and actinides) are significantly elevated and, most notably, Ag is mostly diminished. Several isotopic systematics are identified for potential dating (Rb-Sr, U-Th-Pb) and source tracing (S, Ce).

Compared to nano-Cu silicate, the reddish phase (not zoned) (Fig. 22c; see the Section 5.2 for mineral texture description) shows nearly identical trace element patterns except for Ag (14 ± 7.8 ppm).

5.3.4 Malachite

Seven measurements on malachite of MICA3 and MICA5 were also made. The results are not valid due to two major issues. Firstly, malachite in MICA3 was not easy to target as it was difficult to distinguish it from the other mineral phases using the visual system on the laser device. Secondly, laser spots shifted unexpectedly in the MICA5 so that the spots did not correspond to malachite.

Several results not being affected by the aforementioned issues, yielded high contents of U, and thus, dating was attempted with U-Pb later.

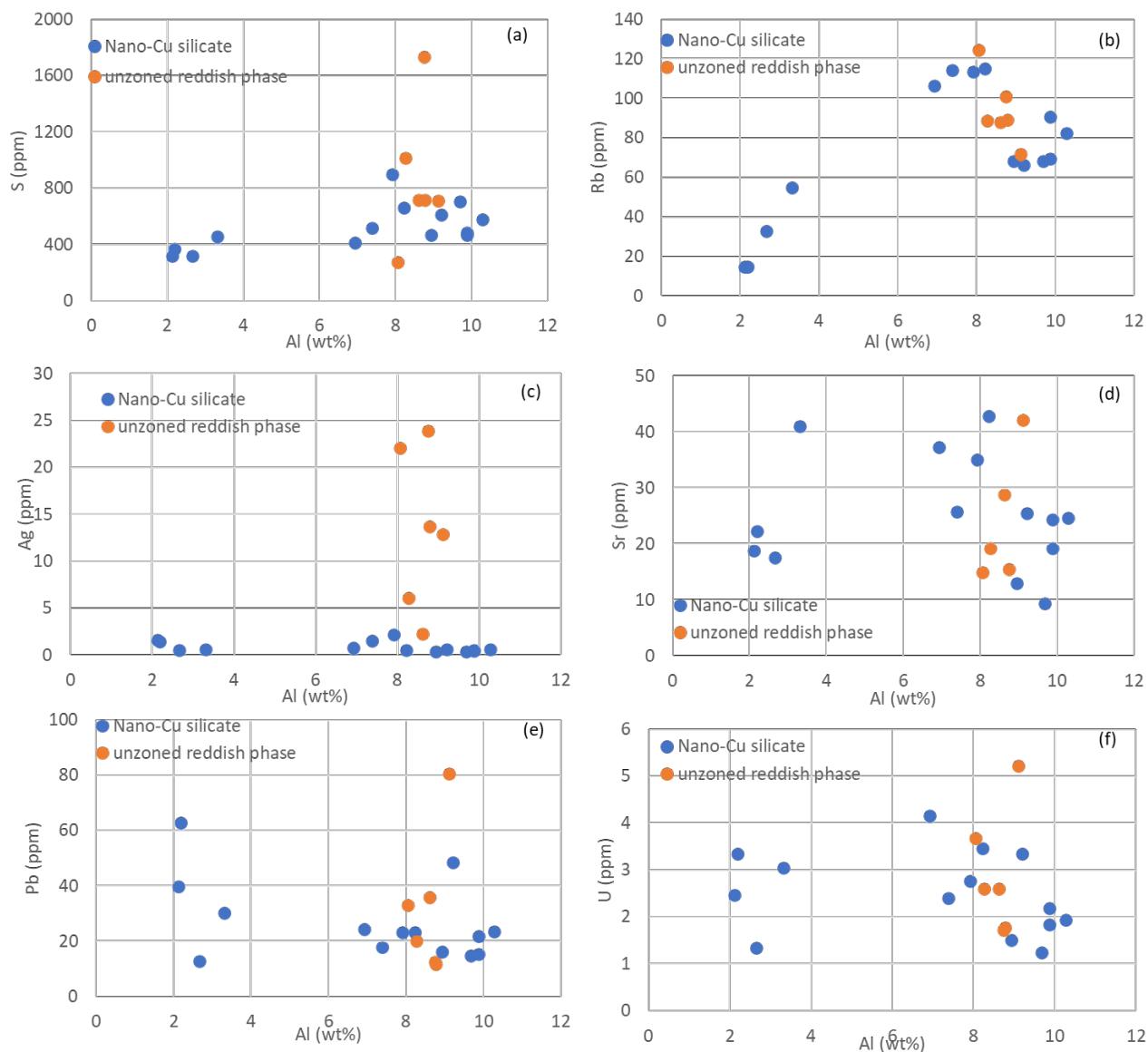


Fig. 22. Trace and minor element plots versus Al for nano-Cu silicate and unzoned reddish phase.

Table 8. Major and trace element contents (ppm) in the nano-silicate and apachite analyzed by LA-ICP-MS.

Sample	Spot	Li	Na	Mg	Al	S	Ti	V	Cr	Fe	Mn	Co	Ni
MICA3	7	9.43	135	8876	21193	319	11309	222	134	88952	711	9.34	
	8	12.9	78.7	8716	21914	367	12198	426	172	174532	787	11.5	11.0
	9	9.33	225	6862	26571	319	5330	65.1	48.6	31531	247	6.53	7.51
	10	7.31	564	4645	33122	456	12438	140	78.1	72351	439	5.40	10.7
	3	38.7	1993	26775	92086	613	24571	135	146	34125	989	31.1	34.1
	4	79.0	1318	55293	96837	703	4234	88.9	185	28147	1280	60.7	212
	5	64.5	1987	47756	98713	486	6022	108	194	31234	1086	49.5	106
	6	77.3	1552	50900	89395	465	4534	89.7	211	29570	1262	59.0	235
	7	45.7	1277	23106	98768	467	14409	77.5	198	19301	556	21.5	64.9
	8	56.5	1644	39141	102776	579	5685	94.6	236	27791	1118	46.9	146
	21	64.9	1932	32468	69217	411	19921	122	185	32559	875	35.7	117
	22	70.4	1222	33727	73819	519	6683	99.1	83.1	25516	813	34.3	91.1
	23	73.2	1325	38892	82220	661	8666	119	182	34903	1041	40.0	138
	24	56.0	1330	34911	79138	900	8086	99.4	124	29788	881	35.3	177
	9	46.8	1742	29174	86156	716	22165	107	273	30549	976	34.2	126
	10	58.4	2132	36819	91126	709	46784	244	634	59443	1726	41.4	24.9
	19	45.7	1239	31720	82690	1012	10098	106	61	24130	705	31.6	30.6
	20	43.9	2063	29913	87813	714	7279	106	80	17170	688	37.6	377
	25	49.6	1748	31439	87467	1734	5130	108	178	24723	593	27.0	102
	26	53.9	1811	30992	80553	275	10199	172	103	29543	788	30.9	115
MICA7	6	b.d.l.	20.3	1281	6193	b.d.l.	52.2	281	10.7	b.d.l.	18.0	b.d.l.	b.d.l.
	7	b.d.l.	20.0	1266	5771	b.d.l.	39.3	197	b.d.l.	b.d.l.	21.5	b.d.l.	b.d.l.
	8	b.d.l.	28.7	1231	5735	b.d.l.	47.2	292	15.29	678	19.9	b.d.l.	b.d.l.
	9	b.d.l.	51.3	1362	5120	b.d.l.	25.6	358	8.99	222	23.8	b.d.l.	b.d.l.
	10	b.d.l.	77.8	1378	5334	b.d.l.	27.8	381	7.68	b.d.l.	26.2	b.d.l.	b.d.l.
	11	b.d.l.	50.6	1485	5396	b.d.l.	28.8	373	6.61	600	25.1	b.d.l.	b.d.l.
	12	b.d.l.	30.4	1558	5312	b.d.l.	29.9	372	8.87	2721	23.2	b.d.l.	b.d.l.
	13	b.d.l.	34.0	1544	5332	b.d.l.	24.5	373	7.05	795	25.7	b.d.l.	b.d.l.
	14	b.d.l.	24.5	1578	5340	b.d.l.	28.5	396	6.82	304	24.2	b.d.l.	b.d.l.
	15	b.d.l.	30.2	1792	7730	b.d.l.	29.0	301	6.28	b.d.l.	21.9	b.d.l.	b.d.l.

b.d.l.: below detection limit. Note that Cu was used as an Internal Standard for calibration. The values were measured by SEM-EDS.

Table 8. Cont.

Zn	Ga	Ge	As	Rb	Sr	Ag	Ba	La	Ce	Sm	Pb	Th	U
55.8	17.5	1.59	6.59	14.7	18.8	1.57	84.0	47.2	79.4	5.03	39.8	17.3	2.47
56.9	20.1	2.39	7.74	14.7	22.2	1.47	96.8	61.7	102	5.29	62.8	20.7	3.35
33.9	24.2	1.56	3.17	32.9	17.6	0.500	172	29.9	47.7	3.20	12.7	8.81	1.34
24.8	44.2	2.69	7.39	54.9	41.1	0.625	395	66.2	108	7.55	30.1	19.4	3.04
172	49.8	5.67	12.7	66.1	25.5	0.605	201	39.6	83.5	7.49	48.5	15.5	3.35
231	50.4	3.08	2.96	68.2	9.42	0.324	162	18.3	37.5	3.42	14.9	5.44	1.24
190	50.8	3.97	6.71	69.5	19.2	0.455	192	32.3	68.4	4.38	21.9	9.65	1.84
266	47.5	3.90	6.98	68.1	12.9	0.341	172	24.3	50.0	3.13	16.3	7.07	1.50
134	52.8	3.56	6.71	90.6	24.4	0.484	230	31.1	62.6	4.26	15.4	9.39	2.18
245	58.4	3.39	9.06	82.3	24.6	0.605	226	25.5	49.3	3.21	23.5	9.48	1.93
187	70.9	3.88	12.3	106	37.3	0.779	389	50.3	97.4	6.75	24.3	16.0	4.15
207	68.6	2.45	9.23	114	25.7	1.55	314	40.2	67.1	4.71	18.0	10.1	2.40
188	76.2	4.83	10.3	115	42.8	0.496	396	56.3	110	6.51	23.2	16.6	3.45
220	73.2	4.63	11.6	114	35.0	2.21	384	42.0	70.7	5.13	23.2	15.1	2.76
214	64.7	2.24	9.48	88.1	28.8	2.27	315	35.9	67.7	4.54	35.8	12.0	2.59
345	62.1	7.28	21.0	71.9	42.1	12.8	229	68.6	144	11.1	80.7	24.5	5.21
226	50.2	3.15	13.3	88.8	19.2	6.04	153	38.4	64.3	3.98	20.2	12.7	2.6
312	49.4	2.19	12.6	89.2	b.d.l.	13.7	115	25.7	46.8	1.52	11.6	9.42	1.77
259	48.8	10.3	15.2	101	15.5	23.9	114	32.4	63.5	3.46	12.6	10.5	1.71
225	65.6	2.63	16.7	124	14.9	22.1	237	59.3	117	8.42	33.2	19.7	3.67
11.2	52.7	b.d.l.	3.85	0.270	19.6	b.d.l.	b.d.l.	0.704	17.5	0.940	0.299	0.14	174
b.d.l.	56.1	b.d.l.	b.d.l.	b.d.l.	22.6	b.d.l.	b.d.l.	2.32	20.7	b.d.l.	0.450	0.400	171
14.8	55.2	b.d.l.	3.67	0.26	18.7	b.d.l.	b.d.l.	0.707	18.3	0.880	0.308	0.14	177
19.5	92.0	b.d.l.	4.02	b.d.l.	20.0	b.d.l.	b.d.l.	0.562	31.8	0.860	0.431	b.d.l.	132
170	91.3	b.d.l.	4.46	0.31	17.5	b.d.l.	0.800	0.656	32.9	0.940	0.328	b.d.l.	142
17.3	82.7	b.d.l.	b.d.l.	0.32	18.7	b.d.l.	b.d.l.	0.593	31.4	b.d.l.	0.499	b.d.l.	129
14.3	84.8	b.d.l.	4.56	b.d.l.	19.8	b.d.l.	b.d.l.	0.600	32.0	0.830	0.307	b.d.l.	130
20.7	90.9	b.d.l.	b.d.l.	0.25	20.0	b.d.l.	b.d.l.	0.660	34.0	0.980	0.325	b.d.l.	141
14.1	80.5	b.d.l.	b.d.l.	b.d.l.	18.6	b.d.l.	b.d.l.	0.609	32.4	0.980	0.250	b.d.l.	141
b.d.l.	37.2	b.d.l.	b.d.l.	b.d.l.	17.1	b.d.l.	b.d.l.	0.539	18.2	0.760	0.250	b.d.l.	190

b.d.l.: below detection limit. Note that Cu was used as an Internal Standard for calibration. The values were measured by SEM-EDS.

Table 9. Major and trace element contents (ppm) in the malachite analyzed by LA-ICP-MS.

Sample	Spot	Na	Mg	Al	Si	P	S	K	Ti	V	Cr	Fe	Mn	Co	Ni
MICA3	1	13125	1518	17532	205206	168	674	2246	1675	14.6	31.4	2116	49.2	3.42	10.2
	2	3022	1123	18491	205206	166	587	1476	1860	9.93	28.8	860	58.6	3.80	4.67
MICA5	21	9.37	4.19	3553	7055	68.7	b.d.l.	33.5	16.9	94.0	10.9	16880	b.d.l.	b.d.l.	b.d.l.
	22	b.d.l.	b.d.l.	509	b.d.l.	b.d.l.	b.d.l.	167	b.d.l.	25.7	b.d.l.	b.d.l.	b.d.l.	b.d.l.	b.d.l.
	23	b.d.l.	2280	1268364	599063	53989	b.d.l.	b.d.l.	b.d.l.	65322	b.d.l.	2E+07	b.d.l.	b.d.l.	b.d.l.
	24	5.32	1.76	1265	867	45.3	b.d.l.	21.0	b.d.l.	46.8	7.22	5634	b.d.l.	b.d.l.	b.d.l.
	25	b.d.l.	b.d.l.	5425171	2610062	158713	b.d.l.	294631	b.d.l.	118932	26585	2E+07	b.d.l.	b.d.l.	b.d.l.

Table 9. Cont.

Zn	Ga	Ge	As	Rb	Sr	Ag	Ba	La	Ce	Sm	Th	U
58.2	5.4	0.764	6.10	3.48	1.81	4.04	26.4	15.4	28.7	2.31	0.412	0.255
27.1	4.16	2.62	3.48	1.36	6.57	3.53	20.3	16.0	30.9	3.07	0.346	0.374
15.0	1.42	b.d.l.	27.0	b.d.l.	b.d.l.	21.0	1.29	0.520	1.42	b.d.l.	0.277	2.89
b.d.l.	b.d.l.	b.d.l.	b.d.l.	b.d.l.	b.d.l.	4.93	b.d.l.	b.d.l.	b.d.l.	b.d.l.	b.d.l.	1.20
30048	1199	b.d.l.	15862	b.d.l.	b.d.l.	87254	1443	614	1502	b.d.l.	180	1982
7.87	0.360	b.d.l.	16.2	b.d.l.	b.d.l.	96.5	0.80	0.444	1.56	0.410	0.160	0.960
75681	2496	b.d.l.	38009	b.d.l.	b.d.l.	356362	b.d.l.	1697	4584	b.d.l.	458	2891

b.d.l.: below detection limit. Note that Cu was used as an Internal Standard for calibration. The values were measured by SEM-EDS.

5.3.5 Apachite

Ten measurements of trace elements have been made on apachite in the MICA7 (Fig. 23, Table 8). Results suggest that they contain an average of 1448 ± 167 ppm Mg, 5726 ± 731 ppm Al; 887 ± 845 ppm Fe, 153 ± 22 ppm U; 72 ± 19 ppm Ga, 37 ± 17 ppm Na, 35 ± 51 ppm Zn, 33 ± 9 ppm Ti, 27 ± 6.8 ppm Ce, 23 ± 2.5 ppm Mn, 19 ± 1.5 ppm Sr; 9 ± 2.7 ppm Cr, 4 ± 0.3 ppm As, 0.8 ppm Ba, 1 ± 0.5 ppm La, 0.9 ± 0.0 ppm Sm, 0.3 ± 0.03 ppm Rb, 0.3 ± 0.1 ppm

Pb, 0.2 ± 0.1 ppm Th. Silver is below detection limit ($0.2\text{--}0.5$ ppm).

From textural evidence, it is apparent that nano-Cu silicate might have formed via reaction of a fluid with surrounding cuprite. Apachite is so far the only copper silicate observed, so the same fluid source between apachite and nano Cu-silicate is expected. Textual evidence clearly indicates that apachite were precipitated directly in the interstices of the conglomerate from a parent fluid with no fluid-rock interaction.

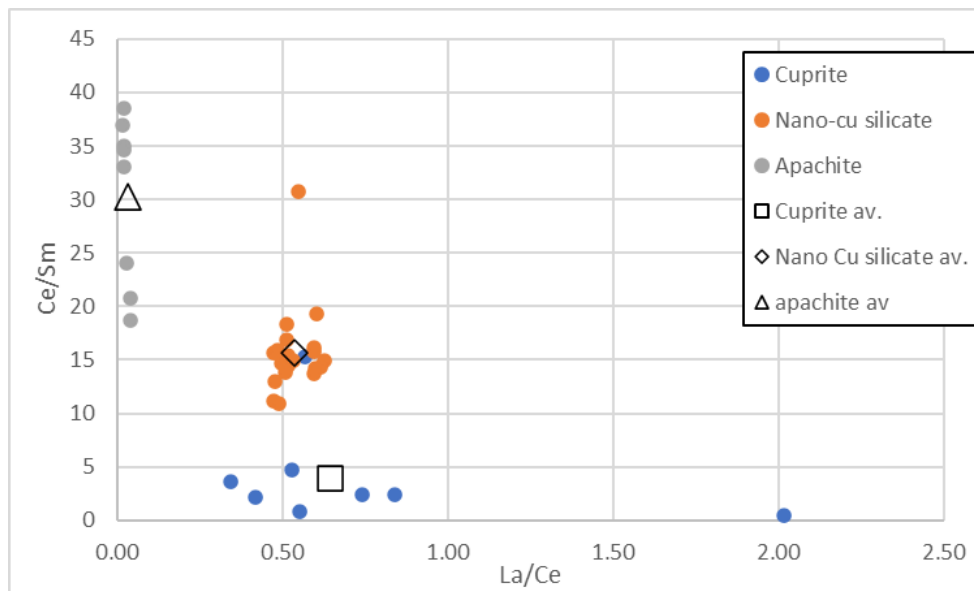


Fig. 23. A Ce/Sm versus La/Ce plot, showing potential relation between cuprite, nano-Cu silicate, and apachite. Individual spots are shown with solid circles, averaged values are shown in open square (cuprite), diamond (nano Cu silicate), and triangle (apachite).

Since rare earth elements have been widely used as geochemical tracer thanks to a resemblance in geochemical properties, Ce/Sm ratio is plotted against La/Ce ratio to see potential relation amongst cuprite, nano- Cu silicate and apachite. In the Figure 23, it is apparent that the La/Ce ratio of nano Cu silicates are close that of cuprite, which probably indicates cuprite as a source for REE and other materials. It is also noted that the nano-Cu silicates have slightly lower average La/Ce but

higher Ce/Sm ratios, which requires an extra source if La, Ce, Sm did not fractionate during the fluid/rock interaction process. This extra source could be the parental fluids of apachite. Apachite data plots in the top left suggesting apachite may be the end-member of the precipitation process. However, detailed modeling would be needed in order to confirm the relation. In addition, a similar age for both nano-Cu silicate and apachite should be obtained before it is possible to make a definitive conclusion.

5.4 U-Pb and common Pb geochronology

5.4.1 Cuprite

Due to the low content of U, common lead method was used to provide a preliminary age of the cuprite. In total, eighteen measurements have been made for MICA11 (eight spots) and MICA3 (ten spots). Laser spots are seen in the Figure 19. Results suggest that Pb signals (in counts per second, cps) are much lower than 1000, which cannot generate precise isotope ratios, and thus are discarded.

Five out of ten measurements for MICA1 produced relatively high cps (1000–2000 cps for ^{206}Pb , ^{207}Pb , and ^{208}Pb), but ^{204}Pb signals are abnormal due to the presence of Hg. Therefore, common lead ages are obtained from only $^{207}\text{Pb}/^{206}\text{Pb}$ ratios based on Stacy and Kramers (1974) model. The selected spots yielded an averaged $^{207}\text{Pb}/^{206}\text{Pb}$ ratios of 0.89926 ± 0.07133 (1σ , $n=5$) that correspond to a model age of

882 Ma. It should be noted that this age has a fairly large uncertainty due to the low cps even though an error estimation has not been attempted. At this time, these results are deemed not reliable.

5.4.2 Nano- Cu silicate

A total of twenty-six measurements of U-Pb isotopes have been made to the nano-Cu silicates of MICA3. The ablation spots are shown in the Figure 21. In general, Pb (about 10–40 ppm, see the Section 5.3.3) yielded 1500 cps on ^{204}Pb , 28000 cps on ^{206}Pb , 24000 cps on ^{207}Pb , 61000 cps on ^{208}Pb ; Th (5–15 ppm, see Section 5.3.3) yielded 28000 cps on ^{232}Th ; U (about 2–3 ppm, see Section 5.3.3) yielded 8000 cps on ^{238}U . The low counts on ^{238}U means low precision.

The presence of ^{204}Pb clearly indicates the presence of common lead in the sample, which means

there are non-radiogenic ^{206}Pb , ^{207}Pb , ^{208}Pb inherited from previous Pb source. The presence of common lead poses challenge for U–Pb geochronology, which essentially uses time-dependent radioactive decay of U and Th to ^{206}Pb , ^{207}Pb , ^{208}Pb . Common lead correction is crucial yet quite challenging for these samples. Currently, no reliable ages can be obtained unfortunately. These results are deemed not reliable.

Based on trace element observation in Section 5.3.5 (Fig. 23), it is assumed that common lead in the nano-Cu silicate was mainly from the cuprite and the fluid itself that precipitated apachite. This assumption is not built on solid ground since the age of apachite is unknown (even though we also tried to date apachite, but no definitive answers have been derived so far). The Pb isotopic composition of cuprite was measured (shown in Section 5.4.1), and that of apachite was taken from Stacy and Kramer's common lead model (1974). Mixing between these two sources with different proportion is considered. Calculation employing Tera–Wasserburg technique (Vermeesch 2021) yielded $^{206}\text{Pb}/^{238}\text{U}$ intercept ages between 180 Ma to 5 Ga, which is unreasonable. Another method attempted in this test study was to use Th–Pb technique. Using the same common lead correction method described above, obtained $^{208}\text{Pb}/^{232}\text{Th}$ ages are highly scattered, even though some of them (about 40 Ma at a mixing proportion of 0.5) appear reasonable.

While U–Th–Pb dating of the nano-Cu silicate seems possible at this time results are deemed not reliable.

5.4.3 Apachite

A total of ten measurements have been made for apachite in MICA7. Laser ablation spots are shown

in Figure 14. In general, Pb (about 0.3 ppm, see the Section 5.3.5) yielded 100 cps on ^{204}Pb , 600 cps on ^{206}Pb , 300 cps on ^{207}Pb , 1000 cps on ^{208}Pb ; Th (0.2 ppm, see the Section 5.3.5) yielded 100 cps on ^{232}Th ; U (about 150 ppm, see the Section 5.3.5) yielded 1,000,000 cps on ^{238}U . $^{206}\text{Pb}/^{238}\text{U}$ and $^{207}\text{Pb}/^{235}\text{U}$ ages are discordant. $^{206}\text{Pb}/^{238}\text{U}$ ages show that the apachites are younger than 4 ± 0.3 Ma (1σ), whereas $^{207}\text{Pb}/^{235}\text{U}$ show ages older at 45 ± 5.3 Ma (1σ). The two apparent ages are considered unreliable. One issue is the low cps on Pb, which can severely affect analytical precision and accuracy. The other is the low Th/U ratio of the apachite, which might indicate existence of U– ^{230}Th disequilibrium. This phenomenon can cause underestimation of $^{206}\text{Pb}/^{238}\text{U}$ ages. Associated with this is that little is known about isotopic closure temperature for U–Pb systematics. To solve these issues, a higher sensitivity instrument or method (e.g., maybe larger laser spot or higher laser fluence) should be used. Likewise, correction for potential U–Th disequilibrium should be applied, which is currently not possible as the U/Th ratio of the original fluid is not known.

5.4.4 Malachite

A total of ten measurements have been made for malachite in MICA5. Laser ablation spots are shown in the Figure 20. In general, Pb yielded 1700 cps on ^{204}Pb , 700 cps on ^{206}Pb , 550 cps on ^{207}Pb , 1400 cps on ^{208}Pb ; Th yielded 3000 cps on ^{232}Th ; U yielded 12000 cps on ^{238}U . $^{206}\text{Pb}/^{238}\text{U}$ and $^{207}\text{Pb}/^{235}\text{U}$ ages are also discordant. $^{206}\text{Pb}/^{238}\text{U}$ ages are younger at 3 ± 1.1 Ma (1σ), whereas $^{207}\text{Pb}/^{235}\text{U}$ ages are older at 52 ± 18 Ma (1σ). Similar to apachite, these are not reliable ages for malachite.

5.5 Cu isotope geochemistry

Copper isotopes in different Cu mineral phases have been measured. For native copper, solution method was used to characterize the Cu isotopic compositions of two copper standards (ERM–EB75 and ERM–EB74, please refer to the Sections 4.5 and 4.7 for details) and two MICA copper samples (MICA2 and MICA3). For cuprite, nano-Cu silicate, and malachite, only laser ablation mode was used because of availability of external standards (please refer to the Section 4.7 for details).

5.5.1 Solution work

Forty-two sub-samples of native copper were sampled from EB75 and EB74 ($n=7$ each), MICA2 ($n=17$), and from MICA3 ($n=11$) for Cu isotopic analysis by drilling. $^{23}\text{Isotopic}$ homogeneity was tested by spreading out the drill holes across the entire sample (Fig. 24).

Results show that the EB standards and MICA samples are homogeneous within the ana-

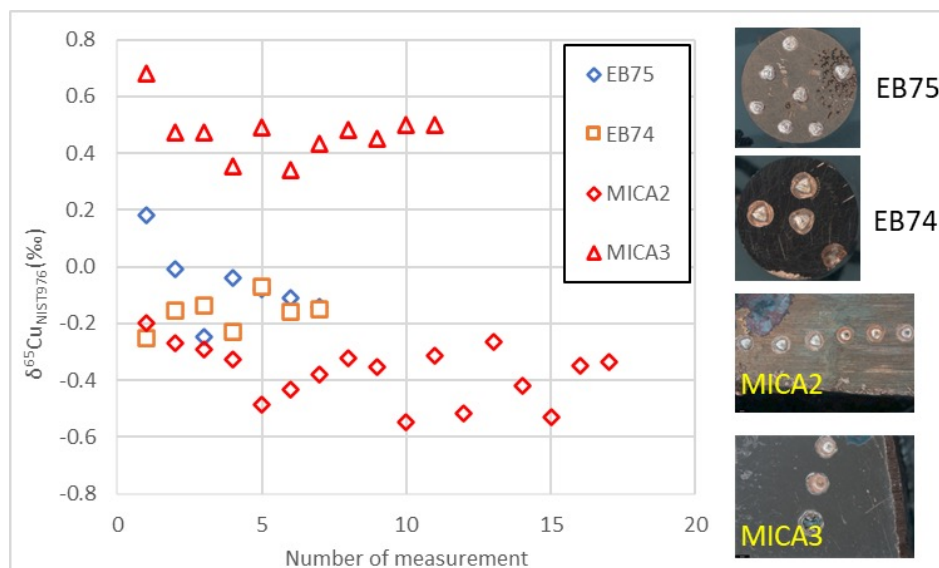


Fig. 24. Plots of $\delta^{65}\text{Cu}_{\text{NIST976}}$ values for EB75, EB74, MICA2, and MICA3 with images showing drilling locations.

lytical uncertainty (0.05–0.1‰). EB75 yielded $\delta^{65}\text{Cu}_{\text{NIST976}} = -0.1 \pm 0.1\text{‰}$ (1 σ , n=7); EB75 yielded $\delta^{65}\text{Cu}_{\text{NIST976}} = -0.2 \pm 0.1\text{‰}$ (1 σ , n=7); MICA2 yielded $\delta^{65}\text{Cu}_{\text{NIST976}} = -0.4 \pm 0.1\text{‰}$ (1 σ , n=17); MICA3 yielded $\delta^{65}\text{Cu}_{\text{NIST976}} = +0.5 \pm 0.1\text{‰}$ (1 σ , n=11).

5.5.2 Laser ablation work

In total, 68 measurements have been made for 6 copper samples by laser ablation method (Table 7). Laser ablation spots are shown in Figure 25.

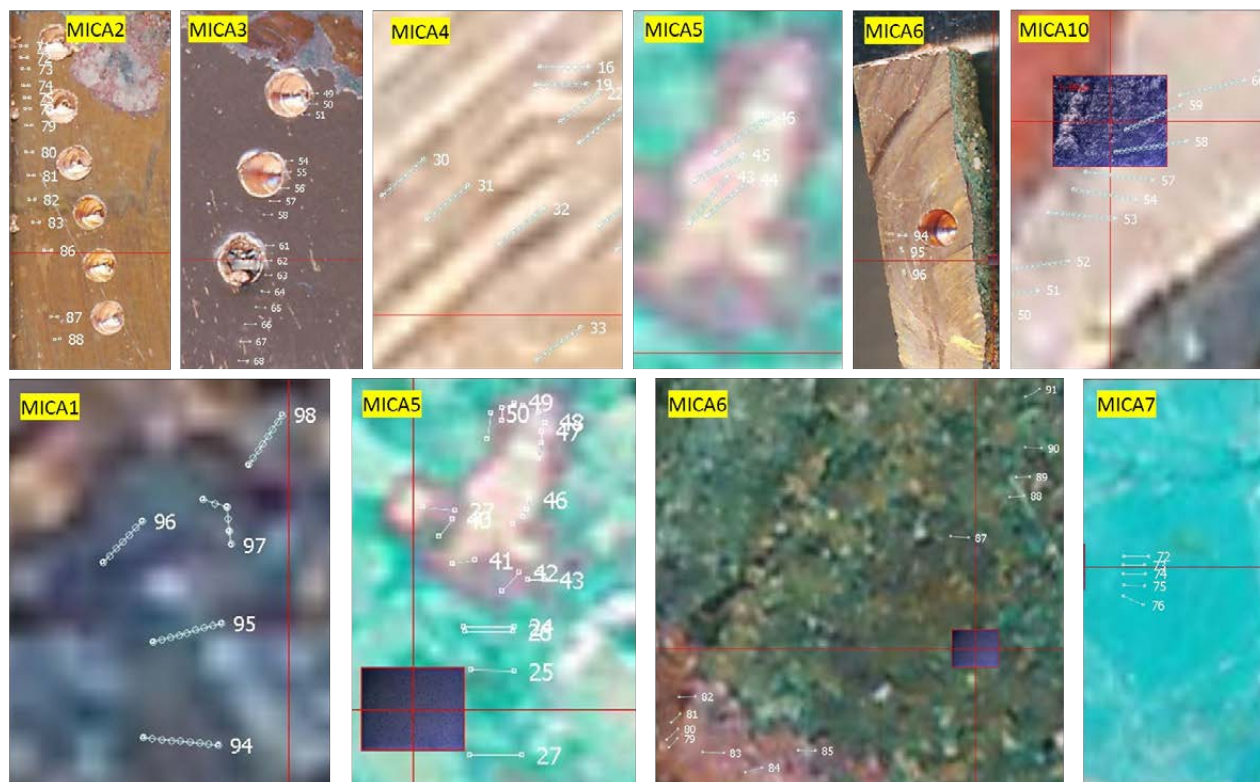


Fig. 25. Laser ablation spots of MICA samples. The upper panel shows native copper; the lower panel shows cuprite, apachite and malachite.

MICA2 yielded $\delta^{65}\text{Cu}_{\text{NIST976}} = -0.2 \pm 0.02\text{‰}$ (1σ , $n=17$); MICA3 yielded $\delta^{65}\text{Cu}_{\text{NIST976}} = 0 \pm 0.02\text{‰}$ (1σ , $n=18$); MICA4 yielded $\delta^{65}\text{Cu}_{\text{NIST976}} = -0.1 \pm 0.01\text{‰}$ (1σ , $n=10$); MICA5 yielded $\delta^{65}\text{Cu}_{\text{NIST976}} = -0.1 \pm 0.01\text{‰}$ (1σ , $n=8$); MICA6 yielded $\delta^{65}\text{Cu}_{\text{NIST976}} = -0.1 \pm 0.02\text{‰}$ (1σ , $n=4$); MICA10 yielded $\delta^{65}\text{Cu}_{\text{NIST976}} = -0.1 \pm 0.02\text{‰}$ (1σ , $n=10$).

Compared to values obtained by solution method, laser ablation overestimated the $\delta^{65}\text{Cu}$ of MICA2 by 0.2‰ , whereas it underestimated MICA3 by 0.5‰ . However, it should be noted that this method pro-

duced the right values for EB74 (Fig. 26). This apparent deviation might be related to “matrix effects” in relation to contrast in texture (artificial vs. natural) and composition as EB is quite pure, but MICA contains more impurities (about 300 ppm impurities in MICA vs 20–50 ppm in EB). Currently, we have not figured out potential causes for this unknown matrix effect. So, it is concluded that laser ablation method adds 0.7‰ uncertainty in addition to the analytical errors.

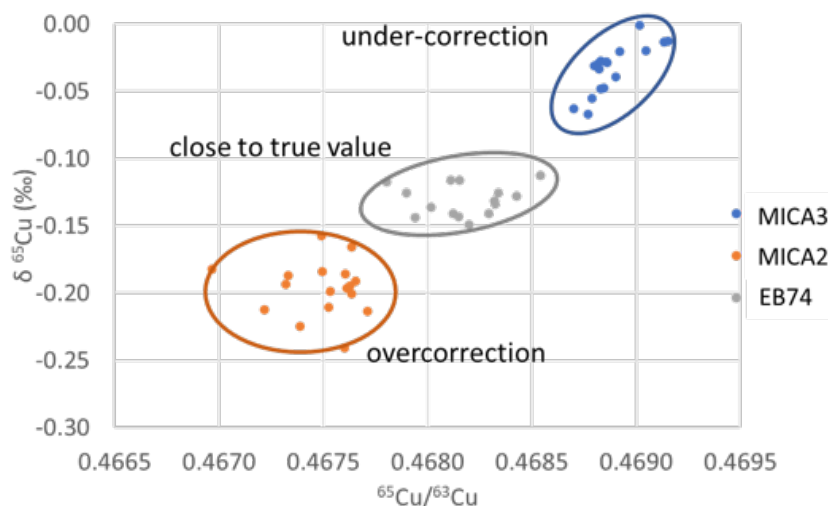


Fig. 26. A plot of $\delta^{65}\text{Cu}_{\text{NIST976}}$ value vs measured $^{65}\text{Cu}/^{63}\text{Cu}$ value for EB74, MICA2, and MICA3.

In total, 29 measurements have been made for cuprite in 3 samples (Fig. 27). Results show that MICA1 yielded $\delta^{65}\text{Cu}_{\text{NIST976}} = 1.3 \pm 0.3\text{‰}$ (1σ , $n=5$); MICA5 yielded an averaged $\delta^{65}\text{Cu}_{\text{NIST976}} = 1.3 \pm 0.6\text{‰}$ (1σ , $n=19$); MICA6 yielded $\delta^{65}\text{Cu}_{\text{NIST976}} = 3.0 \pm 0.5\text{‰}$ (1σ , $n=5$).

In total, 5 measurements have been made for apachite in MICA7, producing $\delta^{65}\text{Cu}_{\text{NIST976}} = -1.6 \pm 0\text{‰}$ (1σ , $n=5$).

In total, 21 measurements have been made for malachite in 3 samples. Results suggest that MICA1 yielded $\delta^{65}\text{Cu}_{\text{NIST976}} = 0.01 \pm 0.3\text{‰}$ (1σ , $n=5$); MICA5

yielded $\delta^{65}\text{Cu}_{\text{NIST976}} = 0.22 \pm 0.23\text{‰}$ (1σ , $n=11$); MICA6 yielded $\delta^{65}\text{Cu}_{\text{NIST976}} = -0.5 \pm 0.6\text{‰}$ (1σ , $n=5$).

Comparing the different mineral phases, it is apparent that cuprite is relatively enriched in ^{65}Cu whereas malachite can be either enriched or depleted compared to their native copper host. This is most obvious in the MICA6, where copper host has ^{65}Cu of around -0.1‰ , but after oxidation cuprite has ^{65}Cu of up to 4‰ which decreases to -0.5‰ in malachite after carbonation. In total, Cu isotopic fractionation between cuprite and native copper is up to 4‰ .

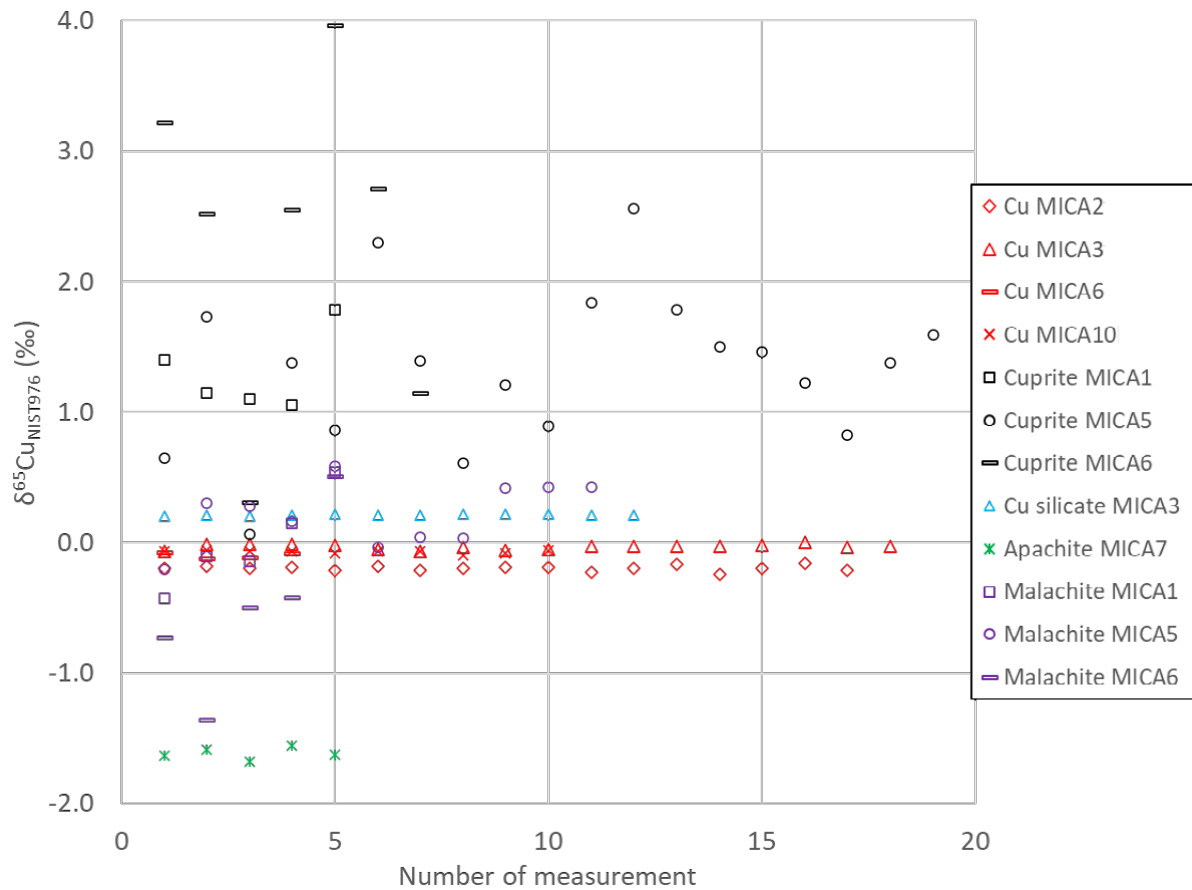


Fig. 27. $\delta^{65}\text{Cu}_{\text{NIST976}}$ values in different mineral phases in the MICA samples. Native copper (in red), cuprite (in black), Cu silicate (in blue), apachite (in green), and malachite (in purple). Different samples are denoted with shapes in MICA1 (rectangle), MICA2 (diamond), MICA3 (triangle), MICA5 (circle), MICA6 (dash), MICA7 (star), and MICA10 (cross).

It should be pointed out that a non-matrix match standard (Cp1, a chalcopyrite) was used for calibrating mass bias in cuprite, nano-Cu silicate, apachite, and malachite, and thus there might exist unknown

matrix effects. Nevertheless, the distinct Cu isotope signatures in copper host and corrosion phases provide a potentially viable proxy for redox conditions and related processes.

6 FEASIBILITY AND USABILITY ASSESSMENT FOR PHASE II

The proposed methodology is aimed at pinpointing corrosion mechanism and if possible constraining the time for native copper samples to be collected from the Keweenaw Peninsula. The method for achieving these goals is the ability to systematically study minerals (mineralogy, texture, structure) to elements (trace elements and isotopes).

Overall, based on the work presented herein:

- Mineralogy and sequencing of corrosion products are readily determined by optical, XRD, and SEM methods.
- Corrosion geometry in 2D and 3D space can be described by XCT.

- Attempts at geochronology using U-Pb and common Pb has failed to produce reliable ages and may not be possible for Phase II.
- Some trace elements in the native copper and other minerals can be determined by LA-ICP-MS. Due to low abundance and/or analytical constraints some trace elements cannot be determined by this method.
- Copper isotopes can be readily determined.

A much more reliable evaluation can be made regarding the usefulness of the analytical methods proposed and used in this test study.

First of all, SEM-EDS has proven most effective in identifying silicate minerals (e.g., apachite). However, it has two drawbacks linked to instrumental limitation. First is its inefficiency in detecting and thus quantifying light elements, particularly C and O, which are common elements in Cu corrosion minerals. Second are the relatively small areas that can be mapped in a limited time frame, which generally means the instrument is not quite cost-effective for large scale elemental mapping. These two drawbacks can be complemented by XRD and μ -XRF. XRD is a technique looking into mineral structure instead of chemistry, so it can easily differentiate carbonates and oxides. μ -XRF is a good technique for visualizing elemental distribution in a large sample within a fairly short amount of time. But for other atomic scale investigations, Atom Probe Tomography might be a good option.

Second, LA-ICP-MS has proven to be a very powerful tool to study analogue samples with thin layers of corrosion products. It can provide quite precise and accurate trace element and isotopic data at high spatial resolution and low sample consumption. Similarly, there might be three limitations to this technique. First is sample preparation: while LA-ICP-MS requires minimum sample preparation compared to other chemical methods, a relatively

flat and big enough ($>100\text{ }\mu\text{m}$) surface is required for good precision and accuracy. Second is the availability of external standards: LA-ICP-MS is a technique that suffers severe matrix effect, which means data quality relies on using matrix match standards. Currently, standards are available for trace elements. Third, laser ablation can cause large isotopic fractionation, especially for native copper with nano-second pulse width laser. It is preferable to use femto-second laser for this purpose.

Micro-XCT has proven to be an effective and efficient technique for studying 3D geometry of corrosion zones. One minor limitation would be related to resolution. To obtain higher resolution, small samples needed to be prepared, which generally means scarifying representativeness. If sample representativeness is compensated by large sample volumes, analytical costs would be another constraint. XCT work in this test study has revealed deformation features in MICA6 (Fig. 7). Regardless of the origin of the deformation event, it may provide an opportunity for studying corrosion responses to deformation. If this research direction is to be performed, detailed sampling work of representative samples with clear background information are needed prior to comprehensive analyses. A preferable addition would be Atom Probe Tomography for structural study at atom scale and femto-second laser for Cu isotope study.

7 CONCLUSIONS

The first objective of determining instrumental limits is relatively straightforward and has been fully achieved by the time of drafting this report. The proposed technologies (instrument and analytical techniques at GTK) are sufficient to acquire the required data, even though, some instrumental limitations have emerged when distinguishing copper silicate from malachite and cuprite from tenorite. The issues have been solved by adding powder XRD in the workflow. In addition, new methods for precise and accurate measurement of trace elements and Pb-Cu isotopes in copper metal by LA-ICP-MS have been vigorously explored and successfully established. Instrumental sensitivity might be a limiting factor for precise measurement of Pb isotopes in Cu metal and Cu oxides, which usually contain low contents of Pb. Even though

laser parameters such as fluence may compensate low sensitivity, instruments with higher sensitivity than the one GTK houses should be sought. μ -XCT has proven to be an effective tool for elucidating spatial distribution of corrosion layers in three dimensions. Nonetheless, depiction of finer features such as Cu/corrosion product contact requires further tests. Limited penetration of X-ray in thick copper slabs may impede visualization of crystal-line structures. APT may provide such information.

The preliminary interpretation has confirmed the presence of corrosion minerals including cuprite, tenorite, and a nano-mixture of chlorite and cuprite, malachite and discovered a new alteration mineral, apachite. The elemental and isotopic shifts of corrosion minerals from their copper hosts seem to be related to physical and chemical

conditions prevailed during the reactions. Radiometric dating with common lead in cuprite and U–Pb in apachite and malachite have not yet proven

to be feasible due to significant complications regarding data reproducibility, U–Th disequilibrium, and common Pb correction.

ACKNOWLEDGEMENTS

This test study has received tremendous analytical supports from researchers at the Espoo Research Lab of the Geological Survey of Finland. I acknowledge Jukka Kuva for conducting XCT scanning, Ester Jolis for conducting XRF mapping, and Pasi Heikkilä for conducting XRD analyses. I am grateful to Sari Lukkari for her assistance during SEM

analyses, to Hugh O'Brien, Matti Kurhila, Minna Myllyperkiö, and Leena Järvinen for their kind help during LA-ICP-MS analyses. I am particularly indebted to Yann Lahaye for invaluable inputs at the beginning of the project as well as thoughtful discussions throughout the study.

REFERENCES

- Belousova, E. A., Griffin, W. L. & O'Reilly, S. Y. 2006. Zircon crystal morphology, trace element signatures and Hf isotope composition as a tool for petrogenetic modelling: examples from Eastern Australian granitoids. *Journal of Petrology* 47(2), 329–353.
- Bogaerts, A., Chen, Z., Gijbels, R. & Vertes, A. 2003. Laser ablation for analytical sampling: what can we learn from modeling? *Spectrochimica Acta Part B, Atomic Spectroscopy* 58(11), 1867–1893.
- Huhma, H., Mänttari, I., Peltonen, P., Kontinen, A., Halkoaho, T., Hanski, E., Hokkanen, T., Hölttä, P., Juopperi, H., Konnunaho, J. & Lahaye, Y. 2012. The age of the Archaean greenstone belts in Finland. In: Hölttä, P. (ed.) *The Archaean of the Karelia Province in Finland*. Geological Survey of Finland, Special Paper 54, 74–175. Available at: https://tupa.gtk.fi/julkaisu/specialpaper/sp_054_pages_074_175.pdf
- Lazarov, M. & Horn, I. 2015. Matrix and energy effects during in-situ determination of Cu isotope ratios by ultraviolet-femtosecond laser ablation multicollector inductively coupled plasma mass spectrometry. *Spectrochimica Acta Part B, Atomic Spectroscopy* 111, 64–73.
- Liu, X., Reijonen, H., Aaltonen, I., Ruskeeniemi, T., Lilja, C., Liebscher, A., Norris, S., Watt, N., Diomidis, W. & Lahaye, Y. 2022. Geochemical and isotopic fingerprinting of Cu metal using Laser ablation mass spectrometry. *Nordic Geological Winter Meeting 2022*. Available at: <https://jfi.is/wp-content/uploads/2022/05/NGWM-2022.pdf>
- Müller, W., Shelley, M., Miller, P. & Broude, S. 2009. Initial performance metrics of a new custom-designed ArF excimer LA-ICPMS system coupled to a two-volume laser-ablation cell. *Journal of Analytical Atomic Spectrometry* 24(2), 209–214.
- Stacey, J. S. & Kramers, J. D. 1975. Approximation of terrestrial lead isotope evolution by a two-stage model. *Earth and planetary science letters* 26(2), 207–221.
- Van Achterbergh, E., Ryan, C. G. & Griffin, W. L. 2001. GLITTER on-line interactive data reduction for the LA-ICPMS microprobe. Sydney: Macquarie Research Ltd.
- Vermeesch, P. 2021. On the treatment of discordant detrital zircon U–Pb data. *Geochronology* 3(1), 247–257.



All GTK's publications online at hakku.gtk.fi